I. Negative Incremental Impedance of Fluorescent Lamps

II. Simple High Power Factor Lamp Ballasts

Thesis by

Edward E. Deng

In Partial Fulfillment of the Requirements

for the Degree of

Doctor of Philosophy

California Institute of Technology

Pasadena, California

1996

(Submitted September 1, 1995)

Dedicated to my parents Jiati Deng and Baomei Ni

Acknowledgements

I wish to express my sincere gratitude to my advisor, Professor Slobodan Ćuk, for accepting me into the Caltech Power Electronics Group, for the freedom to direct my research, for his invaluable advice, steady encouragement and strong support during the course of this work. I also wish to thank my co-advisor, Professor R. D. Middlebrook, for his wise guidance.

I gratefully acknowledge the financial support of Caltech by way of several graduate teaching assistantships and the following corporations by way of graduate research assistantships: General Electric Co., Day-Ray Products Inc., Rockwell International Inc., Apple Computer Inc., GEC Ferranti Defense Systems Ltd., Southern California Edison Inc., Italtel Inc., MagneTek Inc., Dong Ah Electric Co., Ltd. and International Rectifier.

Thanks also go to my predecessors for what they have left behind and to every member of the Power Electronics Group for the open exchange of ideas and of course, the pleasure of friendships. I am very grateful to many people for what I have learned from them and for the good times we have shared which make my days at Caltech a unique and memorable experience.

Finally, of great personal importance to me have been the understanding, encouragement and love of my wife Shihua through my years at Caltech.

Abstract

Two important subjects in high frequency fluorescent lighting are investigated. Part I presents a fundamental understanding of the negative incremental impedance of fluorescent lamps. Search for simple, high power factor, lamp ballast topologies, a more practical aspect of lighting electronics, is presented in Part II.

Part I

Fluorescent lamps have a special v-i characteristic. Their incremental or small-signal impedance is defined and studied in the frequency domain. It is found that the negative incremental impedance of a fluorescent lamp can be characterized by a right half plane zero. The existence of such a result is explained by the modified Francis equation. Two approaches are proposed in order to set up a stable operating point for the lamp. First, a resonant matching network, which provides impedance transformation, is placed between a voltage source and the lamp. Second, a feedback loop is closed from the lamp current to control the magnitude of the voltage source. Stability criteria based on the Nyquist criterion are developed for the impedance of the resonant matching network and for the loop gain in the above two cases, respectively.

It is found that the input impedance of a switching dc-to-dc regulator, which is another case with the negative incremental impedance, and the fluorescent lamp impedance, are two dual cases and thus can be analyzed in a unified manner based on the stability of one-port circuit.

The small-signal lamp impedance is measured in the most practical case of a sinusoidal carrier, and it is fit by a real rational function with a right half plane zero. The small-signal models describing low frequency variations of sinusoidal magnitude are developed and are experimentally verified for the three major resonant matching networks. Stability analysis for resonant matching networks at parallel resonance are performed. It shows

that the *LCC* network is the simplest resonant matching network that a fluorescent lamp needs. It is also predicted, and experimentally verified, that the resonant matching networks at series resonance are feasible as ballasts when the lamp current feedback loop is closed.

Part II

Unlike conventional high power factor ballasts requiring two cascaded power conversion stages, the proposed new lamp ballasts achieve near unity input power factor and high frequency sinusoidal lamp current in a single power conversion stage.

A single-stage, high power factor lamp ballast is proposed, which is derived from the Ćuk converter. A new discontinuous inductor current mode of its input inductor makes this possible by separating the input current-shaping from the output high frequency inversion. The desirable mode of operation is presented with major waveforms. The high efficiency is further enhanced by the soft-switching improvement, which is provided naturally through the lagging current of the resonant matching network. Design equations are given. The performances of the proposed single-stage, high power factor lamp ballast are verified by the experimental results.

Single-switch, unity power factor ac-to-ac converter topologies based on proper integrations of automatic current shapers and single-switch inverters, such as the Class E converter, are presented, which are suitable for lamp ballast applications. Descriptions of the desirable mode of operations and a first order analysis are given. The ballasts have the compact structure of single active switch, high input power factor and low crest factor lamp current as well as soft-switching. Experimental results confirm all the performance advantages.

Contents

Part I

Negative Incremental Impedance of Fluorescent Lamps

Chapter 1

Introduction

1.1 Fluorescent Lamp

We commonly think of ourselves as living in an era when information super highway and worldwide transportation have changed the entire nature of human life. But reflect briefly on the fact that information super highway would be of little or no value if half the world at any given moment was shut down for being in the dark. Making light is one of man's most important achievements in the industrialized history.

Light is a kind of electro-magnetic radiation which stimulates our eyes and enables us to see. Today most man-made light is generated from electricity through an apparatus named as lamp. There are mainly two kinds of lamps, i.e., incandescent filament lamp and gas discharge lamps.

The incandescent lamp has a (tungsten) filament which emits light when the electricity flows through. The spectrum of energy radiated from an incandescent lamp is continuous. Unfortunately the major part of the energy is radiated in the infrared region and is converted into heat. Only a relatively small quantity of energy is emitted at various visible lengths as light. Thus the efficiency of an incandescent lamp is low although it may be more convenient to use than gas discharge lamps.

All electric gas discharge lamps convert electrical energy into light by transforming electrical energy into the kinetic energy of moving electrons, which in turn is converted into radiation as a result of some kind of collision process. The primary process is collisional excitation of (mercury) atoms in a gas to high-energy states from which they relax back to the lowest-energy atomic levels by means of the emission of electromagnetic radiation. The unique advantage of the atomic radiation from a gas discharge is that by a suitable choice of the atoms of which the gas is composed, intensity of the radiation

can be concentrated on a few spectral lines at the characteristic frequencies determined by the distribution of permitted energy levels of the particular atoms, thereby making exceptionally efficient light sources. Of all the gas discharge lamps, fluorescent lamp is one of the most efficient and widely used.

A fluorescent lamp consists of a glass tube coated on the inside with a phosphor powder. The tube contains a mixture of one or more noble gases (neon, argon, krypton) at a certain pressure and a small amount of mercury vapor. The lamp is operated by maintaining a gas discharge in it, with the help of two electrodes, one at each end of the glass tube. In the discharge, free electrons are accelerated by a potential difference applied across the lamp; mercury atoms are then excited and ionized in the discharge column. Ultraviolet radiation is emitted when the exited mercury atoms return to lower energy states, which is converted into visible light by the phosphor coating on the tube wall. The added noble gas is to increase the efficiency of the discharge. The phosphor plays a key role in determining the color and color rendering of the lamp. The life of a fluorescent lamp is determined by its electrode's life.

Incandescent lamp is easy to use due to its simple electric behavior. The v-i relation of the incandescent filament lamp is determined by the resistance of the tungsten filament, which is close to the v-i characteristic of a linear resistor. The v-i characteristic of a fluorescent lamp, however, is nonlinear and time-variant since various physical processes which are responsible for the light generation are involved in the gas discharge. Therefore, fluorescent lamp needs a so-called "ballast" circuitry to run with it.

As a example, Figure 1.1 shows a typical curve of discharge potential drop versus current when lamp is operated from a dc power source [1] [2]. Because the slope of the I-V curve is negative, that is, $r \equiv dV/dI < 0$, the discharge is said to have a "*negative incremental resistance.*" This poses a circuit problem for operating lamps. In general, a voltage V_s higher than the steady-state operation voltage is needed to establish initial ionization in the gas. After the discharge gets started, the operating point (i,v) of the discharge lies somewhere on the line of $V = V_s$ which is above the steady state operating curve, where the ionization rate exceeds the loss rate or $dn_e/dt > 0$. Thus the discharge current rises without any regulation, which eventually causes system failure.

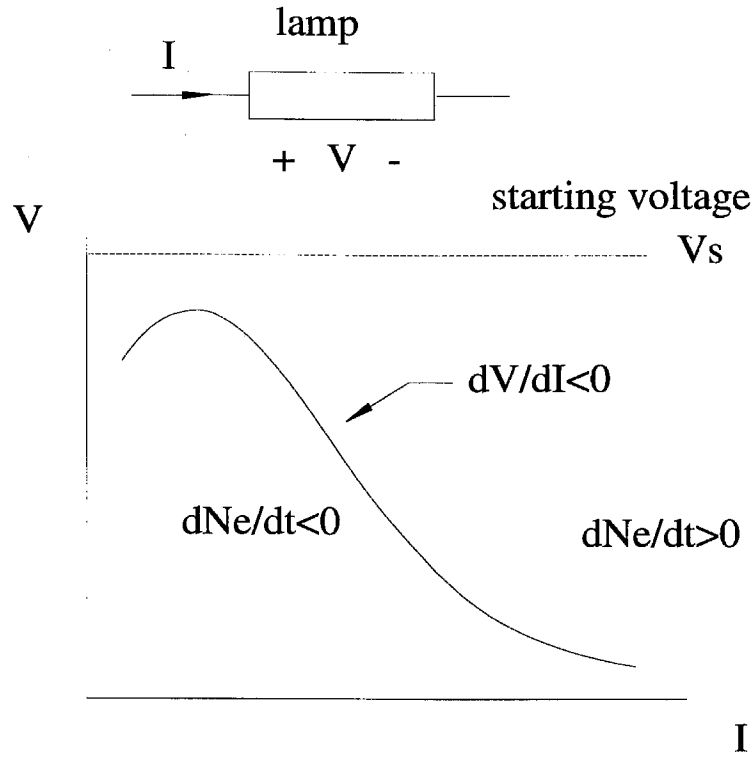

Figure 1.1: A typical I-V curve of a gas discharge lamp operated from a dc power.

As a result, a certain impedance must be placed in series with a fluorescent lamp as a means to limit the lamp current. For dc operation, a resistor R is needed so that the I-V curve of the series-connected circuit has a positive slope as shown in Figure 1.2. Suppose the lamp current is higher than its steady state value. The operating point is to the right and below the steady state operating curve, so the potential applied across the lamp would be less than normal due to the voltage drop across the resistor R and thus $dn_e/dt < 0$. Accordingly, electron density would have to decrease with time and operating current would have to shift to lower currents. In this way, the operating point is brought back to the steady state (i_{ss}, V_s). Similarly, any current smaller than i_{ss} would be also brought back to the steady state (i_{ss}, V_s) so it is a stable operating point. The resistor R which helps to establish the stable current i_{ss} through the gas discharge

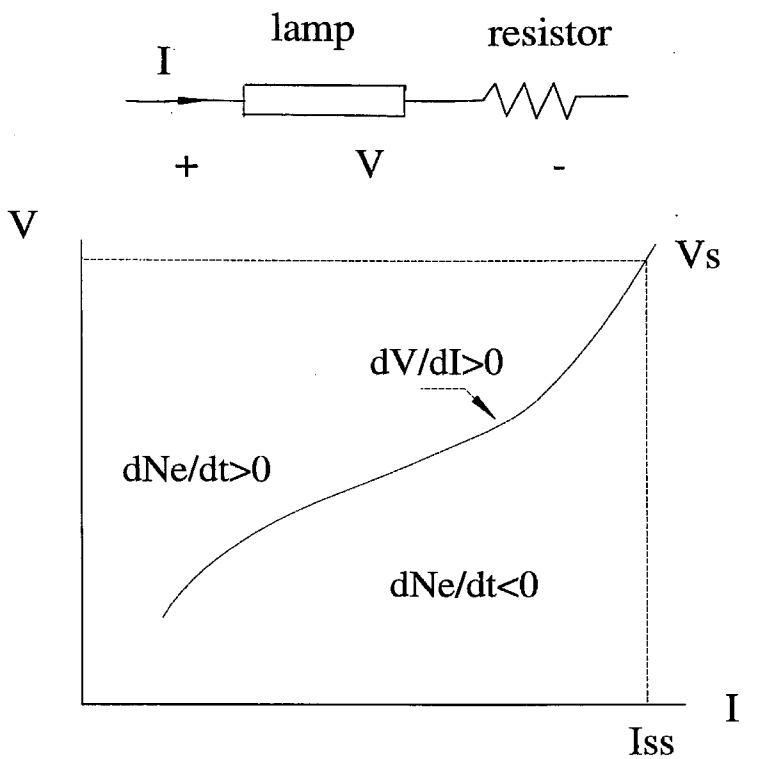

Figure 1.2: An I-V curve of a gas discharge lamp in series with a resistor R operated from a dc power.

acts as a *ballast.* To obtain the positive slope on I-V curve as in Figure 1.2, R has to be larger than $|r|$.

In general applications, a fluorescent lamp is usually driven with an ac power. Reactive components are used in the ballast to avoid the ohmic loss of a resistor. Ac operation also balances the wearing of two electrodes and maintains a longer lamp life. At 60Hz operation, a ballast mainly consists of inductive components. It strikes the lamp every halfline cycle as well as limits the lamp current. Lamp voltage and current waveforms are quite dissimilar and both contain a fairly large amount of high harmonics due to the lamp's nonlinear *v-i* characteristic [2].

1.2 High Frequency Operation of Fluorescent Lamps

The study of high frequency operation of fluorescent lamps started quite early [3] and has grown very fast recently due to the pronounced lamp efficacy increase at high frequencies. It has been shown that the lamp efficacy can be increased by 15% when the operating frequency rises to 20KHz [4]. High frequency operation also makes lamp start easily and eliminates the stroboscopic effect.

Another advantage of high frequency operation is that the use of solid-state ballast has a lower power loss due to the non-inductive nature of the resonant circuits [5]. The size of the ballast is also significantly reduced. Audio noise associated with the 60Hz magnetic ballast is removed. In addition, voltage regulation and power factor correction can be easily incorporated into the ballast. High frequency operation of fluorescent lamps also offers new possibilities for intelligence and energy management. For example, lamp light can be controlled in combination with the daylight change by using a dimmable ballast. The major disadvantage of high frequency operation at present is in the increased cost of the ballast.

Coincident with the rise in luminous efficiency are the changes in lamps *v-i* characteristic. With sinewave of power applied, the apparent lamp power factor changes from about 90% at 60Hz to unity at 400Hz and all higher frequencies [3], [9]. Within the frequency range of our interest, voltage and current waveforms of a fluorescent lamp are almost proportional. If drawn in the *v-i* plane, the characteristic curve can be considered as a straight line passing through the origin so the lamp can be approximated as a resistor. However, this resistor is not linear but varies as a function of time and current which will be studied further in the following chapters.

1.3 Terminology

Some terminology is introduced in this section which summarizes the above discussions and also provides the necessary background knowledge for the contents of the thesis.

Efficacy: Efficacy is a measure of the lamp efficiency performance, i.e., the ratio of total light output over the input electrical power. It is given in lumens per watt (lm/W).

For example, the efficacy of a high frequency fluorescent lamp and ballast system can be as high as 100 lm/W [6]. The efficacy of a typical incandescent lamp, on the other hand, is less than $20 lm/W$.

Current Crest Factor: Crest factor is a measure of the lamp current waveform, i.e., the ratio of the peak current over the rms current. The electrode life is very sensitive to the current crest factor. The lower the current crest factor is, the longer a lamp lasts. Sinewave has a crest factor of 1.4. Triangular wave has a crest factor of 1.7. Usually a current crest factor less than 1.7 is required to ensure a normal lamp life of 20,000 hrs. For high frequency operation, current crest factor is not only determined by the lamp current waveform during each switching cycle but also depends on the low frequency modulation on top of it. To maintain a low crest factor, low frequency ripple also has to be minimized.

Lamp Ballast: Generally it is the circuitry between an electrical power source and a fluorescent lamp. A 60Hz ballast comprises several reactive (mainly inductive) components where power is completely processed at low frequency. A high frequency ballast is in general an ac-to-ac converter, where the input power is of 60Hz and the output power is in the range of tens of kHz to several hundred kHz. It includes a rectifier stage and an inverter stage; usually a *resonant matching network* is placed between the inverter output and the lamp. A high frequency ballast is expected to perform the following functions: supply proper starting and operating voltage for the lamp; maintain a running current at the designed value with a low crest factor; regulate the lamp current output against supply voltage variations and have a high overall efficiency. A relatively new requirement is to maintain a high (near unity) input power factor. In addition, since a ballast is a commercial product, low cost and high reliability are also highly desirable.

Resonant Matching Network: It is a network of reactive components inside the high frequency ballast, which is usually placed between the inverter output and the lamp. Its major functions are to shape the switching waveform into the sinewave as well as to provide an impedance matching for the lamp. Isolation can be also offered by inserting a transformer in it.

Carrier: The waveform that a lamp is operated with. If a lamp is driven by a dc power source, then the carrier is dc. If a lamp is operated by a high frequency sinewave current source, then the carrier is sinusoidal. A carrier could also be a squarewave, etc.

1.4 Summary of Contents

General study of the negative incremental impedance of fluorescent lamps and the corresponding stability analysis are presented in Chapter 2. The lamp incremental impedance is characterized in a small-signal sense in the frequency domain. The result is explained by the modified Francis equation. Two approaches which stabilize the lamp operation are proposed, and the stability criteria are developed based on Nyquist criterion. As a brief aside, another case of the negative incremental impedance, the input impedance of a switching dc-to-dc regulator, is reexamined and its relation with the lamp impedance is revealed.

Chapter 3 concentrates the investigation on one of the most practical case where a lamp is operated with a high frequency sinusoidal carrier. The incremental lamp impedance is measured and fit. Small-signal models which descibe low frequency variations of magitude of sinusoidal carrier are developed and experimentally verified for the three major resonant matching networks. Stability analysis for resonant matching networks at parallel resonance are performed. It is also shown and experimentally verified that the resonant matching networks at series resonance are feasible as ballasts when the lamp current feedback loop is closed.

Chapter 2

Negative Incremental Impedance and Stability of Fluorescent Lamps

It is a well known fact that a fluorescent lamp, like most other electric discharge lamps, has a negative incremental impedance characteristic and therefore must be operated in series with a current controlling circuit or a ballast. The above statement merely gives a qualitative description of the lamp's distinctive electrical characteristic and its requirement. The primary issue is that the ballast should be designed to ensure stability when operated with such a special circuit element. Therefore, it is necessary to develop an accurate model to describe the lamp's v-i characteristic.

Several studies [7], [8], [9] have been reported in the literature which intend to establish a mathematical model for the gas discharge. The authors of [7] presented a model with a set of six constants based on the physical principles inside the discharge. The parameters are obtained from the measurements of lamp voltage, current, and the relative light intensity waveforms. The approach gives accurate simulation of lamp's terminal v-i characteristic in the time domain. However, this physics-oriented model is too complicated to give a clear picture of lamp negative incremental impedance. Another approach is more empirical and electrical where physical theory only suggests aspects of the form of the mathematical model. Francis [2] proposed a simple differential equation which satisfactorily describes the first order effect of lamp behavior but also fails to show the negative incremental impedance. Various modifications [8] and [9] were made to the Francis' equation in order to increase its accuracy. The final forms of the model are a set of differential equations which are shaped to best duplicate the experimental waveforms. The parameters of equations are obtained from the measurement. The final goal of all the above modeling approaches is to accurately match the lamp's voltage and current

waveforms in the time domain.

The interest of lamp modeling here is to characterize its salient feature, negative incremental impedance, and to provide a good base for the ballast design. As we know, at high frequency or dc operation, a lamp's steady-state impedance can be considered as a resistor R. Thus instead of studying a lamp's steady-state behavior, our efforts are focused on the change of operating point or its incremental impedance. As opposed to the previous approaches, a lamp's incremental or small-signal model is studied in the frequency domain where the negative impedance can be clearly presented in poles and zeroes. In addition, stability analysis of the lamp and ballast is also easy to perform in the frequency domain because of convenience and the availability of existing analytical tools.

General study of the lamp negative impedance and stability are performed in this chapter. The study of the most practical case where the carrier is a high frequency sinewave will be presented in the next chapter. First, both steady-state and incremental lamp impedances will be defined. Only the incremental impedance is important in stability analysis. Based on the results in previous publications, Section 2 introduces a general shape of the lamp incremental impedance and the way to characterize it in the frequency domain. Physical interpretation of the above property is given based on the modified Francis equation. Stability analysis of the lamp and ballast is treated as a one-port circuit stability problem. Another kind of negative incremental impedance in power electronics, the incremental input impedance of a dc-to-dc switching regulator, which is the dual case of a lamp's impedance, is described in Section 3.

2.1 Lamp Impedance: Steady-state and Incremental

As mentioned earlier, lamp v-i characteristic at high frequency approximates a resistor. Figure 2.1 shows the waveforms of lamp voltage and current where they are completely in phase and share nearly the same shape. To better demonstrate its terminal behavior, the same waveforms are shown in i-v plane of Figure 2.2. The trace shown contains a little hysteretic loop but is very close to a straight line passing through the origin. This is because at high frequency the switching period is much smaller than the

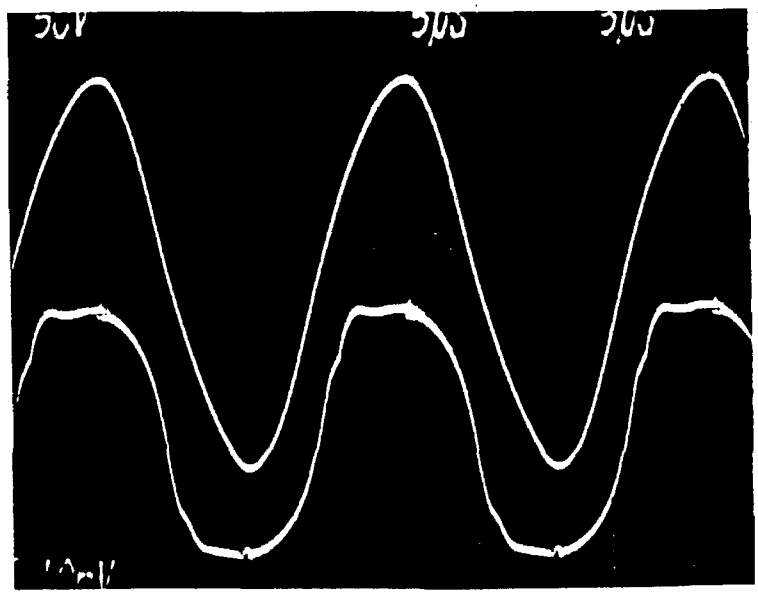

Figure 2.1: Voltage (upper trace) and current waveforms of a fluorescent lamp at high frequency operations.

gas ionization constant. Gas does not have enough time to ionize and recombine within a switching cycle so that its impedance looks like a pure resistor.

When the lamp current varies as in a dimming ballast, however, the slope of the straight line also changes. So the lamp resistance is not linear but a function of lamp current. The trace of the moving operating point is plotted in Figure 2.3, which is similar to the lamp steady-state curve at dc operations as in Figure 1.1. Now we have two curves to describe the lamp impedance. One is the straight line $A - O$ through the origin which has a positive V/I slope and describes a lamp's *steady-state* behavior. Another curve $A - B$ has a negative dv/di slope which describes the change of the operating point or its *incremental* behavior.

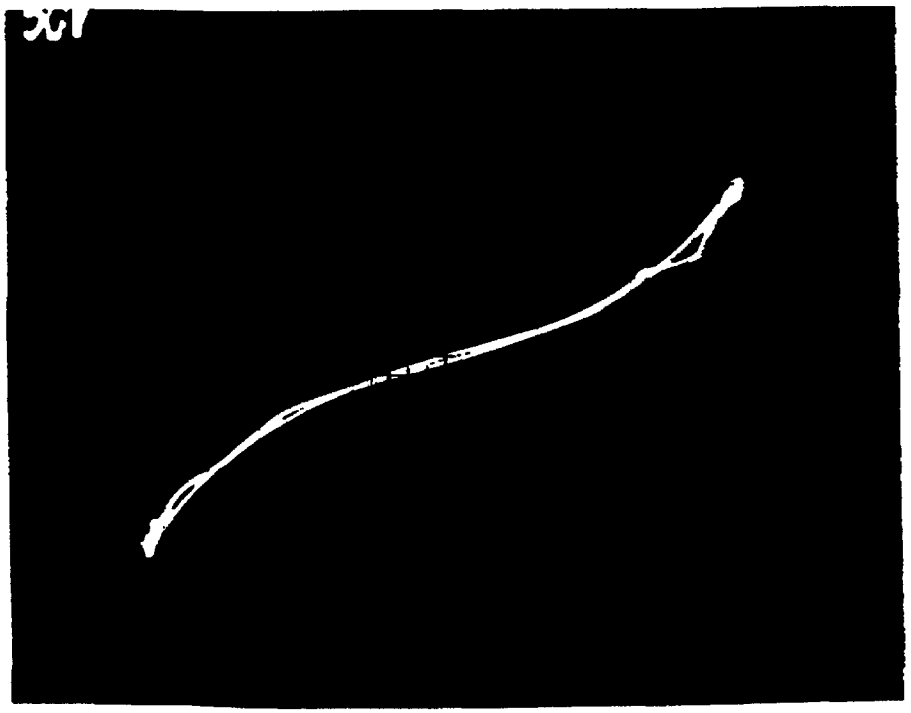

Figure 2.2: Lamp voltage and current waveforms in i-v plane at high frequency operations.

To study a lamp's incremental impedance, a perturbation which is sufficiently small in magnitude is applied around the operating point so that a linear small-signal model can be obtained. The ballast can also be analyzed to a good approximation based on the small-signal model. For example, when lamp is driven by a dc power source superimposed with a small-signal perturbation, its voltage and current are:

$$v = V + \hat{v} \tag{2.1}$$

$$i = I + \hat{i} \tag{2.2}$$

where the applied perturbation voltage $\hat{v}$ and the resulting current $\hat{i}$ are:

$$\hat{v} = |\hat{v}|cos(\omega_m t)$$

$$\hat{i} = |\hat{i}|cos(\omega_m t - \phi_m) \tag{2.3}$$

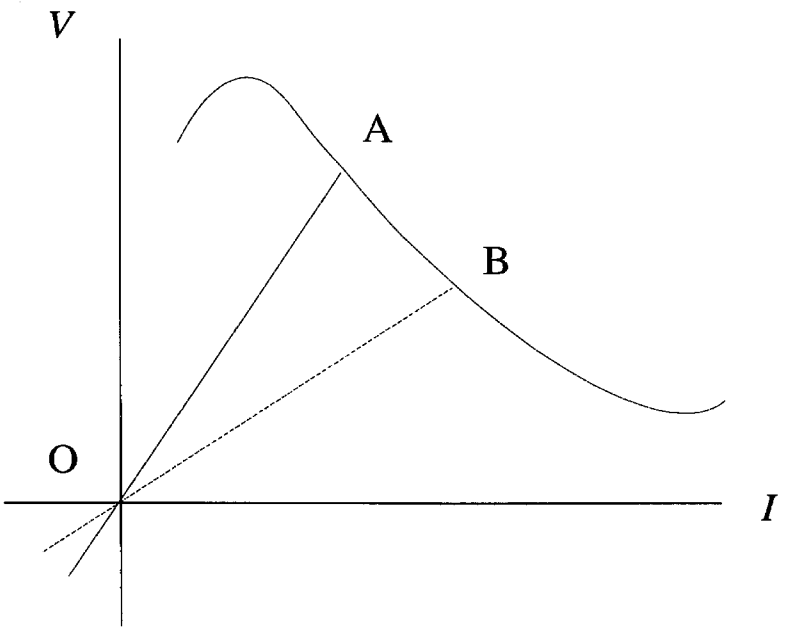

Figure 2.3: Plot of change of lamp operating point in i-v plane at high frequency operations.

and the small-signal condition is

$$\frac{|\hat{v}|}{V} \ll 1,$$
$$\frac{|\hat{i}|}{I} \ll 1. \tag{2.4}$$

The incremental impedance is

$$Z_l(j\omega_m) = \frac{|\hat{v}|}{|\hat{i}|}\angle\phi_m. \tag{2.5}$$

As another example, if carrier is a perturbed sinusoidal, then

$$v = (V + \hat{v})sin(\omega_s t) \tag{2.6}$$

$$i = (I + \hat{i})sin(\omega_s t) \tag{2.7}$$

where $\hat{v}$ and $\hat{i}$ can be expressed as in Eq. (2.3) and satisfy the small-signal condition. The incremental impedance can be also defined as in Eq. (2.5).

As a summary of the above discussions, the steady-state impedance and incremental impedance are set forth in the following definitions:

Steady-state impedance: Magnitude ratio of lamp voltage over current at a steady-state operating point. If the carrier is dc then the steady-state impedance is the dc voltage over dc current. If the carrier is high frequency sinewave, then the steady-state impedance is the ratio of their rms values. In both cases, it is a positive value.

Incremental impedance: Ratio of small-signal magnitude perturbations in lamp voltage over that of lamp current. Usually it is a complex number, and a function of the perturbation frequency ω_m. Incremental impedance is also called as small-signal impedance.

A steady-state impedance is usually associated with a large-signal operating point while an incremental impedance is concerned with small-signal perturbations of an operating point. Since lamp carrier waveforms include sinewave, squarewave and dc, etc., the steady-state point is not necessarily a dc operating point.

An interpretation of the above definition is illustrated in Figure 2.4 where a lamp is driven by a high frequency sinewave at the frequency ω_s whose amplitude is modulated by a slow-varying signal at the frequency ω_m. The incremental impedance of the lamp thus can be defined as the ratio of the slow-varying signals which modulate lamp voltage and current, respectively. It is the incremental impedance that appears to be negative at low frequency as shown by the curve A-B in Figure 2.3. In the mean time, lamp voltage and current waveforms are still proportional. Large-signal impedance remains resistive because lamp is a passive component which always consumes power.

Stability problem is closely related to the change of lamp operating point. The lamp incremental impedance will be studied first before stability analysis is performed.

2.2 Negative Incremental Impedance and Stability of Fluorescent Lamps

Fluorescent lamp has a negative incremental impedance and it needs a ballast circuitry to set up a stable operating point. This statement will be fully explained in this

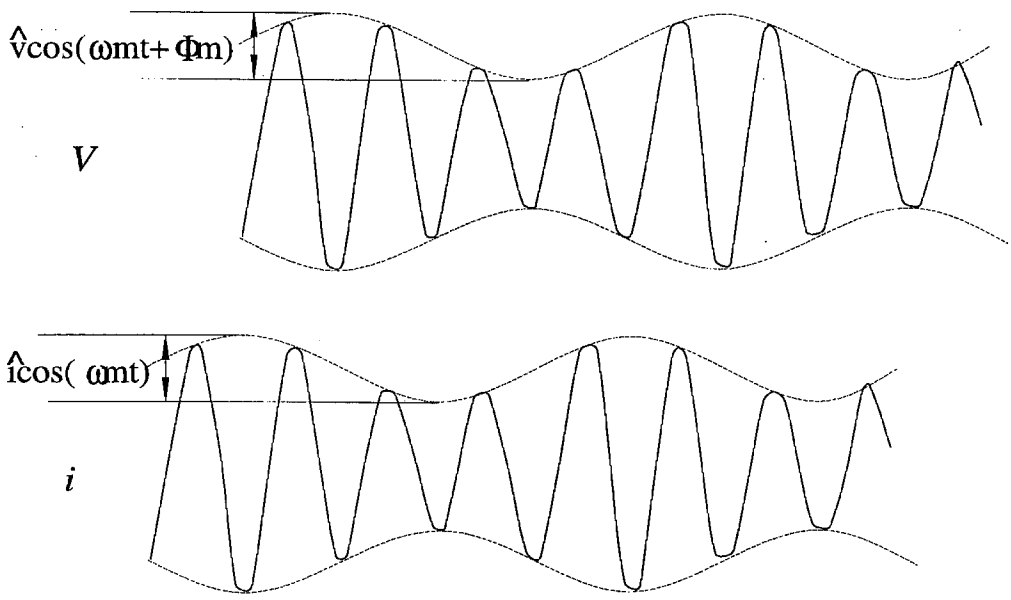

Figure 2.4: Illustration of the incremental impedance with high frequency sinusoidal carrier.

section within the scope of linear circuit theory. Based on the measurements in the frequency domain, the distinctive property of the lamp incremental impedance $Z_l(s)$ is studied first. It turns out that the negative impedance can be effectively modeled by a right half plane (RHP) zero in the frequency domain. The physical interpretation of this simple result is given based on the modified Francis equation. To establish a stable operating point, an equivalent ballast component $Z_B(s)$ has to be placed between the lamp $Z_l(s)$ and the voltage source v_s. Certain stability criteria for $Z_B(s)$ in terms of $Z_l(s)$ are also derived.

2.2.1 Negative Incremental Impedance of Fluorescent Lamps

The small-signal impedance $Z_l(s)$ of fluorescent lamps in various carriers were measured and reported by several authors [7], [9], [10]. Results of measurement in the case of high frequency sinewave will be shown in Chapter 3. They all share a common shape

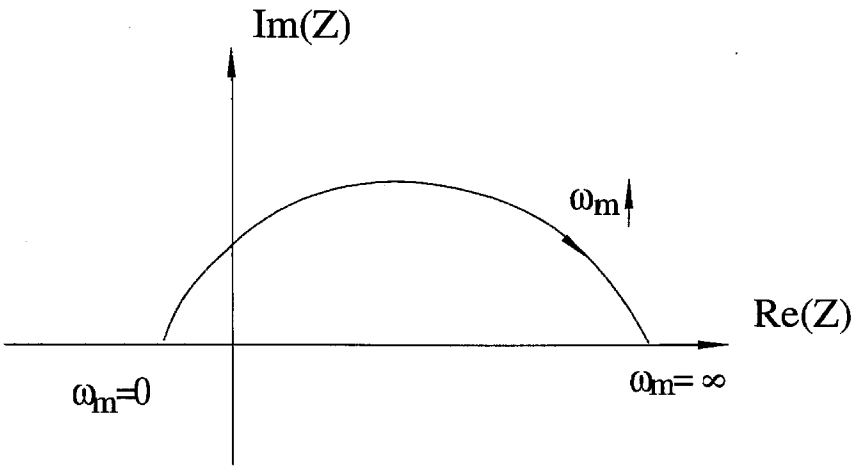

Figure 2.5: A typical plot of lamp incremental impedance $Z_l(s)$ in complex plane.

as shown in Figure 2.5 where the impedance $Z_l(s)$ is plotted in the complex plane as a function of modulation frequency $\omega_m = s/j$. When ω_m is close to zero, $Z_l(s)$ has a negative value with a phase of 180^o. As the modulation frequency ω_m increases, the magnitude of $Z_l(s)$ rises but its phase decreases. When the modulation frequency ω_m approaches the switching frequency ω_s, $Z_l(s)$ is close to a positive value.

From the previous plot in Figure 2.3, we can infer that incremental impedance $Z_l(s)$ must be negative when ω_m is zero since the slope of $A - B$ curve in i-v plane is negative. Since the trace is plotted by dimming the lamp manually, its slope can be considered as the dc value of the incremental impedance or $Z_l(s)|_{s=0}$. On the other hand, when the modulation frequency ω_m approaches the switching frequency ω_s, the small-signal impedance $Z_l(s)$ should be close to the positive slope of the straight line $A - O$. [9] illustrated how the phase of the small-signal perturbations changes when lamp is driven by dc power.

A *real rational function*, which is the ratio of two polynomials with real coefficients in the factored form as shown below, can be used to fit the measurement.

$$Z_l(s) = K\frac{\left(\frac{S}{Z_1}+1\right)\left(\frac{S}{Z_2}+1\right)...\left(\frac{S}{Z_n}+1\right)}{\left(\frac{S}{P_1}+1\right)\left(\frac{S}{P_2}+1\right)...\left(\frac{S}{P_n}+1\right)} \tag{2.8}$$

where K is a multiplication factor, Z_i, P_i, $i = 1...n$ are real zeros and poles, respectively. Certain properties of the above rational function can be derived from the special shape of lamp impedance. First the lamp impedance has definite values at both zero and high frequencies so that the numerator and denominator of the impedance function must have equal orders. In addition, since $Z_l(s)$ is negative when ω_m or s is zero, so $K < 0$. Finally $Z_l(s)$ is positive when $\omega_m = s/j$ approaches infinity, so the product of all Ps ands Zs are negative. Now assume $Z_l(s)$ does not have any RIIP poles (which makes sense since the lamp can be directly driven by a current source) and note the phase of $Z_l(s)$ monotonically decreases from 180^o to 0^o. It is thus concluded that **there is a right half plane zero in** $Z_l(s)$.

According to the linear circuit theory, an impedance with a RHP zero can not be driven directly by a voltage source since otherwise the transfer function of its current would contain a RHP pole. The above statement indicates if the lamp is directly connected to a voltage source, its current would not be stable. Certain measures need to be taken to stabilize the lamp current. For example, a ballast circuitry with an impedance of $Z_B(s)$ can be inserted between the lamp and a voltage source.

The RHP zero in $Z_l(s)$ uncovers the mystery of the lamp's negative incremental impedance in a rather straightforward way. It would be interesting to find any inherent connections between this simple model and physical principles in the gas discharge as described next.

2.2.2 Interpretation of RHP Zero from Modified Francis Equation

Francis [2] proposed a first order linear differential equation to describe the gas discharge behavior:

$$\frac{dy}{dt} = Aw - By \tag{2.9}$$

where y is lamp conductance, w is lamp power and A, B are positive constants. It states that the change of lamp conductance is proportional to its power and in reverse proportionality to its conductance. At steady-state, it becomes

$$AW = BY \quad or \quad V^2 = B/A \tag{2.10}$$

when $W = VI$ and $Y = I/V$ are substituted. If the lamp carrier is dc, then the steady-state solution is just its dc operating point. If the lamp carrier is a high frequency sinewave, then the steady-state operating point represents its rms values since switching period is much smaller than the ionization constant and conductance can be considered as constant.

From Eq. (2.9) the small-signal impedance $Z_l(s)$ can be derived. First y can be presented by:

$$y = \frac{i}{v}, \tag{2.11}$$

then i and v are decomposed into:

$$i = I + \hat{i}, \quad v = V + \hat{v}. \tag{2.12}$$

Substitute Eqs. (2.11), (2.12) and (2.10) into Eq. (2.9) and apply Laplace transform; $Z_l(s)$ can be obtained as (derivations are shown in Appendix A)

$$Z_l(s) = \frac{V}{I} \frac{s}{s + AV^2(A^2 - 1)}. \tag{2.13}$$

It does not show a RHP zero!

Reflect briefly on the fact that the RHP zero in $Z_l(s)$ is related to the negative incremental impedance or more specifically it relates to the negative slope of lamp's v-i curve $A - B$. But the steady-state solution in Eq. (2.10) says V is a constant or $Z_l(s)|_{s=0} = 0$, which means Francis equation does not predict a negative impedance. That is why $Z_l(s)$ derived does not have a RHP zero even though it satisfactorily explains the first order effect of the gas discharge behavior. In fact, this observation may also even explain why several modifications [8] [9] were made to the Francis equation for a better simulation in the time domain.

Thus a modified model which can better handle this issue is proposed as

$$\frac{dy}{dt} = \frac{Ai}{G(i)} - By \tag{2.14}$$

where $G(i)$ is a monotonically decreasing function of i. Its steady-state solution is

$$V = \frac{B}{A}G(I) \tag{2.15}$$

and it has a negative slope since $G'(I) < 0$. In [11] a lamp model is proposed and verified

$$V = \frac{V_{max}}{\sqrt{2}} - R_s I \tag{2.16}$$

which is a specific case of Eq. (2.14) when

$$G(i) = \frac{A}{B}\left(\frac{V_{max}}{\sqrt{2}} - R_s I\right). \tag{2.17}$$

The small-signal impedance derived from Eq. (2.14) is

$$Z_l(s) = \frac{V}{I}\frac{s + AVIG'(I)/G^2(I)}{s + VA/G(I)} \tag{2.18}$$

which indeed has an RHP zero $-AVIG'(I)/G^2(I)$.

In conclusion, the negative slope in the lamp's v-i plot and the modified Francis equation inherently generate a RHP zero in the small-signal impedance $Z_l(s)$. However, the above discussion only discovers the existence of an RHP zero in the lamp model. To accurately fit the measurement, zeros and poles have to be properly chosen in Eq. (2.8). Generally, the higher the order of the polynomials are, the better the rational function will fit the measurement.

2.2.3 Stability Analysis

Since $Z_l(s)$ has a RHP zero, it can not be directly connected to a voltage source $v_s(s)$. One way to stabilize its operation is to place a ballast network having an impedance of $Z_B(s)$ in series with it. The stability problem is considered as an example of the more general one-port circuit stability problem [12] as illustrated in Figure 2.6. There are three elements: voltage source $v_s(s)$, a ballast network with an impedance of $Z_B(s)$ and a lamp represented by its incremental impedance $Z_l(s)$. After $Z_l(s)$ is given, certain conditions have to be met by $Z_B(s)$ to ensure the stability of lamp current $i_l(s)$ as developed next.

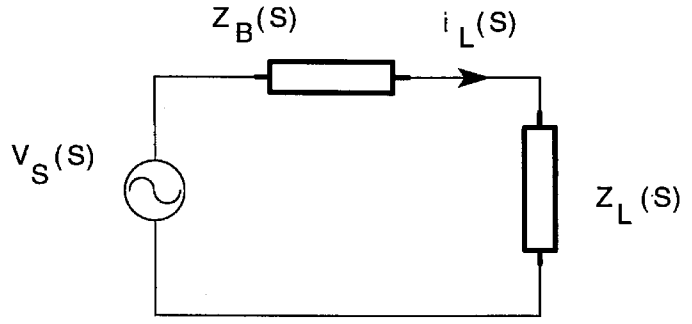

Figure 2.6: A block diagram of ballast/lamp system comprising a voltage source $v_s(s)$, an equivalent ballast impedance $Z_B(s)$ and a lamp model $Z_l(s)$.

Lamp current $i_l(s)$ can be expressed as

$$i_l(s) = \frac{v_s(s)}{Z_B(s)} \frac{1}{1 + Z_l(s)/Z_B(s)}. \tag{2.19}$$

The *necessary and sufficient condition* of its stability is $1 + Z_l(s)/Z_B(s)$ does not have any RHP zeroes, which means, from Nyquist criterion, **The Nyquist plot of $Z_l(s)/Z_B(s)$ does not encircle $(-1, 0)$ point.**

A stronger or a *sufficient condition* can be easily seen

$$\left| \frac{Z_l(s)}{Z_B(s)} \right| < 1. \tag{2.20}$$

Physically this criterion implies that a lamp wants to see a current source. In a special case of resistive ballast with dc carrier, the necessary and sufficient condition simply reduces to $R > |r|$, where $r \equiv Z_l(s)|_{s=0}$ as discussed in Figures 1.1 and 1.2.

Placing a circuit network $Z_B(s)$ between the voltage source $v_s(s)$ and a lamp $Z_l(s)$ is a simple way to set up a stable operating point. $Z_B(s)$ provides an impedance transformation, but at the same time this added network will incur certain power loss and reduce the system efficiency. For example, if a lamp is operated from a dc voltage source, then the resistor R which is to stabilize lamp current will significantly decrease the system efficiency. At high frequency sinewave operation, usually a resonant matching network

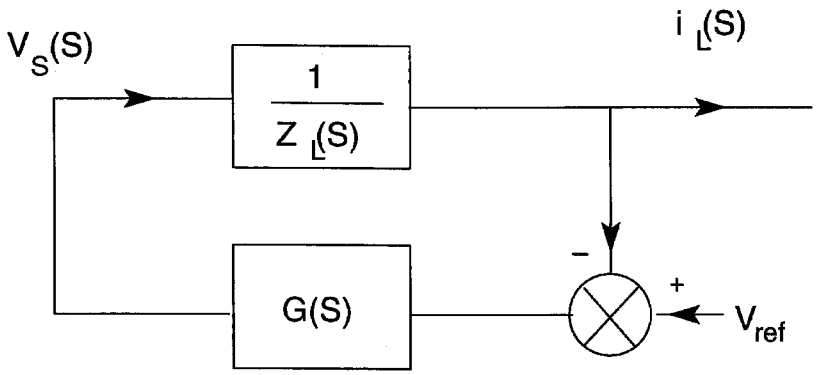

Figure 2.7: A block diagram of a close-loop ballast where lamp current $i_l(s)$ is sensed to control the input voltage $v_s(s)$.

(which has a output impedance $Z_B(s)$) at parallel resonance provides the impedance transformation required by the lamp. It inevitably causes certain conduction losses due to the excessive circulating current flowing through the parallel branch. This problem can be avoided by another approach as explained below.

Another way to stabilize the lamp current $i_l(s)$ is to operate the lamp in a close-loop manner as shown in Figure 2.7. Lamp current $i_l(s)$ is obtained from $v_s(s)/Z_l(s)$. $i_l(s)$ is sensed, amplified by the compensation network $G(s)$, then compared with the reference V_{ref}. The error signal then controls the magnitude of the voltage source $v_s(s)$ which is applied across the lamp to regulate its current $i_l(s)$.

According to the control theory, a system which is open-loop unstable or has an unstable plant (due to the RHP zero in $Z_l(s)$) can be always stabilized by closing the loop [13]. This can be shown by using the complete version of Nyquist criterion [14]. The system characteristic equation is:

$$1 + \frac{G(s)}{Z_l(s)}. \tag{2.21}$$

Since $Z_l(s)$ has a RHP zero, then $\frac{G(s)}{Z_l(s)}$ has a RHP pole, or system is open-loop unstable. Therefore *necessary and sufficient condition* for a stable close-loop system is **the Nyquist plot of $\frac{G(s)}{Z_l(s)}$ counterclockwise encircles $(-1, 0)$ once.**

Physically, the feedback loop converts the voltage source into a current source in order to build up a stable operating point. This impedance transformation is accomplished without adding any components in the power conversion circuit but at the price of increased complexity of the control circuitry. A ballast based on this concept is introduced in Chapter 3.

To make the above analysis complete, appropriate models which can effectively represent the circuit small-signal low-frequency behavior of various carriers are also needed so that the above classical linear circuit theory can be legitimately applied. If the carrier is dc then the circuit model is the original circuit itself. If the carrier is the squarewave as in the PWM switching converter, then state space averaging approach [15] would be a useful tool to derive the small-signal model which describes the low frequency behavior of the squarewave magnitude.

In the previous measurement [9] [10], the carriers are either dc or squarewave. In most high frequency applications, however, a lamp is connected to a resonant matching network. The carrier can be approximated as a high frequency sinewave. The models which describe the low frequency behavior of sinewave envelopes for resonant matching networks will be developed in Chapter 3.

2.3 Two Dual Cases of Negative Incremental Impedance in Power Electronics

The distinctive property of lamp incremental impedance has been revealed in the frequency domain. The general shape of its polar plot has a negative dc value and a decreasing phase as the modulation frequency ω_m increases which is accredited to the RHP zero as demonstrated. On the other hand, it would be interesting to find its dual case, an impedance that has a negative dc value but an increasing phase as ω_m goes up. Fortunately it does exist. It is the input impedance $Z_i(s)$ of a dc-to-dc switching regulator as presented in [16], which is shown in Figure 2.8.

Intuitively a switching regulator acts as a constant power source P at low frequency; its incremental input impedance is

$$R_i = \frac{dV_s}{dI_s} = \frac{d}{dI_s}\frac{P}{I_s} = -\frac{P}{{I_s}^2} = -\frac{V_s}{I_s} = -\frac{V}{M^2 I} = -\frac{R}{M^2} \tag{2.22}$$

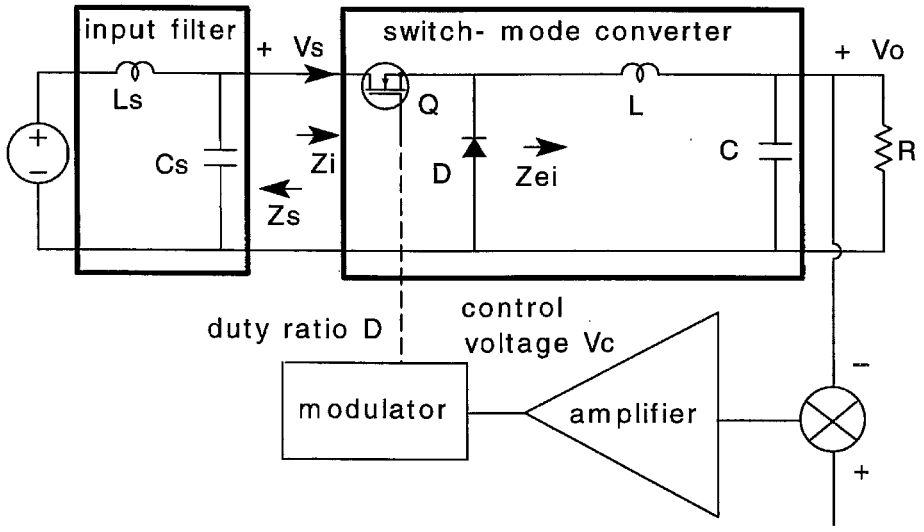

Figure 2.8: A block diagram of input filter and a switching dc-to-dc regulator.

where R is load resistance and M is the voltage conversion ratio V_o/V_s. At frequencies way above the crossover frequency, regulator can be considered in open-loop. The input impedance $Z_i(s)$ is just a transformed version of $Z_{ei}(s)$ which appears to be inductive. The small-signal input impedance $Z_i(s)$ of a dc-to-dc switching regulator is defined as dv_s/di_s.

The expressions for the input impedance is [16],

$$\frac{1}{Z_i(s)} = -\frac{T}{1+T}\frac{M^2}{Rf(s)} + \frac{1}{1+T}\frac{M^2}{Z_{ei}(s)}. \tag{2.23}$$

At low frequency, loop gain T satisfies $|T| >> 1$ so that the input impedance $Z_i(s)$ is dominated by the first term and is negative at dc. At high frequency, $|T| << 1$, $Z_i(s)$ is dominated by the second term and it becomes inductive since $Z_{ei}(s)$ is inductive at high frequency. It is difficult to justify the case of the phase change in general. But from the measurements in Figure 23 of [16] which is copied into Figure 2.9, the phase generally increases from -180^o to $+90^o$.

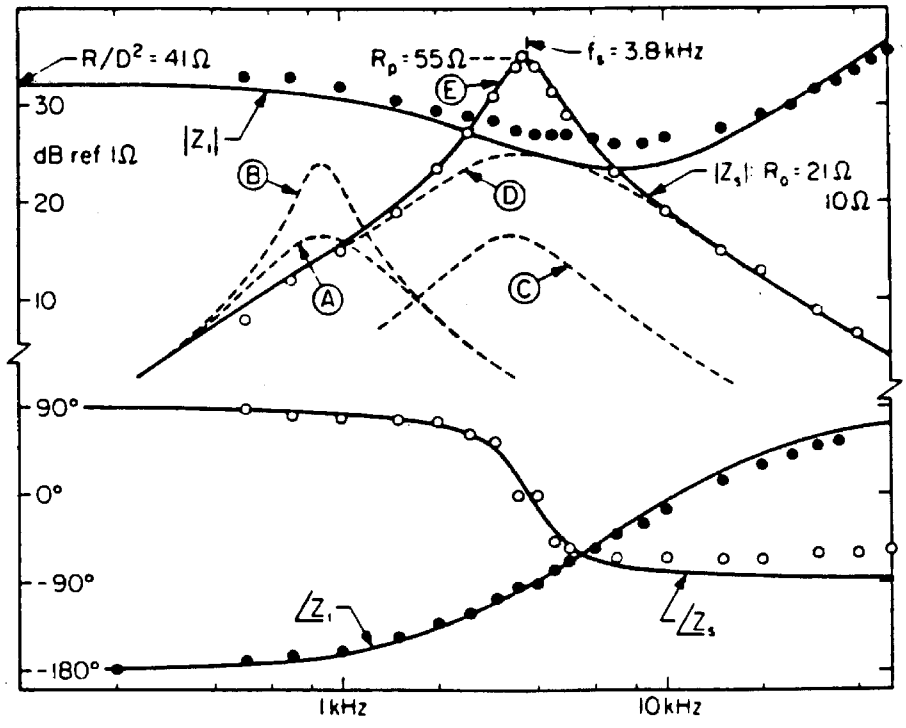

Figure 2.9: Measurement of input impedance $Z_i(s)$ of a switching regulator from [16].

There is one easily interpreted special case when the loop gain crossover frequency is very low, even below the corner frequency of the output filter. In this case, the loop gain T may be expressed as $T = \omega_c/s$ where ω_c is the loop-gain cross-over frequency and for frequency below the corner $1/RC$, Eq. (2.23) reduces to

$$\frac{1}{Z_i(s)} = \frac{M^2}{R}\frac{1-\frac{\omega_c}{s}}{1+\frac{\omega_c}{s}}. \tag{2.24}$$

Therefore, $Z_i(s)$ has a RHP pole–exactly the dual case of the lamp impedance $Z_l(s)$.

Without proof it is thus assumed that $Z_i(s)$ is negative at dc and has an increasing phase which can be simulated by the real rational function shown below:

$$Z_i(s) = K\frac{\left(\frac{s}{Z_1}+1\right)\left(\frac{s}{Z_2}+1\right)\ldots\left(\frac{s}{Z_n}+1\right)}{\left(\frac{s}{P_1}+1\right)\left(\frac{s}{P_2}+1\right)\ldots\left(\frac{s}{P_m}+1\right)} \tag{2.25}$$

where K is a multiplication factor, $Z_i, i = 1...n, P_i, i = 1...m$ are real zeros and poles, respectively. Certain properties of the above rational function can be derived from the

special shape of the $Z_i(s)$. First K is negative since

$$K = Z_i(s)|_{s=0} = -\frac{R}{M^2}. \tag{2.26}$$

Now assume $Z_i(s)$ does not have any RHP zeroes (which makes sense since system oscillation usually occurs in the presence of input filter) and note the phase of $Z_i(s)$ monotonically increases from -180^o to 90^o when its magnitude increases at the slope of $20dB/dec$. It is thus concluded that **there is a right half plane pole in** $Z_i(s)$. Usually the order of the numerator is that of the denominator plus 1. In the special case of Eq. (2.24), both numerator and denominator have the same order.

The stability analysis can be undertaken based on the same one-port circuit model as shown in Figure 2.10. It includes a voltage source $v_s(s)$, output impedance $Z_s(s)$ of the input filter and input impedance $Z_i(s)$ of a dc-to-dc switching regulator. By simple algebraic manipulations and the application of Nyquist criterion, conditions for the system stability when the input filter is added can be derived. The voltage across the input of the switching regulator $v_i(s)$ is expressed as

$$v_i(s) = \frac{v_s(s)}{1 + Z_s(s)/Z_i(s)}. \tag{2.27}$$

The *necessary and sufficient condition* for stability, from Nyquist criterion, is

$\frac{Z_s(s)}{Z_i(s)}$ **does not enclose** $(-1, 0)$ **point.**

A *sufficient condition* is

$$\left|\frac{Z_s(s)}{Z_i(s)}\right| \ll 1. \tag{2.28}$$

The sufficient condition is the same as shown in [16] where it was derived from the minor-loop gain $T_1 = Z_s(s)/Z_i(s)$, but the way it is derived here via the one-port circuit model is more direct.

Note in this case the carrier for input filter is dc so that the dynamic model is the filter itself while the input impedance $Z_i(s)$ of the dc-to-dc switching regulator is associated with squarewave carrier so that $Z_i(s)$ can be either derived by state space averaging approach or directly obtained from measurement.

Up to now it has been demonstrated that there are two entirely different negative incremental impedance problems in power electronics which can be treated in a unified

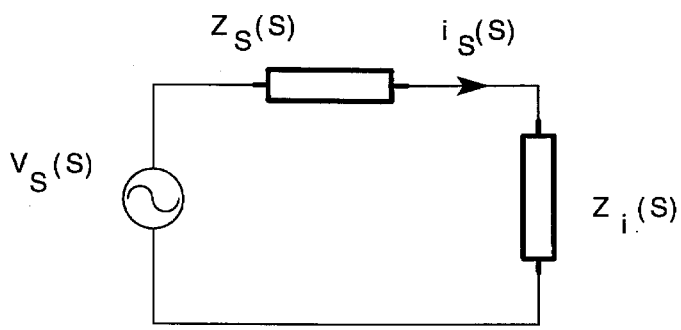

Figure 2.10: A block diagram illustrates analysis of oscillation problem of input filter of a dc-to-dc switching regulator based on one-port circuit model.

way as the dual cases of a more general stability problem of the one-port circuit in linear circuit theory. The stability criteria derived for the two cases are also dual. Physically speaking, a fluorescent lamp needs a current source to drive it while the input impedance of a switching dc-to-dc regulator wants to see a voltage source.

Chapter 3

Lamp Impedance and Stability in Half Bridge Resonant Circuits

In most high frequency applications, a fluorescent lamp is connected to a resonant matching network and is a load of a resonant inverter. The operating waveform is close to a sinewave. This is because resonant circuits are easy to implement and have low switching losses at high frequency operation. The sinusoidal carrier has a current crest factor of 1.4 and also lower radiated EMI since it has much less higher harmonics than squarewave. Therefore, it is of great importance to study lamp incremental impedance with high frequency sinusoidal carrier and consequently conduct the stability analysis of a lamp with various resonant matching networks. One of the most popular ballast topologies is halfbridge circuit which consists of a pair of current bi-directional switches and a resonant matching network loaded by a lamp.

Measurements and modeling of small-signal impedance of the fluorescent lamp are presented in the case of high frequency sinewave carrier. Major resonant matching networks at parallel resonance are modeled and analyzed for stability. A voltage source driven, close-loop ballast based on the LC series resonant network is proposed, built and verified.

3.1 Measurements and Modeling of Lamp Impedance

Now the fluorescent lamp is driven with a high frequency sinewave power. Its current i_l and voltage v_l are proportional due to its resistive impedance, which is expressed below:

$$v_l = vsin(\omega_s t), \quad i_l = isin(\omega_s t). \tag{3.1}$$

A small-signal perturbation of the amplitudes has to be introduced to measure lamp incremental impedance,

$$v_l = (V + \hat{v})sin(\omega_s t), \quad i_l = (I + \hat{i})sin(\omega_s t) \tag{3.2}$$

where

$$\hat{v} = |\hat{v}|sin(\omega_m t), \quad \hat{i} = |\hat{i}|sin(\omega_m t - \phi_m) \tag{3.3}$$

and

$$\begin{aligned} \frac{|\hat{v}|}{V} &\ll 1, \\ \frac{|\hat{i}|}{I} &\ll 1. \end{aligned} \tag{3.4}$$

Then the measured incremental impedance is

$$Z_l(j\omega_m) = \frac{|\hat{v}|}{|\hat{i}|}\angle\phi_m. \tag{3.5}$$

Suitable instrumentation for measurement is shown in Figure 3.1. Lamp is driven by a halfbridge circuit through a resonant matching network. Two switches in the halfbridge configuration turn ON and OFF alternately and generate a sequence of squarewave voltage, which is filtered by the resonant matching network. Only the fundamental component at switching frequency is applied to the lamp. The magnitude of the sinusoidal component v_s is a function of the switching duty ratio:

$$v_s = \frac{2V_{dc}}{\pi}sin(\pi d). \tag{3.6}$$

A perturbation signal at the frequency ω_m is injected at the PWM controller of the switch to produce an amplitude-modulated sinusoidal voltage v_l in the form of Eq. (3.2) across the lamp.

Lamp voltage v_l is rectified and picked up at the channel A of a network analyzer. Lamp current i_l is sensed and rectified through a current transformer and is then measured at the channel B. The display of the network analyzer is user-defined as A/B. The narrowband filters inside the analyzer extract the components at ω_m. Comparison of the magnitude and phase of the ω_m signal of the channel A and channel B waveforms yields

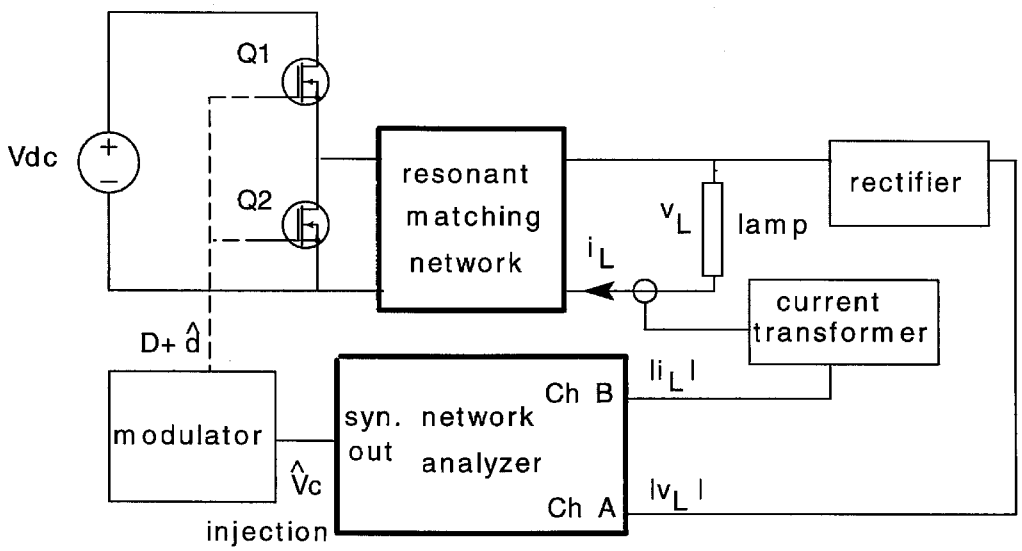

Figure 3.1: Experimental set-up for the measurement of lamp incremental impedance $Z_l(s)$ with high frequency sinusoidal carrier.

the frequency response at ω_m. The synthesizer is stepped through all desired values of the modulation frequency ω_m to obtain a lamp impedance curve.

The results of the measurement are shown in Figure 3.2. The magnitude starts flat, then rises like a single zero and then becomes flat again. The phase begins with 180^o when ω_m is low and then monotonically drops to 0^o when ω_m approaches ω_s, which very well corresponds to the general shape described in Chapter 2.

Measurements can be fit to arbitrary accuracy by the rational function in Eq. (2.9). As a matter of fact, it turns out that a first order bi-linear function which is shown below suffices to fit most measurements satisfactorily.

$$Z_l(s) = K\frac{\frac{s}{Z_1}+1}{\frac{s}{P_1}+1}. \tag{3.7}$$

Several examples of measurements and fits are shown in Figure 3.3. Except for the deviations near half the switching frequency $\omega_s/2$ the rational function shown above

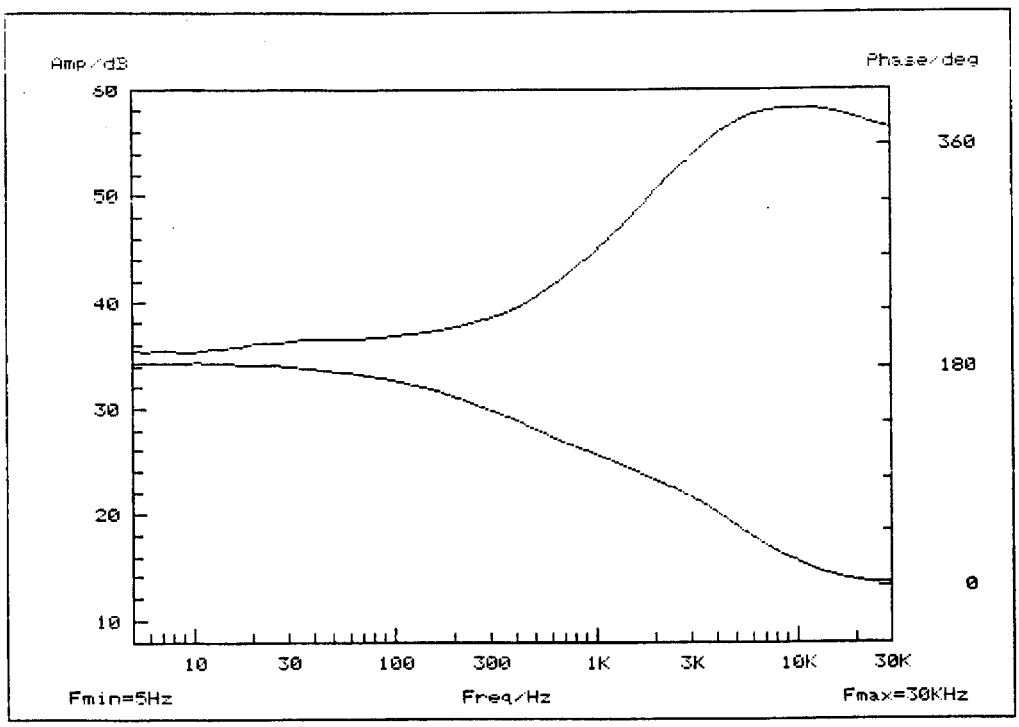

Figure 3.2: Measured lamp impedance $Z_l(s)$ shown in the Bode plot under the following conditions: Sylvania Octron lamp (F017), carrier frequency: 100kHz, rms lamp current: 0.2A

represents the measurement quite well.

Equivalent circuit can be also derived from the fit function of Eq. (3.7) as shown in Figure 3.4. A negative resistor R_1 gives the negative resistance at dc as long as $|R_2| > |R_1|$. Resistor R_2 shows the positive resistance at high frequencies. An inductor L is necessary to introduce both a RHP zero and a LHP pole.

3.2 Modeling of Resonant Matching Networks

The object of the modeling is to derive a linear equivalent circuit so that small-signal, low frequency variation on the *magnitude* of sinusoidal carrier or the low frequency

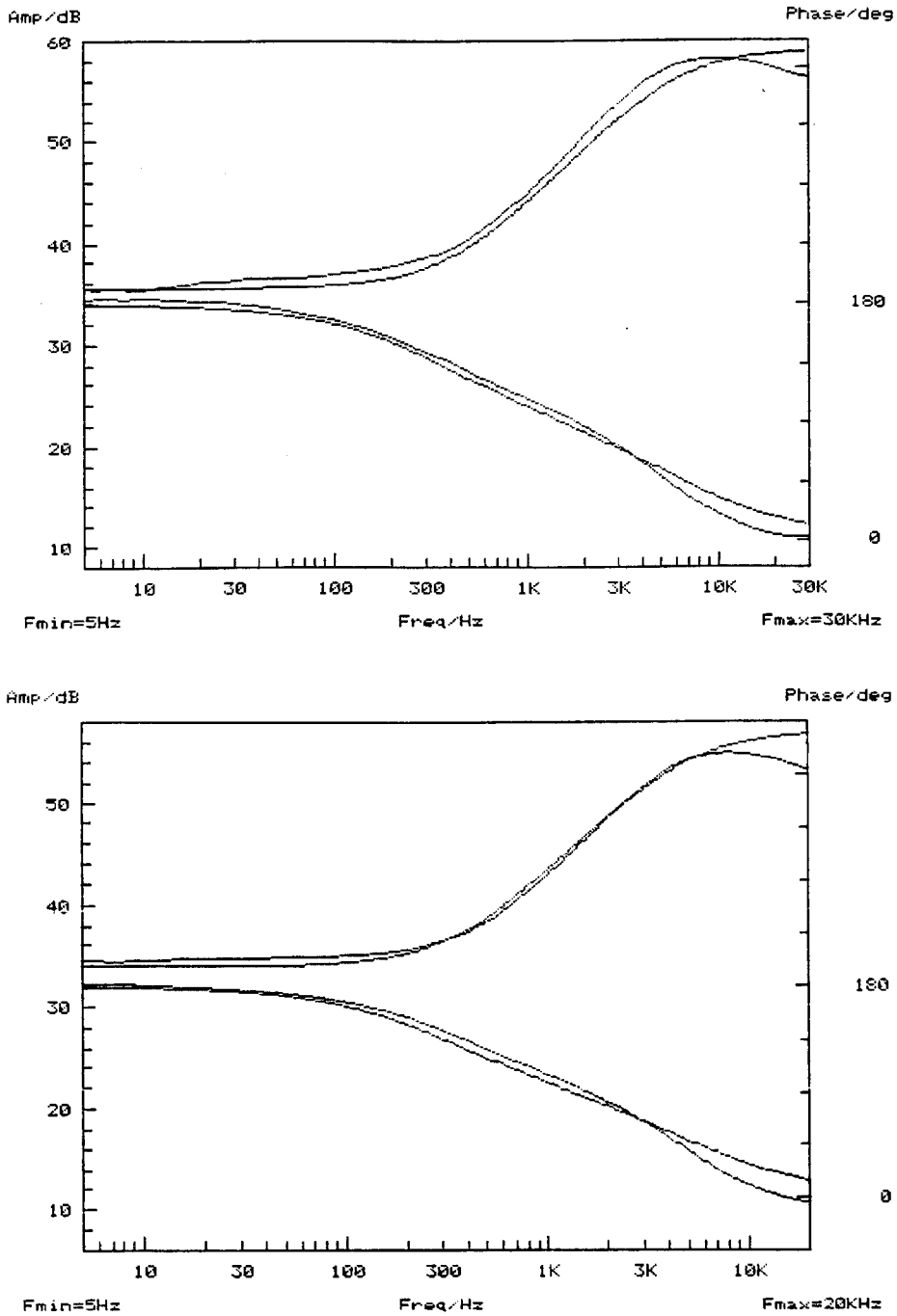

Figure 3.3: Fits of measured and predicted lamp impedance. (a) lamp carrier frequency: 100kHz, fit parameters: K=-60, Z_1=-400Hz, P_1= 4kHz. (b) lamp carrier frequency: 90kHz, fit parameters: K=-50, Z_1=-350Hz, P_1=5kHz. Both currents are 0.2A rms.

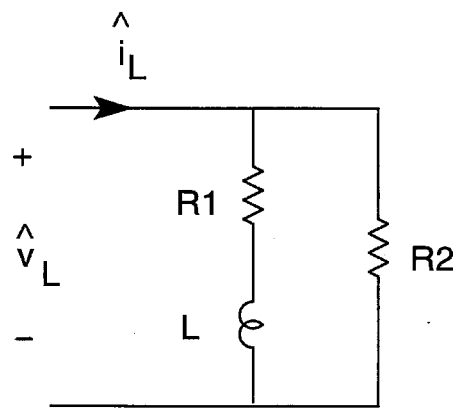

Figure 3.4: Equivalent circuit model of lamp dynamic impedance $Z_l(s)$.

variation of the envelope of the high frequency sinewave is effectively modeled. The model has to be continuous and linear so that the conventional linear circuit theory can be legitimately applied for stability analysis.

The modeling approach will be introduced first. Three resonant matching networks, i.e., LC series resonant network at series resonance, LC parallel resonant network and LCC series and parallel resonant networks at parallel resonance are modeled and verified.

3.2.1 Modeling Approach

The classical state space averaging approach [15] is only suitable for the modeling of PWM converters where the switching ripple is small compared to its dc component. The resonant matching networks to be studied, however, operate in a resonant fashion where dominant component is sinewave so that the state space averaging method is no longer applicable.

More general averaging methods have been proposed by several authors [17], [18], [19] to simplify the analysis of resonant dc-to-dc converters. The averaging approach [17] is based on the fact that any repetitive waveforms can be approximated to arbitrary accuracy with a Fourier series representation which coefficients are slow-varying variables. The Fourier representation can be substituted into the original differential equations

of the switching network. To make a simplified model, only relatively large Fourier coefficients which capture the interesting behavior of the system are retained. Thus a new set of equations describing the amplitudes of the major harmonics in the studied systems are generated. In this way transient response of the resonant converter is easily simulated. As a special case, only dc component is retained in PWM dc-to-dc converter to study the converter behavior, and the general average approach reduces to the state space averaging approach. In the case of resonant converter, where the fundamental component is dominant, only the fundamental harmonic will be retained and the waveforms appear to be amplitude modulated sinusoids.

Similar idea was also proposed in terms of variable phasor transformation [18] where the sinusoidal signal is represented by a variable phasor. First each circuit component is modeled in the "phasor" domain, then the phasor model for the entire resonant circuit is built and analyzed. The approach has the merit of easy establishment of phasor model. Based on the describing function concept, another method was proposed [19]. Following the procedures of decomposing the resonant waveform into sine, cosine and their high harmonics, performing harmonic approximation and harmonic balance, small-signal equivalent circuit and the various transfer functions are obtained. The above general averaging approaches are equivalent to each other. By approximating the switching waveform with its major harmonics, good trade-off between accuracy and complexity in the modeling of resonant converter is achieved.

In the case of resonant matching network, the small-signal low frequency variations of the magnitude of sinusoidal carrier are our major concern. Usually, the fundamental component contains both sine and cosine components. The magnitude square of the fundamental component is the sum of magnitude squares of sine and cosine components, respectively. This operation will in general introduce non-linearity in the small-signal transfer function. To avoid this, the switching frequency ω_s has to be set equal either to the series resonant frequency ω_{ser} or to the parallel frequency ω_{par} so that the output of a resonant matching network has sine or cosine component only. Fortunately, most resonant matching networks are operated close to their resonance. The result of our analysis is still effective in most applications despite this analytical limitation.

The variable phasor approach in [18] will be adopted in our analysis because of its simplicity. The conventional phasor in circuit analysis represents the magnitude and phase of a sinusoidal signal in steady-state. The modified phasor $\mathbf{x(t)}$, which represents a transient sinusoidal signal, is defined below:

$$x(t) \equiv Re\left[\sqrt{2}\mathbf{x(t)}e^{j\omega_s t}\right]. \tag{3.8}$$

Thus a complex phasor $\mathbf{x(t)}$ is associated with the sinusoidal signal $x(t)$. Distinct from the conventional phasor, both $\mathbf{x(t)}$ and ω_s could be time-varying. In our case, only $\mathbf{x(t)}$ is a variable since only PWM modulation is used.

To build an equivalent phasor model from a given circuit, the phasor model for each basic component is derived first. Following example shows how the inductor phasor transformation is derived.

The differential equation for the inductor L is

$$L\frac{di_L}{dt} = v_L. \tag{3.9}$$

The phasor transformation of i_L and v_L are

$$i_L \equiv Re\left[\sqrt{2}\mathbf{i_L}e^{j\omega_s t}\right] \tag{3.10}$$

and

$$v_L \equiv Re\left[\sqrt{2}\mathbf{v_L}e^{\omega_s t}\right]. \tag{3.11}$$

Applying Eqs (3.10) and (3.11) to Eq. (3.9) results in

$$L\frac{d}{dt}\left(Re\left[\sqrt{2}\mathbf{i_L}e^{j\omega_s t}\right]\right) = Re\left[\sqrt{2}\mathbf{v_L}e^{j\omega_s t}\right] \tag{3.12}$$

or

$$LRe\left[\frac{d\mathbf{i_L}}{dt}e^{j\omega_s t} + j\omega_s\mathbf{i_L}e^{j\omega_s t}\right] = Re\left[\left(L\frac{d\mathbf{i_L}}{dt} + j\omega_s L\mathbf{i_L}\right)e^{j\omega_s t}\right] = Re\left[\mathbf{v_L}e^{j\omega_s t}\right]. \tag{3.13}$$

So the phasor model for the inductor L is

$$L\frac{d\mathbf{i_L}}{dt} + j\omega_s L\mathbf{i_L} = \mathbf{v_L}. \tag{3.14}$$

Eq. (3.14) is obtained from the following theorem.

Theorem:

For any $\mathbf{x}$, $\mathbf{y}$ and $\omega_s \neq 0$, then $Re\left[\mathbf{x}e^{j\omega_s t}\right] = Re\left[\mathbf{y}e^{j\omega_s t}\right]$ if and only if $\mathbf{x} = \mathbf{y}$

Proof:

$$\begin{aligned} Re\left[\mathbf{x}e^{j\omega_s t}\right] &= Re\left[|\mathbf{x}|e^{j\angle\mathbf{x}}e^{j\omega_s t}\right] \\ &= |\mathbf{x}|Re\left[e^{j\angle\mathbf{x}+j\omega_s t}\right] \\ &= |\mathbf{y}|Re\left[e^{j\angle\mathbf{y}+j\omega_s t}\right] \end{aligned}$$

which is equivalent to

$$|\mathbf{x}| = |\mathbf{y}| \quad and \quad \angle\mathbf{x} = \angle\mathbf{y} + 2n\pi,$$

where $n = integer$. This is equivalent to

$$\mathbf{x} = \mathbf{y}.$$

The phasor model can be expressed by an equivalent circuit as shown in Figure 3.5(a). Similarly, the phasor model for the capacitor and resistor are

$$C\frac{d\mathbf{v_C}}{dt} + j\omega_s C\mathbf{v_C} = \mathbf{i_C} \tag{3.15}$$

and

$$\mathbf{v_R} = R\mathbf{i_R}. \tag{3.16}$$

Their equivalent circuit models are shown in Figures 3.5(b) and (c).

From Eqs (3.14), (3.15) and (3.16), the relationships for steady-state phasor $\mathbf{X}$ and small-signal variation $\hat{\mathbf{x}}$ are also derived and are listed as follows.

Steady-state phasor relations for L, C and R, respectively:

$$j\omega_s L\mathbf{I}_L = \mathbf{V_L} \tag{3.17}$$

$$j\omega_s C\mathbf{V_C} = \mathbf{I_C} \tag{3.18}$$

$$\mathbf{V_R} = R\mathbf{I_R}. \tag{3.19}$$

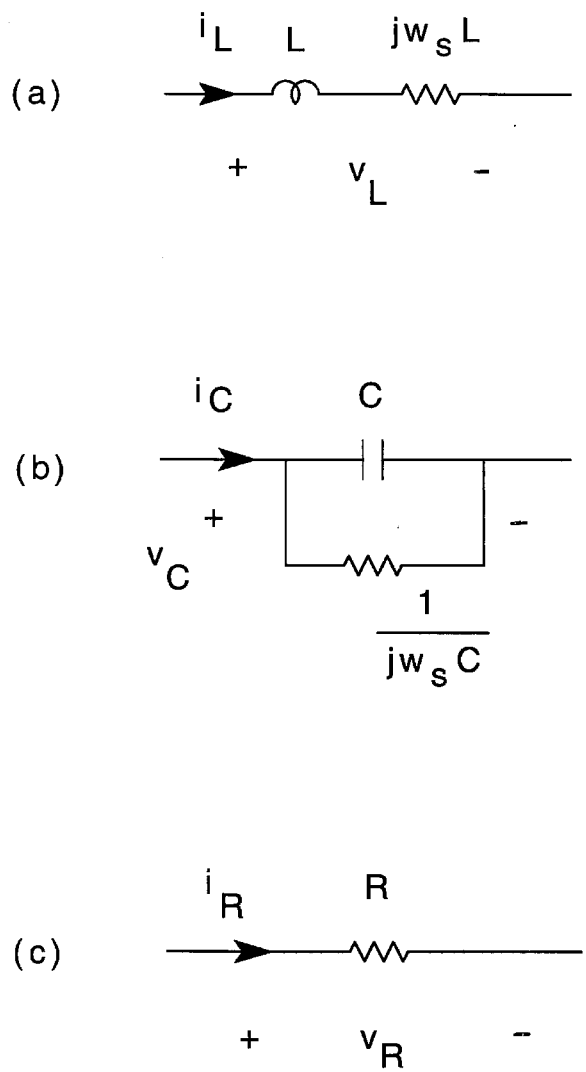

Figure 3.5: Equivalent phasor circuit models of inductor L, capacitor C and resistor R.

Small-signal phasor relation for L, C and R:

$$L\frac{d\hat{\mathbf{i}}_\mathbf{L}}{dt} + j\omega_s L\hat{\mathbf{i}}_\mathbf{L} = \hat{\mathbf{v}}_\mathbf{L} \tag{3.20}$$

$$C\frac{d\hat{\mathbf{v}}_\mathbf{C}}{dt} + j\omega_s C\hat{\mathbf{v}}_\mathbf{C} = \hat{\mathbf{i}}_\mathbf{C} \tag{3.21}$$

$$\hat{\mathbf{v}}_\mathbf{R} = R\hat{\mathbf{i}}_\mathbf{R}. \tag{3.22}$$

Using phasor transformations in Figure 3.5, one can easily draw a phasor circuit from a resonant matching network. Then the phasor transfer function can be directly obtained from the phasor circuit.

3.2.2 Modeling of Resonant Matching Networks

Small-signal models which describe low frequency variations of magnitude of sinusoidal carrier are derived for the three major resonant matching networks, i.e., LC series resonant network at series resonance, LC parallel resonant network and LCC series-parallel resonant networks at parallel resonance.

An LC series resonant circuit and its phasor equivalent circuit are shown in Figure 3.6(a)(b), respectively. The steady-state phasor response can be calculated from the circuit of Figure 3.6(b) by removing the inductors and capacitors. The dc phasor transconductance is

$$\frac{\mathbf{I_R}}{\mathbf{V_S}} = \frac{1}{j\omega_s L + \frac{1}{j\omega_s C} + R} \tag{3.23}$$

when switching frequency ω_s is equal to the series resonant frequency ω_{ser}, i.e.,

$$\omega_s = \omega_{ser} = \frac{1}{\sqrt{LC}}. \tag{3.24}$$

The transfer function is R, which means two phasors are in phase. The small-signal amplitude transfer function is the same as the phasor transfer function.

$$\frac{\hat{i}}{\hat{v}} = \frac{\hat{\mathbf{i}}}{\hat{\mathbf{v}}} = \frac{(s + j\omega_s)C}{(s + j\omega_s)^2 LC + (s + j\omega_s)RC + 1} \tag{3.25}$$

or

$$\frac{\hat{i}}{\hat{v}} = \frac{(s + j\omega_s)C}{sLC(s + 2j\omega_s) + RC(s + j\omega_s)}. \tag{3.26}$$

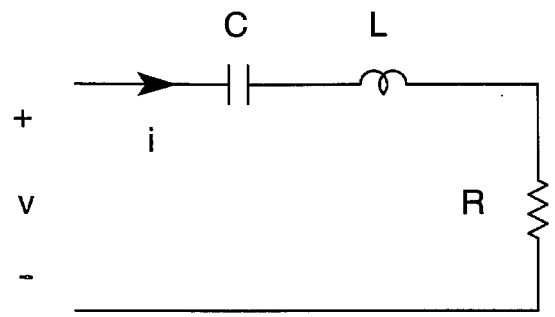

LC series resonant ciruit

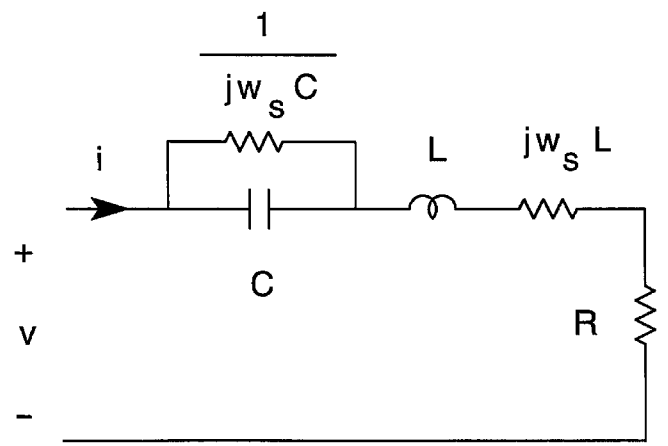

its phasor model

Figure 3.6: LC series resonant circuit and its phasor equivalent circuit at series resonance.

When the modulation frequency $\omega_m = s/j$ is much smaller than the carrier frequency ω_s, we can get

$$2(s + j\omega_s) \simeq s + 2j\omega_s. \tag{3.27}$$

Therefore,

$$\frac{\hat{i}}{\hat{v}} = \frac{1}{2sL + R}. \tag{3.28}$$

From Eq. (3.28) an equivalent circuit model is drawn and shown in Figure 3.7(a).

Quite similarly, the magnitude transfer function can also be derived for LC parallel circuit except for one difference. The dc phasor transconductance for LC parallel circuit is

$$\frac{\mathbf{I}}{\mathbf{V}} = \frac{1}{s^2LCR + sL + R} \tag{3.29}$$

when switching frequency ω_s is equal to the parallel resonant frequency ω_{par}

$$\omega_s = \omega_{par} = \frac{1}{\sqrt{LC}}. \tag{3.30}$$

The transfer function is $1/j\omega_{par}L$ which means two phasors have 90^o phase shift. But model is still linear because if input is an amplitude-modulated sinewave, then output is a pure amplitude-modulated cosine or vice versa.

Equivalent circuits obtained for LC parallel circuit and LCC series and parallel circuit at parallel resonance are listed in Figures 3.7(b)(c).

3.2.3 Experimental Verifications

The above models are experimentally verified to show their validities. The experimental set-up is shown in Figure 3.8.

Two switches are configured in a halfbridge fashion to generate a squarewave voltage source with a magnitude V_{dc}. The fundamental component v_s is determined by the duty ratio d as

$$v_s = \frac{2V_{dc}}{\pi} sin(\pi d). \tag{3.31}$$

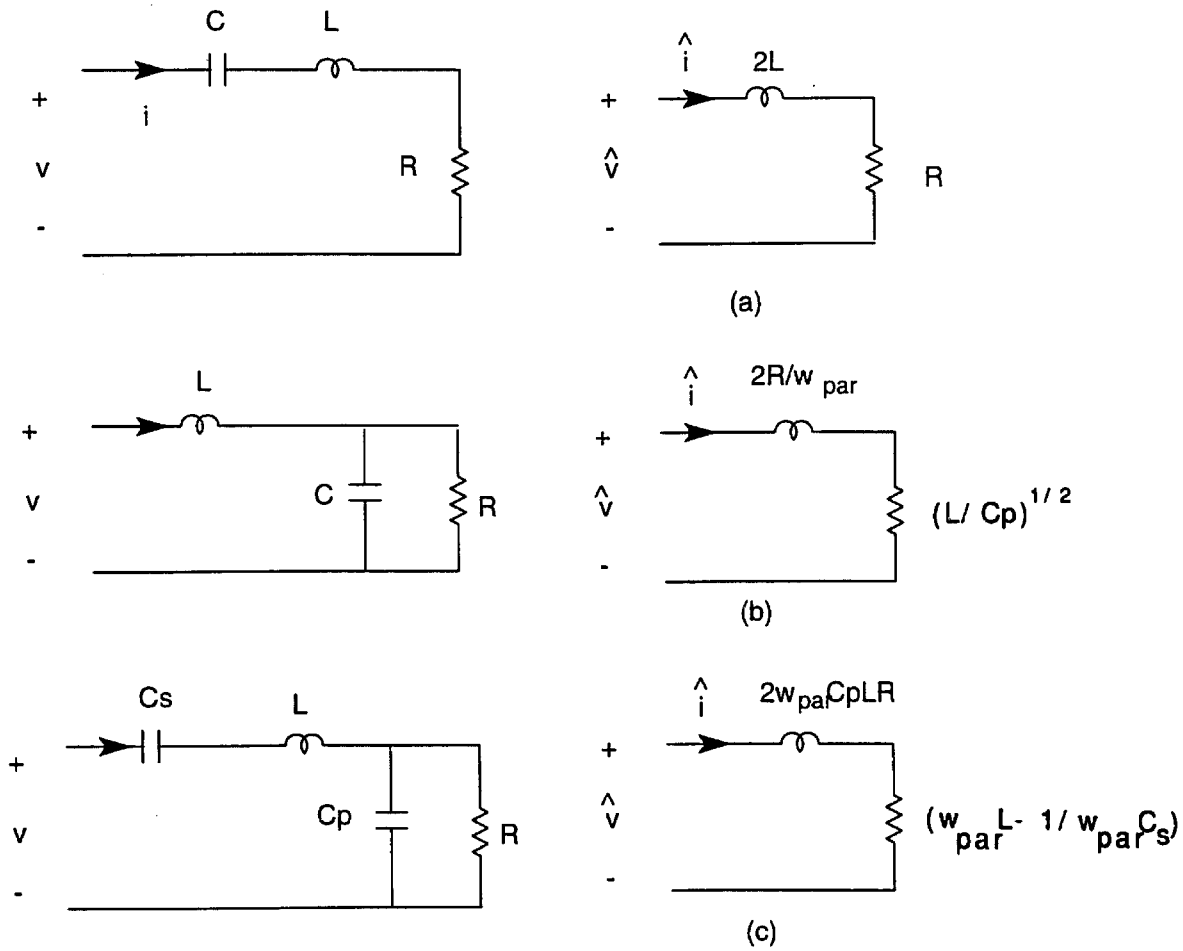

Figure 3.7: Equivalent circuit models describing the small-signal variations of the magnitude of sinusoidal carrier for LC series resonant circuit at series resonance, LC parallel resonant circuit and LCC series and parallel resonance at their parallel resonance.

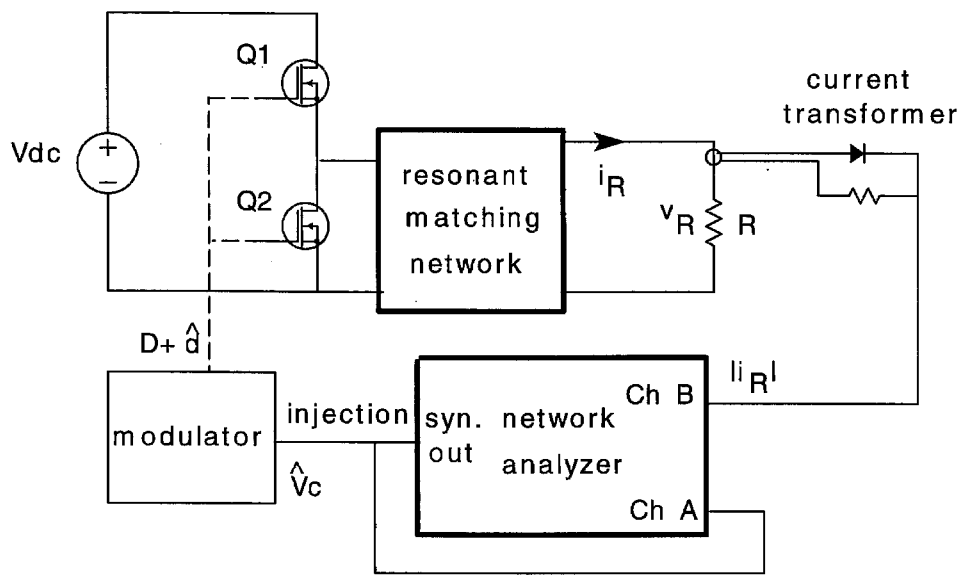

Figure 3.8: Experimental set-up for verifying the small-signal low frequency models of the resonant matching networks.

The perturbation signal is injected at the PWM controller to cause a small-signal variations on duty ratio, i.e.,

$$d = D + \hat{d} \tag{3.32}$$

which in turn causes a small-signal perturbation on the magnitude of sinusoidal voltage at the input of the resonant matching network

$$\hat{v}_s = 2V_{dc}cos(\pi d)\hat{d}. \tag{3.33}$$

Consequently, an amplitude-modulated sinusoidal current i_R is observed at the resistor R which is sensed and rectified by a current transformer. A network analyzer is used to measure the transfer function. Channel A is to measure the controlling input voltage variation $\hat{v}_c$, and channel B is to measure the output current variation $\hat{i}_R$. The injected signal $\hat{v}_c$ is generated by the synthesizer inside the analyzer which sweeps all the desired

value of modulation frequency ω_m. Each input of the analyzer has a narrow-band tracking filter, which is used in amplitude measurement to extract the signal at ω_m. Comparison of the magnitude and phase of the ω_m signal of the channel A and channel B yields the frequency response $\hat{i}_R/\hat{v}_c$.

Figure 3.9 shows the measurements and predictions of several resonant matching networks analyzed above. The componets used are: (a) LC series resonant: $L = 0.18mH$, $C = 8nF$, $R = 50\Omega$, $f_s = 133kHz$, (b) LC parallel resonant: $L = 52\mu H$, $C_p = 51nF$, $R = 100\Omega$, $f_s = 95kHz$, (C) LCC circuit: $L = 52\mu H$, $C_s = C_p = 51nF$, $R = 50\Omega$, $f_s = 138kHz$.

3.3 Stability Analysis

The models to describe the low frequency behavior of the sinewave magnitude for the resonant matching networks are derived and experimentally verified. It is also shown that the lamp can be modeled by a rational function in the frequency domain. Replacing the load resistor R with the lamp model $Z_l(s)$, stability analysis for the halfbridge ballast can be performed using the theory developed in Chapter 2. The results of the analysis are also experimentally verified.

3.3.1 Stability Analysis of Parallel Resonant Ballasts

One of the most popular resonant matching networks is LCC circuit. Its Norton equivalent circuit is shown in Figure 3.10. At the parallel resonance determined by

$$\omega_{par} = \frac{1}{\sqrt{LC_e}} \tag{3.34}$$

where

$$C_e = \frac{C_s C_p}{C_s + C_p}$$

we can see the output impedance $Z_o(S)$ goes to infinitively large. So LCC circuit is a "current source" at its parallel resonance which is able to establish a stable operating point. The above statement only explains the dc case of the small-signal analysis. Complete analysis is given as next based on the modeling tools we have developed.

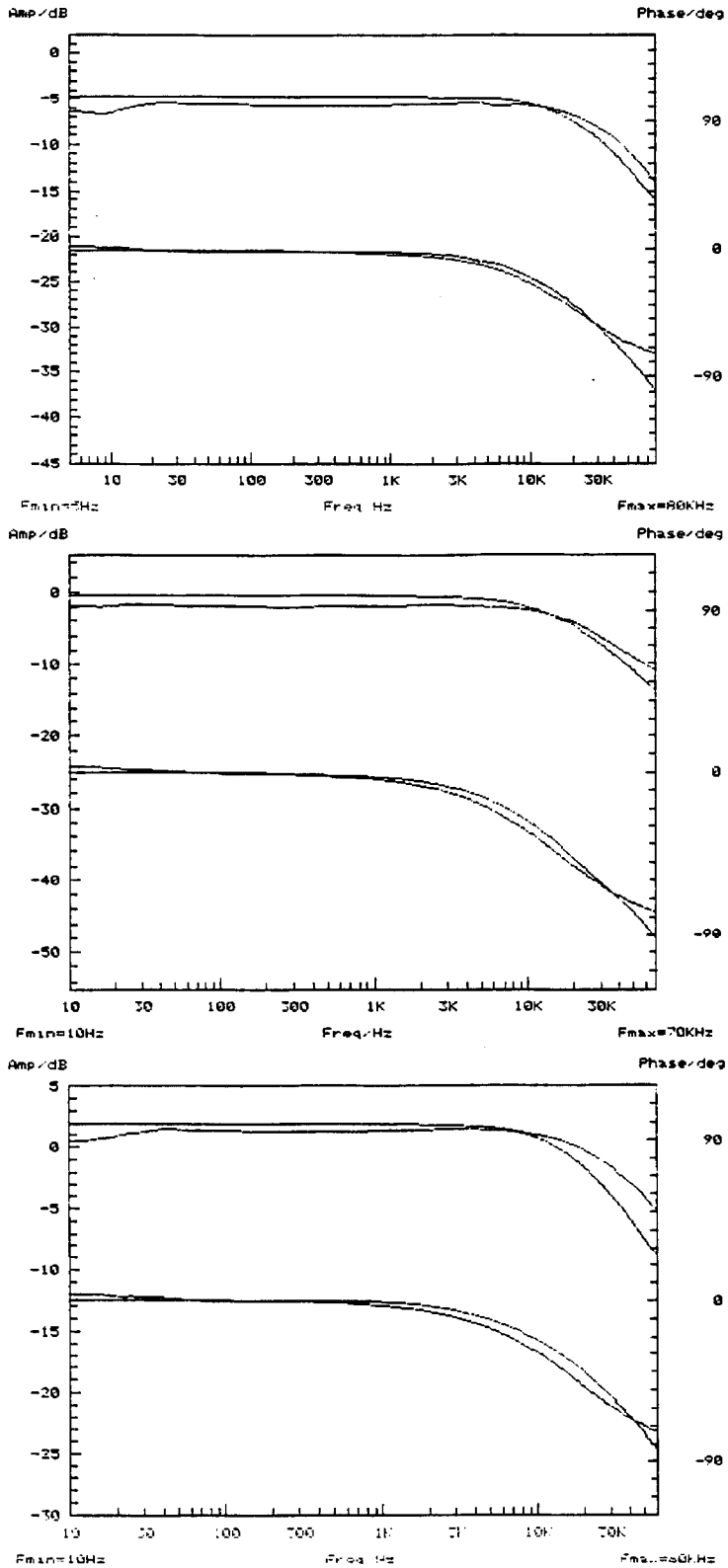

Figure 3.9: Measurements and predictions of transconductance $\hat{i}_R/\hat{v}_c$ of the equivalent circuit models for LC series (a), LC parallel (b), and LCC (c) resonant matching networks.

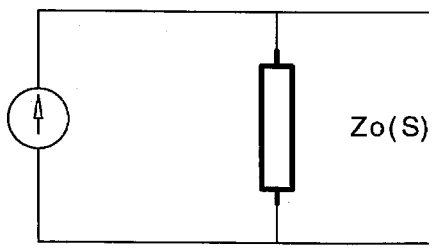

$Zo(S) = (1/jw_S Cs + jw_S L)//(1/jw_S Cp)$

Figure 3.10: Norton equivalent circuit of LCC network.

The transconductance function for the LCC circuit at the parallel resonant frequency ω_{par} is

$$\frac{\hat{i}_R}{\hat{v}_c} = K\frac{1}{(\frac{s}{\omega_c})+1} \tag{3.35}$$

where

$$K = \frac{V_{dc}}{V_M}\cos(\pi d)\frac{2}{\pi}\sqrt{\frac{(C_s+C_p)C_p}{LC_s}}$$

where V_M is PWM modulator ramp height and

$$\omega_c = \frac{C_s}{2RC_p(C_s+C_p)}.$$

When it is used as a ballast, R is replaced with the lamp impedance $Z_l(s)$:

$$Z_l(s) = K_l\frac{s/Z+1}{s/P+1}. \tag{3.36}$$

In the case of $C_s = C_p$, the transconductance function then is

$$\frac{\hat{i}_l}{\hat{v}_c} = K\frac{1}{K_1\frac{s(s/Z+1)}{s/P+1}+1} \tag{3.37}$$

where

$$K_1 = 4C_sK_l.$$

Its characteristic equation is

$$\left(\frac{K_1}{Z}\right)s^2 + s\left(K_1 + \frac{1}{P}\right) + 1. \tag{3.38}$$

Routh's array [14] is applied to find if Eq. (3.38) has any RHP zeroes.

$\frac{K_1}{Z}$	1
$K_1 + \frac{1}{P}$	
1	

Since $K_1 < 0$, $Z < 0$, $P > 0$, so $K_1/Z > 0$. If $(K_1 + \frac{1}{P}) > 0$, then there would be no change of sign in the first column of the Routh's array. That is, there is no RHP zeros in characteristic equation and system is stable. If $(K_1 + \frac{1}{P}) < 0$, however, then system would have two RHP zeroes and is not stable.

Fortunately in most cases, the order of magnitude of negative resistance K_l is small so that $(K_1 + \frac{1}{P}) > 0$. Therefore, LCC circuit does set up a stable operating point even in an open-loop manner.

The transfer function $\hat{v_c}/\hat{i_l}$ is predicted and measured. Both results are displayed in Bode plot in Figure 3.11.

From the Nyquist plot, it can be seen that it is not always true that the Nyquist plot does not enclose origin. From the above analysis it can be seen that even at parallel resonance a parallel resonant network merely offers a "current source" at dc. When the lamp is strongly unstablizable or $|K_l|$ is very large, the Nyquist plot will enclose the origin and the lamp is still not stable. In that case a lamp current feedback loop has to be closed to maintain a stable operating point.

Similar stability analysis for LC parallel resonant network can be conducted. Both the prediction and measurement of the transconductance function are shown in Figure 3.12 to demonstrate the system stability.

3.3.2 Stability Analysis of a Series Resonant Ballast

It seems there is no way to drive a lamp using an LC series circuit especially at series resonance in an open-loop fashion because LC series resonant network at its series resonance only provides a voltage source. The following analysis confirms this speculation.

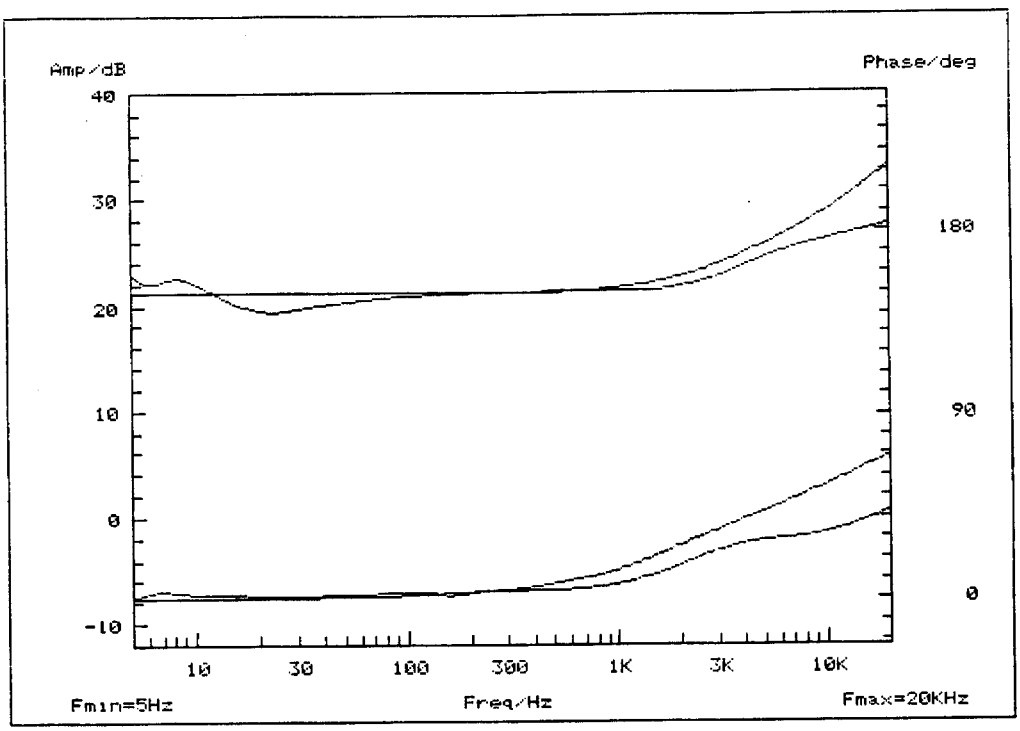

Figure 3.11: Prediction and measurement of transconductance of LCC parallel resonant ballast show the stability of the operation. Conditions: Sylvania Octron lamp (F017), $L = 0.54mH$, $C_p = C_s = 10nF$, $f_s = 97kHz$, lamp current: 0.2A rms.

When the lamp model $Z_l(s)$

$$Z_l(s) = K_l \frac{\frac{s}{Z} + 1}{\frac{s}{P} + 1} \tag{3.39}$$

is plugged into the equivalent circuit model of Figure 3.7(a), its transfer function is

$$\frac{\hat{i_l}}{\hat{v_c}} = \frac{K_1}{K_l} \frac{\left(\frac{s}{P} + 1\right)}{\frac{2L}{PK_l}s^2 + \left(\frac{2L}{K_l} + \frac{1}{Z}\right)s + 1} \tag{3.40}$$

where

$$K_1 = \frac{V_{dc}}{V_M} cos(\pi D) \frac{2}{\pi}$$

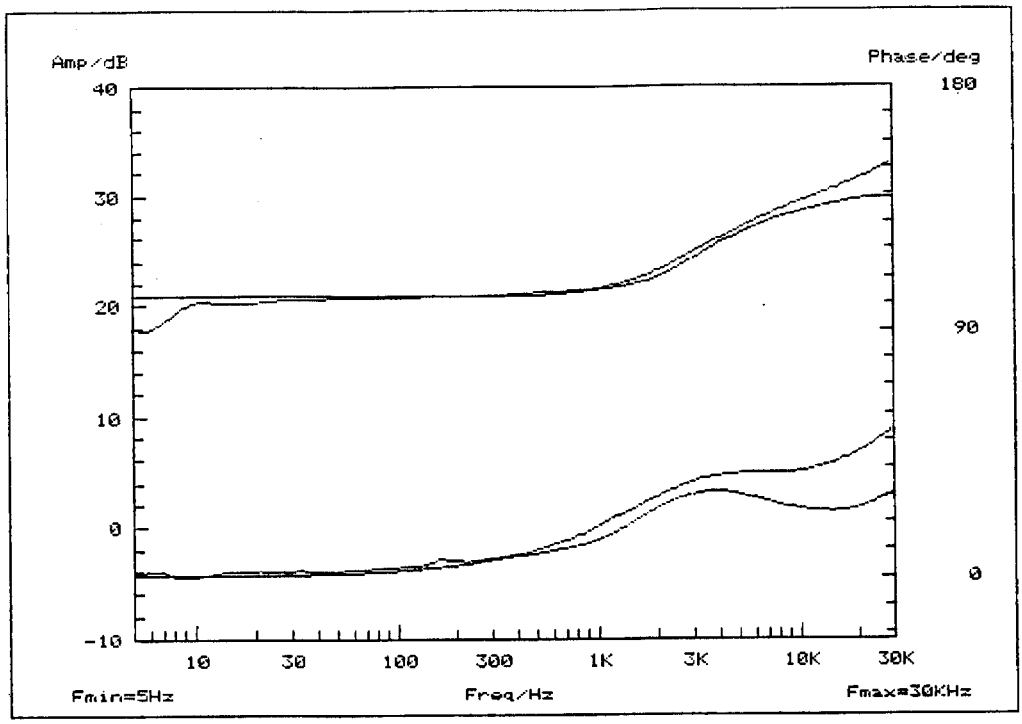

Figure 3.12: Prediction and measurement of transconductance of LC parallel resonant ballast showing the stability of the operation. Conditions: Sylvania Octron lamp (F017), $L = 0.25mH$, $C_p = 10nF$, $f_s = 100kHz$, lamp current: 0.2A rms

and V_M is PWM modulator ramp height. The Routh's array for the characteristic equation is

$$\begin{array}{ll} \frac{2L}{PK_l} & 1 \\ \frac{2L}{K_l} + \frac{1}{Z} & \\ 1 & \end{array}$$

Since $K_l < 0, Z < 0$, so $2L/PK_l$ and $2L/K_l + 1/Z$ are both negative. Thus the first column of the Routh's array has one change of sign which means the lamp-ballast system is not stable as expected since it has one RHP pole.

From control theory, the above case shows that system has an unstable plant. So a lamp can not be directly driven by an LC series resonant matching network. But it is still possible to stabilize the lamp current by adding an appropriate controller and

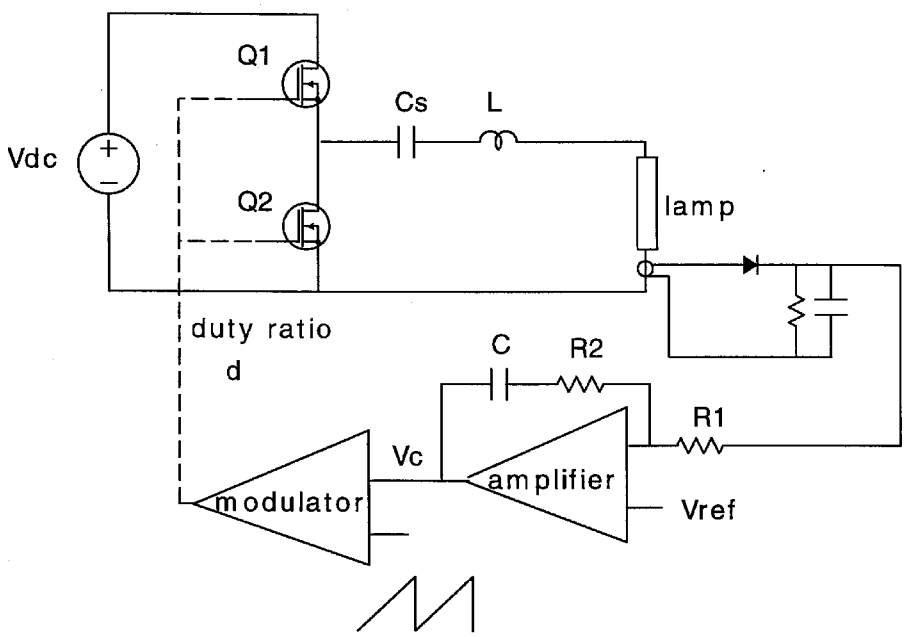

Figure 3.13: The block diagram of the close-loop LC series resonant ballast.

closing the loop as described in Chapter 2.

From the Nyquist criterion, if system open loop-gain has a RHP pole, then to make a close loop system stable the compensation network should be designed in such a way that the Nyquist plot of new open loop-gain should counterclockwise enclose $(-1, 0)$ point once. Figure 3.13 shows the block diagram of such a ballast where lamp current is sensed and fed back to control the duty ratio so that the close-loop system is still stabilizable.

The measured loop gain and prediction are shown in Figure 3.14.

The advantages of the above ballast circuit comes from the LC series resonant network. Since all power flowing through the resonant circuit will drive the lamp so there is no extra conduction loss due to the extra circulating current as in the case of parallel resonant matching network. This efficiency gain is achieved at the price of added feedback circuitry and an addition of lamp start circuit. The concept can be extended to other carriers. In the case of a dc power source, the power efficiency is expected to rise

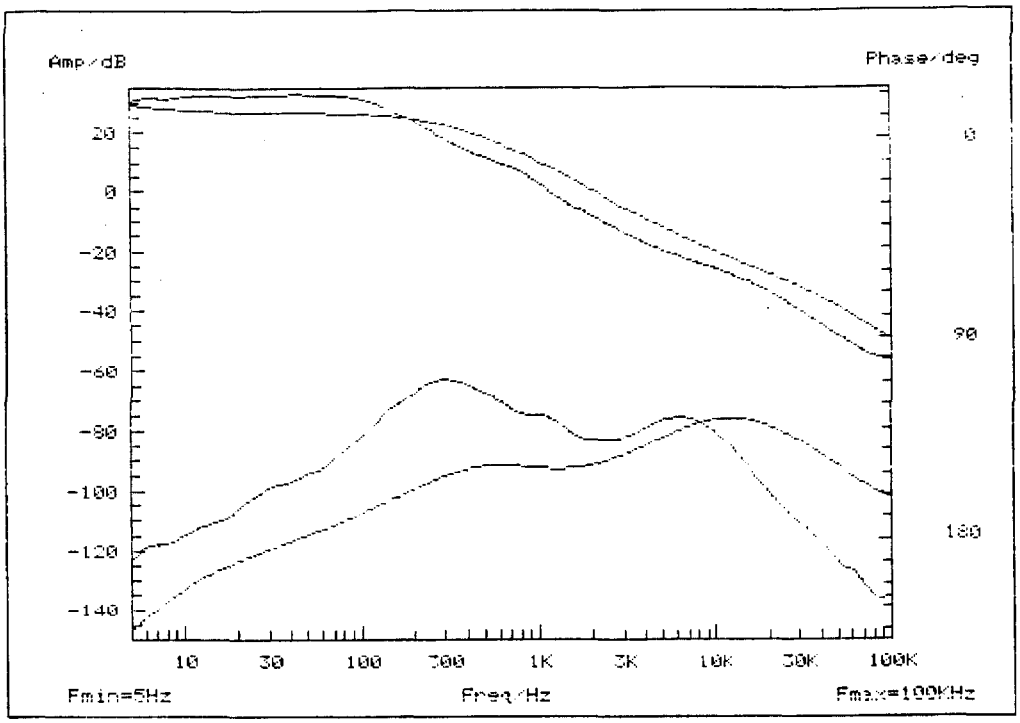

Figure 3.14: Measured and predicted loop gain for the LC series resonant ballast shows the enclosure of the $(-1, 0)$ point. Conditions: Sylvania Octron lamp (F017), $L = 1.2mH$, $C = 2.2nF$, $f_s = 100kHz$, $R_2 = 360k\Omega$, $R_1 = 10k\Omega$, $C = 100nF$, lamp current: 0.25A rms.

significantly since resistor ballast is removed.

Most of the resonant matching networks in the ballast are operated in the vicinity of its resonant frequency. The above analysis can be served as criteria to justify if a resonant network can be used as a resonant matching network. The model can also be used to design a close-loop ballast.

Chapter 4

Conclusions

Fluorescent lamps have a special v-i characteristic due to the various physical processes inside the gas discharge. It needs a ballast to stabilize its operating point. Many previous works were done to accurately model the lamp's terminal behavior in the time domain. The research conducted in this part intends to further uncover this phenomenon and presents it in a way that electrical engineers are familiar with.

The incremental impedance of a fluorescent lamp is defined and studied in the frequency domain. It is found that so-called negative incremental impedance of a fluorescent lamp can be characterized by a right half plane zero so that a lamp can not be directly connected to a voltage source. The existance of such a result is explained by the modified Francis equation. Two approaches are proposed to build up a stable operating point for a lamp. First, a resonant matching network is placed between the voltage source and the lamp. Second, lamp current is sensed and fed back to control the voltage applied across the lamp. The stability criteria based on the Nyquist criterion are developed for the impedance of the resonant matching network and for the loop gain in the above two cases, respectively.

It is found that two cases of negative incremental impedance in power electronics, the fluorescent lamp impedance and the input impedance of a switching dc-to-dc regulator, are two dual cases and can be analyzed in a unified manner based on the stability of the one-port circuit.

The incremental lamp impedance is measured in the most important practical situation, the case of sinusoidal carrier, and is fit by a real rational function with a right half plane zero. The small-signal models for three major resonant matching networks are developed and experimentally verified. Stability analysis for resonant matching networks at parallel resonance are performed. It shows LCC network is the simplest resonant

matching network that a fluorescent lamp needs. It is also shown and experimentally verified that the resonant matching networks at series resonance can be still used as ballasts when the current feedback loop is closed.

The purpose of this research is to gain more fundamental understanding of the fluorescent lamp as a circuit element and to fill the knowledge gap between the lamp and the ballast so that a common ground can be established in order to synthesize more ballast topologies.

Part II

Simple High Power Factor Lamp Ballasts

Chapter 5

Introduction

Most electronic systems draw ac power through an ac-to-dc converter from the utility grid, which supplies power in the form of a low frequency, sinusoidal voltage. Conventional ac-to-dc converters generate poor current waveforms, resulting in such drawbacks as distortion of the line voltage, conducted and radiated electromagnetic interference and poor utilization of the capacity of the power source. As electronic systems evolve, they are becoming more sensitive to the quality of the line voltage. Therefore, as the electronic loads on the utility grid continually increase, the quality of utility power is becoming increasingly important. To maintain the quality of the utility line, current-shaping methods are needed to improve the input-current waveform of ac-to-dc converters.

Power factor is the most common measure of the input-current quality, defined as [20]

$$PF \equiv \frac{P}{V_{i,rms} I_{i,rms}} \tag{5.1}$$

where P is the average power drawn by the load, $V_{i,rms}$ and $I_{i,rms}$ are the rms values of line voltage and current, respectively. Highest value of power factor is unity which implies the ideal line-current waveshape when the input current is propotional to the input voltage, or the input of the ac-to-dc power converter emulates a resistor. *Total harmonic distortions* (THD) is another measure of the input current quality, defined as

$$THD \equiv \sqrt{\frac{\sum_{k=2}^{\infty} I_k^2}{I_1^2}} \tag{5.2}$$

where I_k is the rms value of the kth current harmonics. When input current i_i has no dc component which is true in most applications, the relationship between power factor and total harmonic distortions is

$$PF = \frac{1}{\sqrt{1+(THD)^2}} cos\phi_1 = \frac{I_1}{I_{i,rms}} cos\phi_1. \tag{5.3}$$

The first term, $I_1/I_{i,rms}$, is called the *distortion factor*, which is simply the ratio of the rms value of the fundamental of the current to the rms value of the entire current waveform. The second term, $cos\phi_1$, is called the *displacement factor*, and is the cosine of the angle between the fundamental components of the line current and voltage. To get a high power factor, both distortion factor and displacement factor have to be large. However, in practical situations, THD is usually more concerned. The new standards which regulate the quality of utility power are coming in forcement in terms of allowable minimum power factor and maximum THD.

A high frequency lamp ballast is essentially a single-phase ac-to-ac converter, which draws the low frequency power from the utility grid and converts it into a high frequency ac power to feed the lamp. As lighting equipments represent a significant portion of the total load at many installations, maintaining a high power factor is becoming more and more important for a lamp ballast. As a consequence, a current-shaping or power factor correction stage has to be added to the conventional ballast which makes a typical high power factor lamp ballast consist of effectively two cascaded power processing stages as illustrated in Figure 5.1. The first power conversion stage is to offer a high power factor ac-to-dc rectification from the utility line. The second switching power stage is a dc-to-ac converter to provide the high frequency ballasting function. Major ballast topologies and current-shaping schemes are briefly reviewed next.

5.1 Major Lamp Ballast Topologies

A high frequency ballast provides a high frequency current source for a lamp. Before the lamp turns on, it is an open circuit, and thus a high enough voltage is generated to start the lamp. After the lamp turns on, lamp current is thus stabilized at the designed value. To implement a ballast topology, usually a "*squarewave*" switching scheme is used as it results in simple control and small component count, where several reactive components form a resonant matching network to shape the waveform and provide a high output impedance required by the lamp. The resonant matching network inside the ballast also provides a sinusoidal lamp current with a low crest factor of 1.4. Soft-switching (zero-voltage switching) is also feasible with the "squarewave" switching scheme. Con-

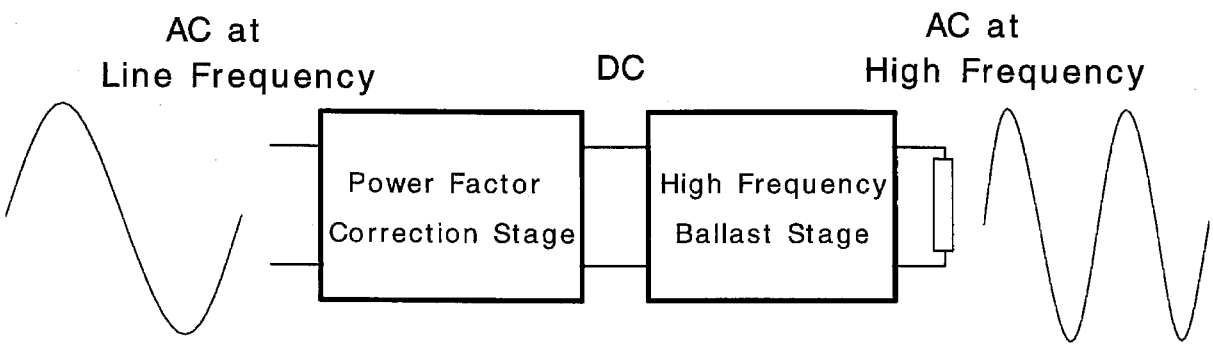

Figure 5.1: Typical configuration of a high power factor lamp ballast.

trollable light output or dimming feature is also desirable to make an intelligent lighting and obtain an extra energy saving.

Two basic squarewave inverter topologies are halfbridge and pushpull resonant inverters [21]. The halfbridge inverter provides a squarewave voltage across the resonant matching network, which is also called "voltage-fed" inverter. The properly designed LCC circuit is the most popular resonant matching network when the halfbridge inverter is used as a ballast [22] as shown in Figure 5.2. The voltage and current waveforms of the switching devices are squarewave and sinusoidal, respectively. Hence the LCC ballast experiences a relatively low voltage stress and a high current stress. Soft-switching is available by operating the resonant matching network above resonance.

The pushpull inverter is kind of the dual form of the halfbridge inverter, where a dc current is chopped alternately by two switches configured in the pushpull manner [21] [23] [24], which is also called "current-fed" inverter. A center-tapped transformer T is necessary to provide an ac power and the voltage step-up. Usually a resonant capacitor C_p is placed across the transformer primary to shape the waveform. The capacitor C_B in series with the lamp is to limit the lamp current. As opposed to the LCC ballast,

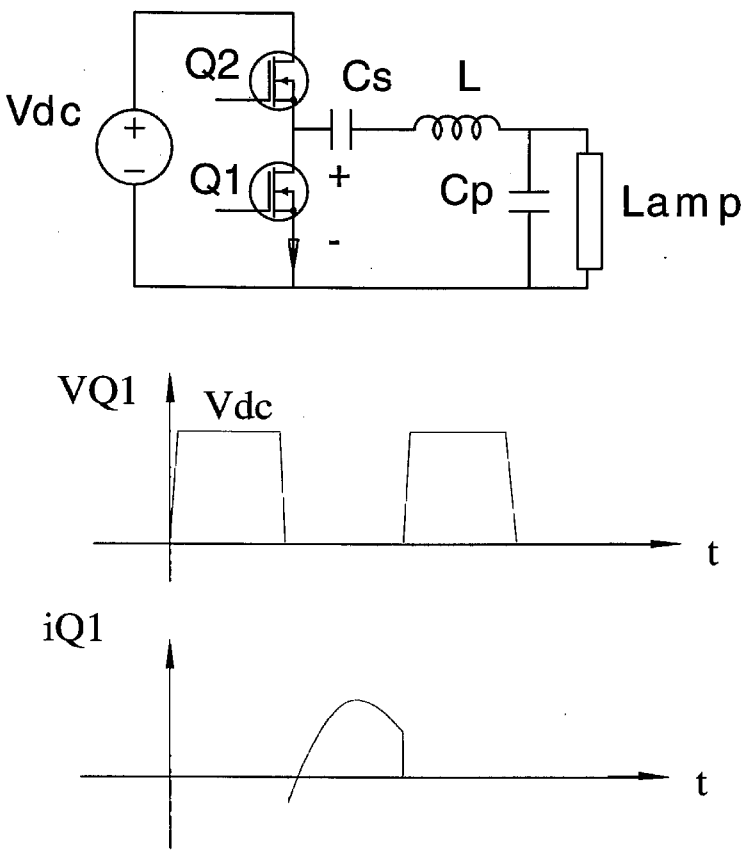

Figure 5.2: Halfbridge LCC ballast and its key waveforms.

current through the switch is basically dc while voltage across the switch is a rectified sinewave whose peak value is at least π times the input dc voltage as shown in Figure 5.3. Soft-switching is also easy to implement in this configuration.

The class E converter is also a good candidate for the ballast applications due to its feasibility of lossless switching and single switch configuration which is suitable for miniaturization [25]. *LCC* resonant matching network is placed between the single-switch and the lamp. However, in this case both voltage and current waveforms for the sinlgle switching device are sinusoidal-like which imposes a severe demand on the device

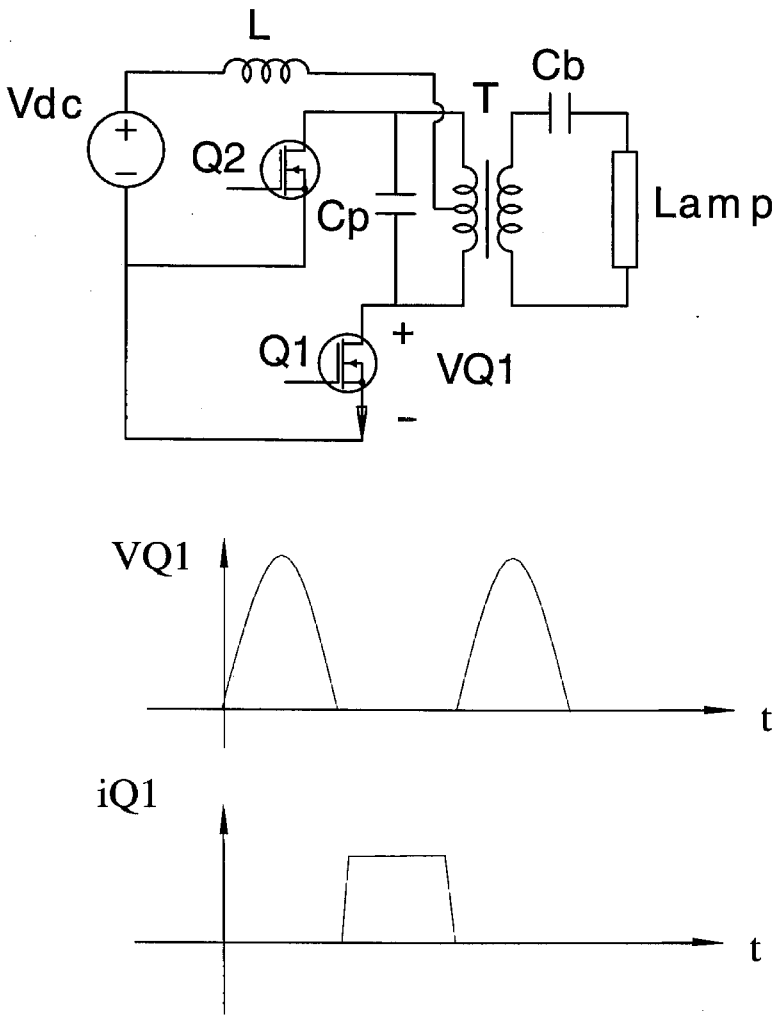

Figure 5.3: Current-fed pushpull ballast and its key waveforms.

ratings [26]. Forward inverter can also be used as a ballast, where voltage stress of the single switch is lower than the Class E converter at the price of added clamping circuit.

Pushpull circuit has the largest component count. The required large inductor and step-up transformer make circuit bulky and lossy. High voltage stress of the two switches also makes it less desirable especially when it is operated after the high power factor preregulator. Class E converter and forward inverter mainly find their applications in the compact fluorescent lamps where size of the ballast is critical. The halfbridge *LCC* ballast, on the contrary, is favored in many applications due to its minimum component

count and inherent current source characteristics at parallel resonance. In the following chapters, the voltage-fed halfbridge and the class E LCC ballasts, based on which new high power factor ballast topologies are generated, will be studied further.

5.2 Power Factor Correction Schemes for Ballasts

Both passive and active circuits are available to perform the function of current-shaping. A so-called "valley-fill" approach which trades part of its energy storage for the input current improvement provides another practical way of current-shaping. Each method has it own advantages and limitations and is favored on the case by case basis.

Passive current-shaping means [20] [23] use only passive components, essentially filters of reactive components and passive switches like diodes. Benefits of passive circuits are their simple structure and robustness as well as the EMI filtering. However, excessive size and weight of the line frequency component, non-ideal power factor correction and lack of regulation limit their applications to the case of low cost and low performance.

The capacitor-input filter generates a stiff voltage source which forces the rectifier to conduct only during a small portion of a line period. Therefore, line current is peaky and a large amount of harmonic currents are generated. Nevertheless, the large capacitor stores the energy and provides a constant power to the output. On the contrary, if a resistive load is directly placed after the bridge rectifier, power line will see a resistance and by definition unity power factor is obtained. The problem with this configuration, however, is that there is no energy storage so that all the line frequency ripple will be passed on to the output. The valley-fill approach [23] is proposed as a compromise between the above two extreme cases in that the circuit operates alternately between the two cases: When the instantaneous line voltage is higher than a certain dc value (nonzero but substantially lower than the peak line voltage) which is determined by the specific circuit, the rectified line voltage will see the load directly and provide line current, which is the resistive load case. Otherwise, the holding capacitor will provide the power to the load during rest of the time and no line current flows, just like capacitor-input filter case. A circuit example is shown in Figure 5.4 to illustrate the shape of input current and dc bus voltage. The valley-fill approach provides an effective way to improve input power

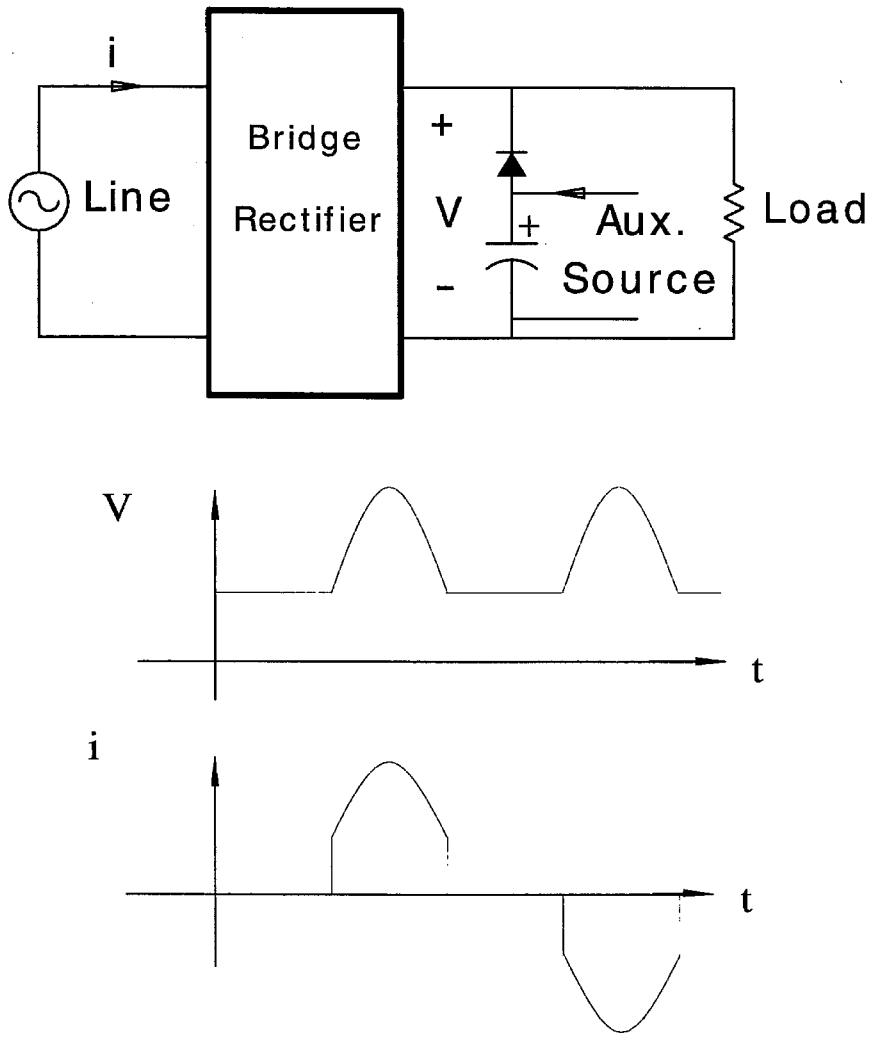

Figure 5.4: Key waveforms in a valley-fill circuit.

factor. But THD is still high due to the discontinuity of the input current. In addition, a fairly large amount of line frequency ripple on the dc side also impairs the lamp current crest factor.

Just opposite to the passive circuits, active current-shaping means have the advantage of providing high quality sinewave input current and the control of power flow. Substantial size and weight reduction is another benefit due to the power processing at the switching frequency. A variety of active current-shaping circuits are offered based on the different dc-to-dc converters, where boost converter is the most popular one [21]

[27]. However, intimately tied to the high power factor controller and active switches, is the circuit complexity making this approach thus less cost-effective.

The quest for low harmonic distortions on the power line requires the addition of a power factor correction stage described above to the conventional electronic lamp ballast. Two-stage ballasts, which can fairly well provide both high input power factor and high frequency lamp ballasting function, also bring a number of deficiencies owing to the two-stage power processing: reduced efficiency; increased size and weight; doubled cost and reduced reliability. This gives the motivation to conduct a research on exploring new topologies which overcome the above shortcomings but still retain the high performance of the two-stage ballast. As a result, numerous single-stage and single-switch, high power factor lamp ballasts have been discovered, which are summarized next.

5.3 Summary of Contents

A single-stage, high power factor lamp ballast is proposed in Chapter 6, which combines the input current-shaping and high frequency ballasting functions within a single power conversion stage. Derivation of the ballast from the Ćuk converter is described. Circuit operation and analysis are presented. Soft-switching is naturally provided as a bonus to eliminate the switching losses and reduce the switching noise which plagues the high frequency lighting. Design formulas are given and experimental results are demonstrated to verify all the desired performances.

Chapter 7 presents a class of single active switch, unity power factor, lamp ballasts, which are derived from proper combinations of automatic current shapers and the single-switch inverters, such as the Class E converter. The desirable mode of operation and the first order analysis are given. The proposed ballasts have the following salient features: close to unity power factor and low crest factor lamp current, single active switch reducing circuit complexity, soft-switching, which are verified by the experimental results.

Chapter 6

Single Stage High Power Factor Lamp Ballast

A single-stage high power factor lamp ballast, which is derived from the Ćuk converter, is proposed in this chapter. The *LCC* circuit, which is a representative of other resonant matching networks in the derivations, is analyzed in Section 1. Derivations of the proposed ballast is described in Section 2, where recognition of the new discontinuous inductor current mode in the Ćuk converter is a crucial step. Operations of the new ballast are illustrated both on switching and line periods in Section 3. The naturally provided soft-switching feature is presented in Section 4. Finally, design equations and experimental results verifying all the advantages of the new lamp ballast are demonstrated in Sections 5 and 6.

6.1 LCC Resonant Matching Network

LCC circuit as shown in Figure 6.1 is one of the most popular resonant matching networks in the current-existing ballasts. It is an example of the more general series and parallel resonant network. Capacitor C_s both blocks dc component and plays part in the resonant operation. Inductor L and capacitor C_p form a parallel-resonant circuit. Several important parameters are defined as follows for the convenience of analysis:

$$\begin{aligned} n &= \frac{C_s}{C_p} \\ \omega_{ser} &= \frac{1}{\sqrt{LC_s}} \\ \omega_{par} = (\sqrt{n+1})\omega_{ser} &= \frac{1}{\sqrt{LC_s//C_p}} \\ R_o &= \sqrt{\frac{L}{C_s}} \\ Q_s &= \frac{R_o}{R} \end{aligned} \tag{6.1}$$

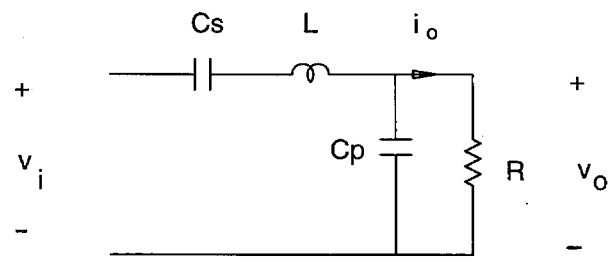

Figure 6.1: LCC resonant matching network.

$$\omega = \frac{\omega_s}{\omega_{scr}}$$
$$x = \frac{i_o R_o}{v_i}$$
$$y = \frac{v_o}{v_i}$$

where ω_{ser}, ω_{par} are the series-resonant and parallel-resonant frequencies, ω_s and ω are the switching frequency and the normalized switching frequency, v_i is the input voltage, i_o, v_o are the output current and voltage, and x and y are normalized output current and voltage, respectively.

The phasor transfer function for the fundamental component is

$$\frac{\mathbf{v_o}}{\mathbf{v_i}} = \frac{1}{1 + \frac{1}{n}(1-\omega^2) + jQ_s(\omega - 1/\omega)}. \tag{6.2}$$

The magnitude transfer function is

$$\frac{v_o}{v_i} = \left|\frac{\mathbf{v_o}}{\mathbf{v_i}}\right| = \frac{1}{\sqrt{\left(1 + \frac{1}{n}(1-\omega^2)\right)^2 + Q_s^2(\omega - 1/\omega)^2}}. \tag{6.3}$$

Since

$$Q_s = \frac{i_o R_o}{v_o} \tag{6.4}$$

we obtain

$$y^2\left[1+\frac{1}{n}(1-\omega^2)\right]^2+x^2(\omega-1/\omega)^2=1. \tag{6.5}$$

So the output characteristic of LCC circuit is described by a family of elliptic curves in the normalized output plane, with ω and n being two parameters.

If ω is 1, the LCC circuit operates at series-resonance. The output will be a constant voltage source. Eq. (6.5) reduces to

$$y=1. \tag{6.6}$$

When ω is $\sqrt{n+1}$, the LCC circuit operates at its parallel-resonance. Eq. (6.5) reduces to:

$$x=\frac{\sqrt{n+1}}{n}. \tag{6.7}$$

When it is used as a resonant matching network in a ballast, LCC circuit is operated in the vincinity of its parallel-resonance where in large-signal sense a current source characteristic is offered. This current source characteristic will generate a high voltage to strike the lamp and set the running current. From the small-signal analysis in Chapter 3, it is also shown that stable operation can also be established in the open-loop fashion.

Another feature of LCC circuit is in its soft-switching. The input impedance of a LCC circuit with a resistive load R is:

$$Z_i(\omega_s)=j\omega_sL-j\frac{1}{\omega_sC_s}+\left(\frac{1}{j\omega_sC_p}\right)//R=A+jB. \tag{6.8}$$

The soft-switching is available when $Z_i(\omega_s)$ becomes inductive, or

$$B=\omega_sL\left(1-\frac{1}{\omega^2}\right)-R\frac{\omega\frac{1}{nQ_s}}{1+(\omega\frac{1}{nQ_s})^2}>0. \tag{6.9}$$

It can be shown on the normalized output plane that the boundary for the soft-switching is determined by:

$$(n+1)y^2+n^2x^2-n^2x^2y^2-n=0. \tag{6.10}$$

The detailed illustration of soft-switching mechanism will be given in Section 4.

Due to the circuit simplicity and the easy operation with lamp, LCC becomes one of the most popular resonant matching networks. Also because of this, LCC will act as a representative of the resonant matching networks in the derivations of the new topologies.

6.2 Derivation of New Circuit

The proposed single-stage, high power factor, lamp ballast is derived from the well-known Ćuk dc-to-dc converter [28] in the following steps. The conventional Ćuk dc-to-dc converter is shown in Figure 6.2(a) where the input switch Q is a MOSFET and the output switch is a diode D. In the continuous inductor current mode (CICM) as in Figure 6.2(b), the sum of the input inductor current i_1 and the output inductor current i_2 is always positive. Diode D which carries the sum current is always conducting. The voltages across the input inductor and output inductor are identical during the two intervals of a switching period which reflects the interdependent nature of the input and output inductor currents: the mode of operation of one inductor imposes the same mode on the other inductor. The discontinuous inductor current mode (DICM) (Figure 6.2(c)) occurs when the effective conduction parameter K_e satisfies the conditions:

$$K_e < K_{crit} \tag{6.11}$$

where

$$K_c \equiv \frac{2L_e}{R} f_s, \quad L_e = L_1 // L_2$$

and

$$K_{crit}(D) = D(1-D).$$

The analysis in [28] shows that there are two entirely different DICM modes. The one shown in Figure 6.2(c) has input inductor current i_1 *negative* for a portion of a switching period, and the output inductor current i_2 is always positive. The second mode (not shown in Figure 6.2(c)) is when output inductor current i_2 is *negative* for a portion of a switching period, but input current i_1 is always positive. The first mode is, however, of interest since it is this mode which will be modified by the addition of the input rectifying diode D_1. The first mode occurs when the condition (6.12) is met:

$$L_2 > ML_1 \tag{6.12}$$

where M is the dc voltage conversion ratio. i_2 is always positive and i_1 can be negative as shown in Figure 6.2(c); thus the sum current drops to zero and a new interval D_3T_s

occurs. The voltages across the input inductor L_1 and output inductor L_2 still share the identical waveform in spite of three intervals in a switching period.

A current bidirectional Ćuk converter can be obtained by replacing the output diode D with a MOSFET switch Q_2 as shown in Figure 6.3. Since both input and output currents can take either positive or negative values, this converter does not permit DICM operation and there are only two switched intervals in a switching period. As before, both inductors L_1 and L_2 share identical voltage waveforms as shown in Figure 6.3.

If another diode D_1 is inserted in series with the input inductor L_1 as in Figure 6.4, behavior of one inductor current may be decoupled from the other under the certain condition when the added switch D_1 becomes active. The input current i_1 becomes unidirectional, and for an inductor L_1 satisfying a critical condition as shown in (6.19), a new DICM operation is discovered as shown by the waveforms in Figure 6.4. The critical condition for the new DICM is expressed in terms of the critical inductance L_{crit}. It can be shown that for given switching frequency f_s and dc load R, the new DICM operation occurs when the input inductor L_1 satisfies:

$$L_1 < L_{crit} \tag{6.13}$$

where

$$L_{crit} = \frac{(1-D)^2}{2D} RT_s.$$

Meanwhile, the output inductor L_2 current i_2 is still bidirectional and does not have DICM operation owing to the two current bidirectional switches Q_1 and Q_2. Thus the input inductor L_1 and output inductor L_2 no longer share identical voltages and are decoupled due to the emergence of the new DICM operation when three switches participate in the converter operation.

The new DICM operation of the converter is retained if it is operated from a rectified ac line, under a new critical condition:

$$L_1 < L_{crit} \tag{6.14}$$

where

$$L_{crit} = \frac{(1-D)^2}{4D} RT_s.$$

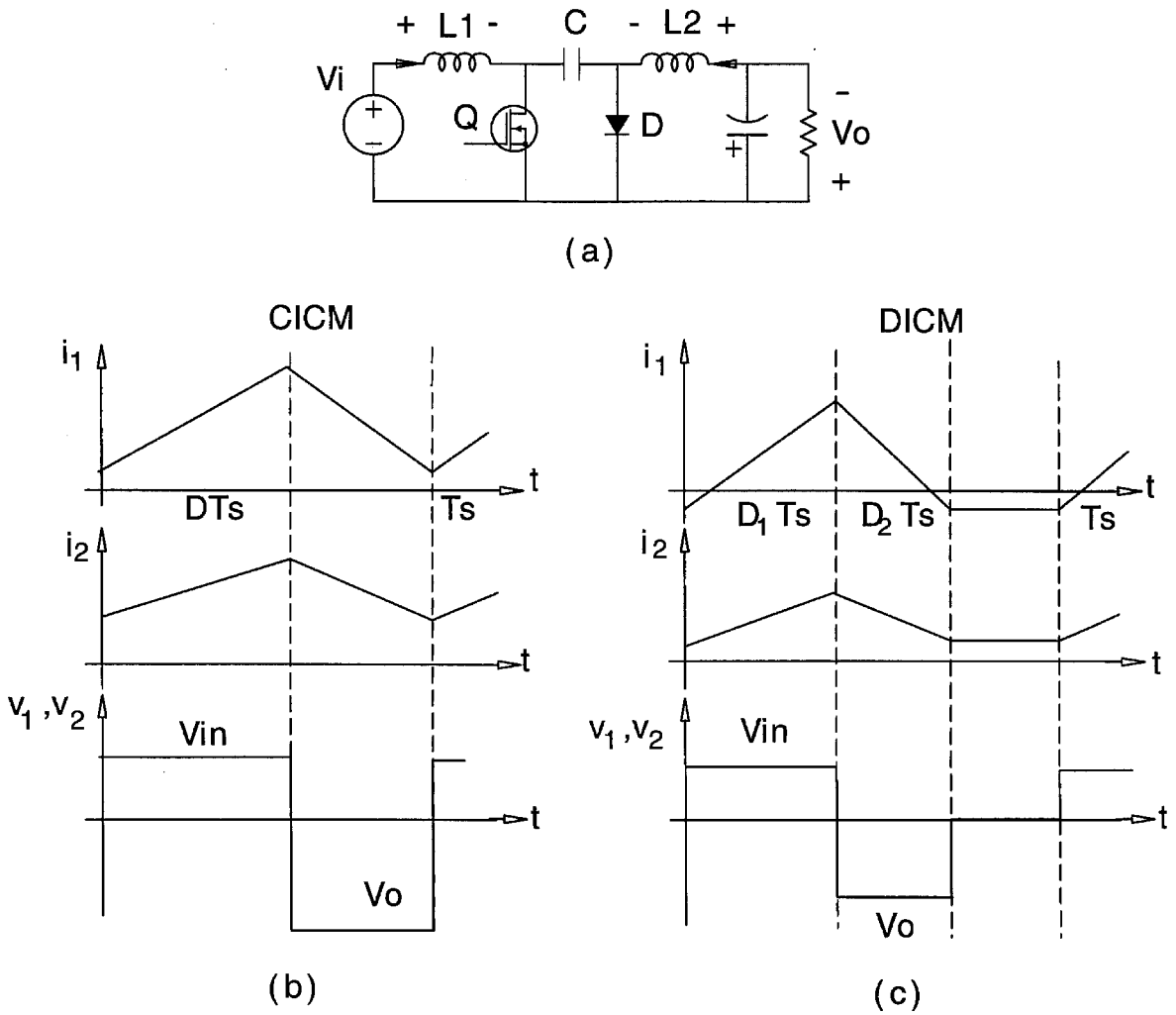

Figure 6.2: Conventional Ćuk converter (a) and its waveforms in CICM mode (b) and DICM mode (c).

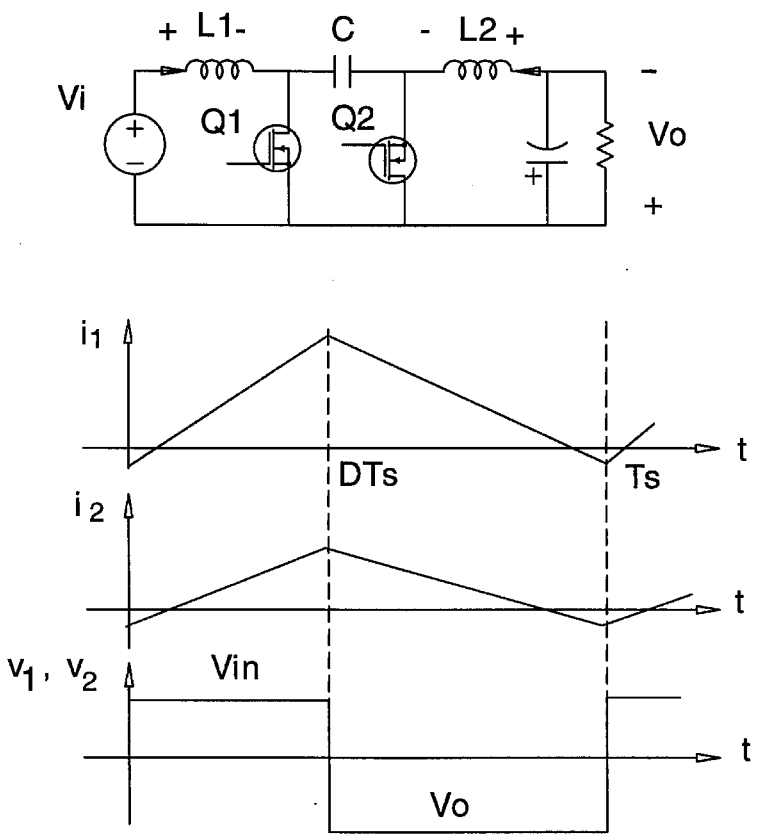

Figure 6.3: Current bidirectional Ćuk converter and its waveforms.

Automatic input current-shaping is provided by simply operating the converter at a constant duty ratio and at fixed frequency, and the energy is internally stored in the energy transfer capacitor C. This automatic current shaping is also described in [29]. However, in [29] only the case of diode rectifier instead of current bidirectional switch Q_2 of Figure 6.4 was analyzed. The current bidirectional switch Q_2 is essential for lamp ballast application analyzed here. Since the two current bidirectional switches Q_1 and Q_2 generate a squarewave voltage before the low-pass filter, an LCC resonant matching network can be also placed to extract the fundamental component of the above

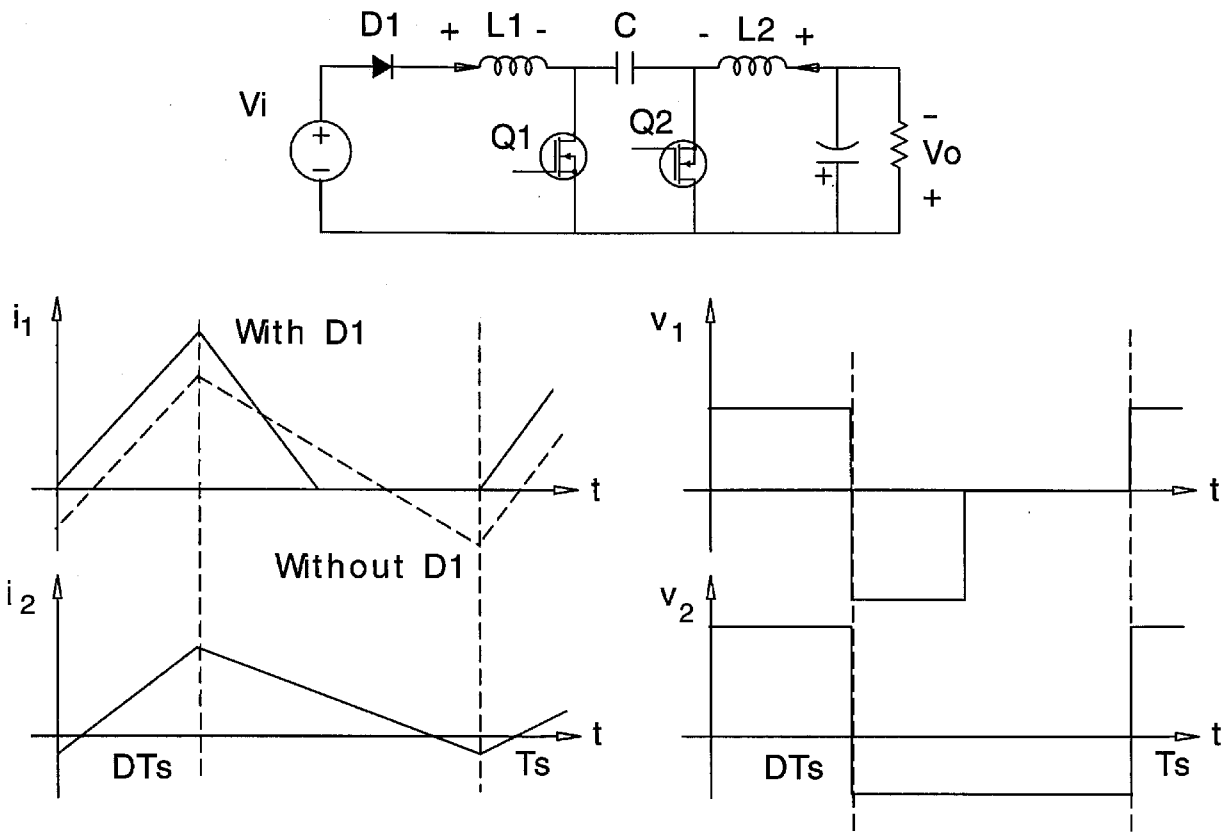

Figure 6.4: New DICM operation in Ćuk converter.

squarewave voltage and then convert it into a sinusoidal current source needed by the lamp. By so doing the single-stage, high power factor ballast is obtained as shown in Figure 6.5.

The new circuit can also be derived following the way Ćuk converter was originally derived [28]. *LCC* ballast can be efficiently regulated via simple duty ratio modulation. The preferred boost current shaper is also PWM controlled. Therefore, the above two stages can be combined by common use of switches, resulting in a single high power factor conversion stage. To remove the line frequency modulation on the lamp current,

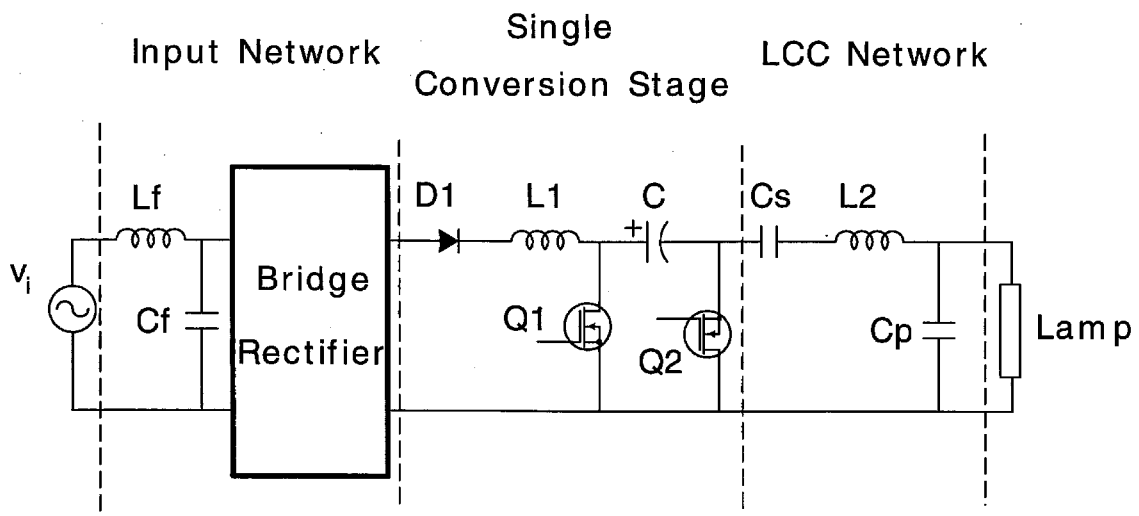

Figure 6.5: Proposed single-stage high power factor lamp ballast.

the duty ratio has to be fixed which requires an automatic current shaper and the front boost-like stage has to be operated in DICM [20]. Unlike other loads, the lamp as a load does not require fast or tight regulation; therefore, a lamp ballast can be operated in open-loop. However, a conventional PWM controller loop can be closed from duty ratio to lamp current so that lamp current can be regulated. A lamp accepts a slow feedback so that input high power factor is not degraded.

6.3 Circuit Operation

The new single-stage, high power factor, gas discharge lamp ballast comprises four parts according to the functions they perform: input network, single power conversion stage, resonant matching network and PWM controller (not shown), as indicated in Figure 6.5.

The input network comprising a full bridge rectifier and low-pass filter provides a rectified sinewave line voltage $v_i = V_m|sin(\omega_l t)|$ to the single conversion stage, and simultaneously unfolds the unidirectional input current i_1 into the sinewave line current

i_i averaged by the low-pass filter. The single conversion stage having the front-end diode D_1, which must be fast-recovery because it switches at the speed of switching frequency, inductor L_1, current bidirectional switches Q_1 and Q_2, and capacitor C converts the rectified sinewave line voltage v_i to a squarewave voltage at the switching frequency controlled by a fixed switching frequency PWM controller. A resonant matching network (typically LCC) converts the high frequency squarewave voltage into a sinewave, ac current source required by the fluorescent lamp. Note that the fast recovery diode D_1 is combined into the bridge rectifier when the bridge rectifier consists of four fast diodes. Details of operation will be described in the following subsections.

6.3.1 Automatic Current Shaping

The input inductor L_1, which is chosen to be less than the critical value L_{crit}, and the front-end diode D_1 force the input inductor current i_1 into the DICM for the nominal lamp power despite the two current bi-directional switches Q_1 and Q_2. Intuitively, smaller values of inductor L_1 and switching frequency f_s tend to move the circuit into DICM operation of L_1. In addition, a smaller value of lamp load impedance R_l also shifts the circuit into DICM operation since the output of the lamp ballast is now a current source i_l which is opposite to that of a voltage regulator. A new parameter R with a dimension of resistance can be defined to reflect the combined effect of the circuit parameters on the operation mode, where

$$R = \sqrt{L_1 R_l f_s}. \tag{6.15}$$

This parameter plays a key role in the DICM, since it combines uniquely all the parameters responsible for such behavior. It can be shown that the critical condition for the ballast operating in the DICM is

$$R < R_{crit} \tag{6.16}$$

where

$$R_{crit} = \frac{\sqrt{D}(1-D)}{2}\frac{MV_m}{i_l} \tag{6.17}$$

where M is an intermediate voltage conversion ratio defined as energy transfer capacitor voltage V_c over the input peak voltage V_m, i_l is lamp current or the value of current source. Similarly, given switching frequency f_s and nominal lamp load R_l, the critical condition could be illustrated in terms of the critical inductance L_{crit},

$$L_1 < L_{crit} \tag{6.18}$$

where

$$L_{crit} = \frac{R_{crit}^2}{R_l f_s}.$$

It can be shown that under the DICM operation the average input current $< i_1 >$ is

$$< i_1 >= \frac{V_m}{R_{em}} |sin(\omega_l t)| \frac{M}{M - |sin(\omega_l t)|} \tag{6.19}$$

where

$$R_{em} \equiv \frac{2L_1 f_s}{D^2},$$
$$M \equiv \frac{V_c}{V_m}.$$

Note that the averaging function is provided by the low-pass filter L_f, C_f in the input network shown in Figure 6.5. When the intermediate voltage conversion ratio M is much larger than $|sin(\omega_l t)|$, effect of the nonlinear term in Eq. (6.19) will be negligible. Therefore, the average input current $< i_1 >$ will closely follow the input voltage v_i where the input resistance is R_{em} and near unity power factor can be obtained. The dependence of input power factor on M is plotted in Figure 6.6 [20]. It can be easily seen that power factor larger than 0.99 can be achieved at M above 2.

6.3.2 Major Waveforms

The new ballast includes three switches: the front-end diode D_1 and two current bidirectional switches Q_1 and Q_2 of the conversion stage. These switches generate three switched networks within one switching period of the controller, as will be described with reference to the waveforms in Figure 6.7.

During the first interval t_1, switch Q_1 closes and switch Q_2 is open. The input voltage v_i is applied across L_1 and the input current i_1 through the input inductor L_1 linearly

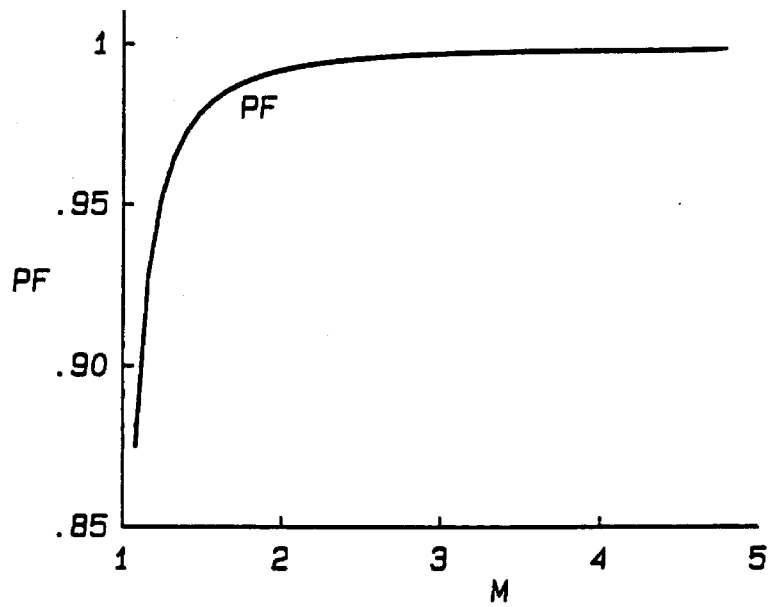

Figure 6.6: Plotted input power factor as a function of conversion ratio M in boost automatic current shaper.

increases. Meanwhile, the energy transfer capacitor C is in series with the LCC network to provide a voltage V_c across the port $A - B_1$. When the switch Q_1 is turned off after a time period t_1 determined by the PWM controller, Q_2 is turned on and the second interval t_2 of the switching period begins. During t_2, the energy transfer capacitor C is connected across the input inductor L_1 and ground, the voltage across L_1 is then $v_i - V_c$, current i_1 decreases linearly and charges the capacitor C until the input current i_1 drops to zero and is blocked by the diode D_1, i.e., D_1 becomes open and the third interval t_3 starts. During t_3, the inductor L_1 current i_1 continues to be zero and the energy transfer capacitor C is idled, while the rest of the network remains the same as in interval t_2. When the switching period ends, Q_2 is turned off and switch Q_1 is turned on and next switching cycle begins with the interval t_1. During the whole period, the output inductor current i_2 is always continuous and in a sinusoidal form due to the two current bidirectional switches and the LCC resonant network.

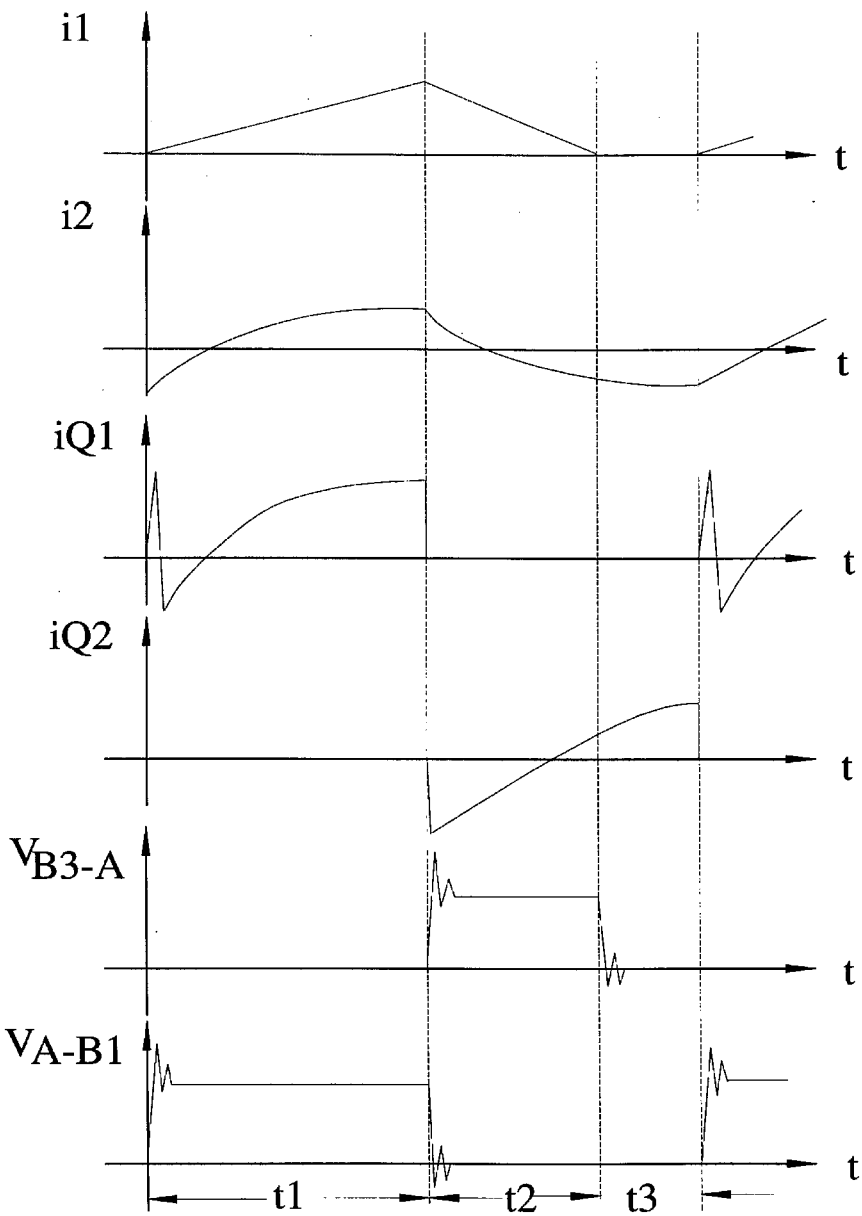

Figure 6.7: Key switching waveforms in the proposed ballast.

Figure 6.8 shows the major waveforms on the line scale. The input inductor current i_1 is discontinuous whose peak value is modulated by the rectified sinewave v_i provided by the input network. The input network also averages and unfolds this current yielding the line current i_i which closely follows the instantaneous line voltage. The energy transfer capacitor C also stores energy to balance the power difference between the line frequency input and high frequency output. Thus its voltage v_c will have modulation at twice the line frequency whose amount depends on the capacitance C. Reasonable large capacitance can reduce those line ripples to the minimum. Finally, the output lamp current i_l is also a sinewave but at switching frequency with a slight line frequency modulation.

A variety of ways can be used to control lamp current, where fixed frequency PWM control is favored because it is easy to be implemented and convenient for harmonics filtering. PWM control modulates both height and width of the squarewave voltage applied to the LCC network which makes the control more sensitive compared to the two stage circuits with separate control where only duty ratio D or dc link voltage v_c is adjusted. Reference voltage at the PWM controller can be adjusted to continuously vary the lamp light output. Adjustment of reference voltage in the PWM controller will adjust the duty ratio D, and then vary the lamp current so that the light is continuously dimmed.

The voltage across the energy transfer capacitor is determined by the equation:

$$M = \frac{V_c}{V_m} = \frac{1 + \sqrt{1 + \frac{2D_1^2}{K}}}{2} \tag{6.20}$$

where

$$K = \frac{2L}{R_e T_s}$$

and R_e is the equivalent dc load to the boost stage. When the lamp is removed, the front-end boost automatic shaper is unloaded or R_e is open. Then M or V_c will blow up, which will destroy the two switching devices Q_1 and Q_2. To avoid this, voltage V_c should be sensed. When it exceeds a threshhold value, the sensor will trigger a controller to shutdown switch Q_1 thus to stop the voltage from overrise.

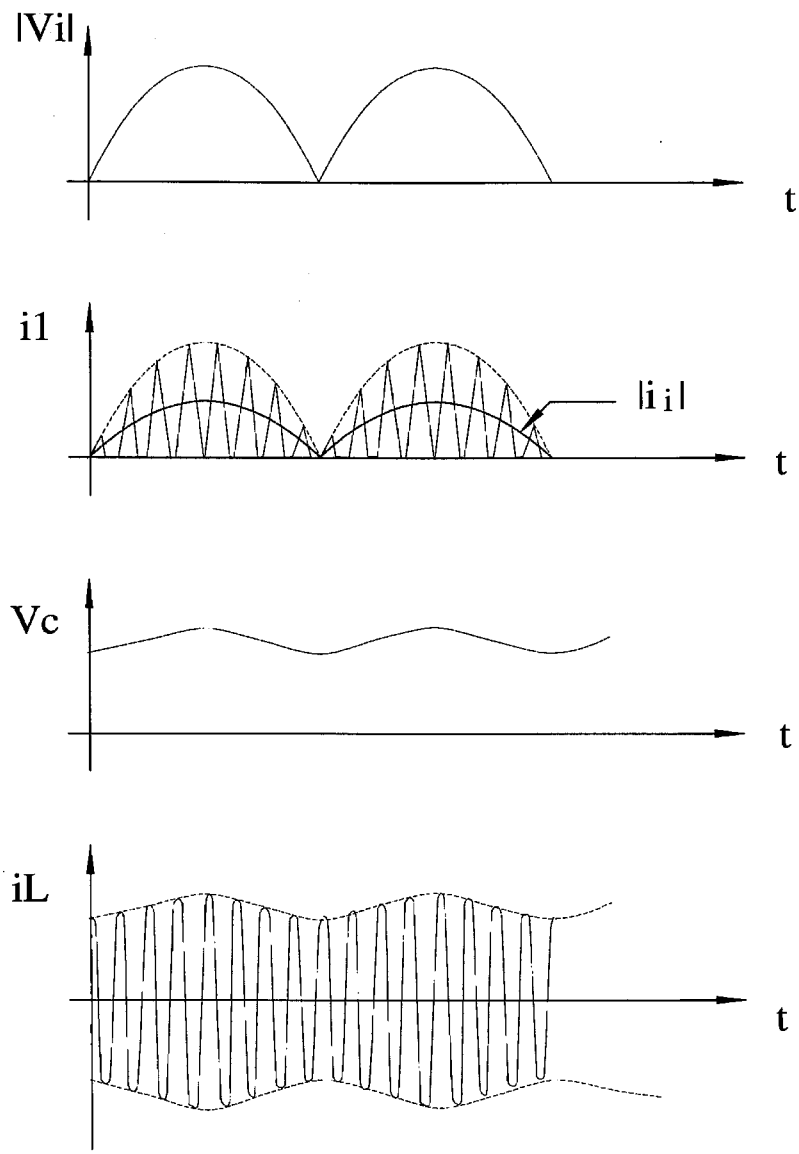

Figure 6.8: Major line scale waveforms in the proposed ballast.

6.3.3 Isolated Versions

Isolation from line is certainly desirable for the safety reasons and when extra voltage step-up is needed to operate the lamp at ultra high voltage. Extra filament heating can be also efficiently provided through the extra windings from the transformer. Similar to the Ćuk converter [28], the energy transfer capacitor C can be split into C_1 and C_2, with the isolation transformer T being inserted in between as shown in Figure 6.9(a). The transformer can be built on the non-gapped core since it doesn't handle any dc flux. The isolation transformer T can also be inserted anywhere past the dc blocking capacitor C_s in the LCC network as shown in Figure 6.9(b). In this case the leakage inductance of transformer is combined into the resonant circuit and thus harmful ringing and associated power loss due to energy stored in leakage inductance are avoided. More circuit variations are disclosed in [31].

6.4 Soft-switching

The switching process in Figure 6.7 of the ballast is called hard-switching since the current bidirectional switches Q_1 and Q_2 in their OFF states store the energy $\frac{1}{2}C_Q V_c^2$ in their parasitic capacitances C_Q (both C_{Q1} and C_{Q2}), which is dissipated as a loss the moment the switches turn ON. This loss of $\frac{1}{2}C_Q V_c^2 f_s$ is proportional to the switching frequency and therefore represents the major obstacle for reducing the size and weight via switching frequency increase. This switch turn-on loss due to the capacitor charge dumping results in current spikes and voltage overshoots. As a consequence, high voltage ratings are needed for the semiconductor switches and EMI noises is also generated. However, all these disadvantages are eliminated by the extra feature of soft-switching of the two MOSFETs. Since the new ballast is built by combining the two power conversion stages, the two current bidirectional switches Q_1 and Q_2 carry both the triangular input current i_1 and the sinewave output current i_2. Either current can be considered to "soften" the switch which benefits the overall power conversion stage.

The key to achieve soft-switching is to provide two transition intervals during which both active switches Q_1 and Q_2 are OFF. Charge transfers from previously OFF device to the one which is just turned OFF. Thus the first device can be turned ON at zero

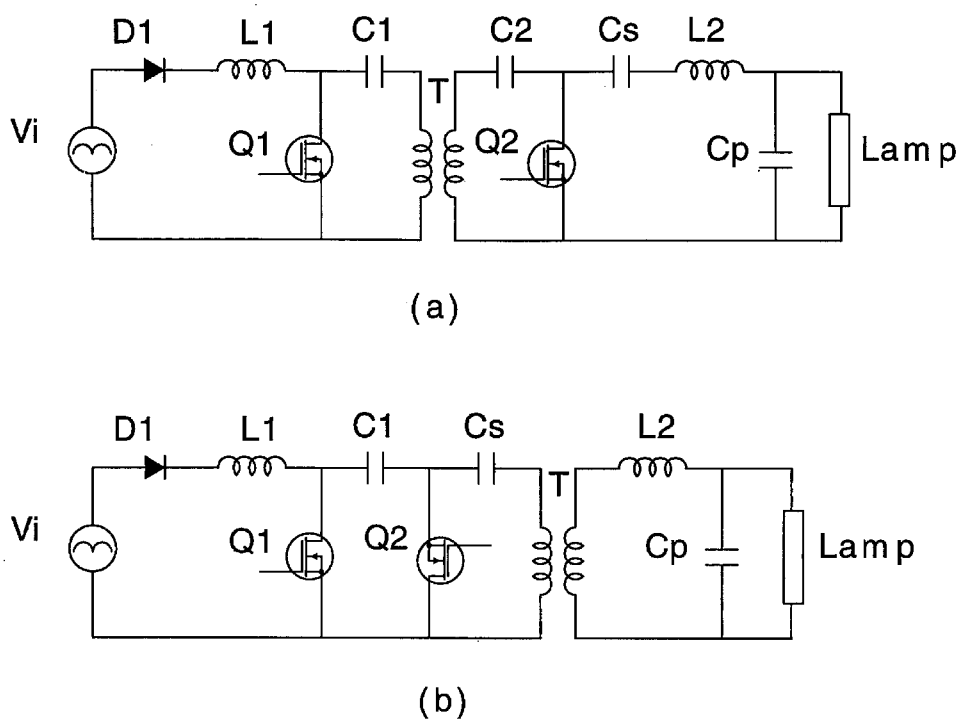

Figure 6.9: Two examples of the isolated single-stage high power factor lamp ballast.

voltage with low switching losses. For the charge transfer to occur during the resonant transitions, the *reverse* current is clearly needed. The current to discharge the capacitance of the second switch Q_2 is easy to get – it mainly comes from the input (inductor L_1) current i_1 since i_1 is peaky due to the DICM operation and at its peak when Q_1 is turned OFF. However, compared to the readily available discharge current for Q_2, the discharge current to "soften" Q_1 is not so obvious even if it does exist. Input current i_1 is helpless this time because it is zero before Q_1 turns on due to the DICM operation. But the output (resonant inductor L_2) current i_2 is available to accomplish the function.

First we should note that in the Ćuk converter as well as in the ballast of Figure 6.5 derived from it, the current in active switches is the sum of input i_1 and output i_2 inductor currents. Since i_1 is zero due to the DICM mode, this leaves the active switch currents to

depend entirely on i_2. If this i_2 current direction could be reversed just prior to turn-ON of Q_1, the parasitic capacitance of Q_1 switch would also discharge naturally to zero. The critical issue then becomes how to achieve such a current reversal. In dc-to-dc converters, this is usually accomplished by large ripple currents of i_2 [30] with related deficiencies. For the lamp ballast circuit, however, such additional and undesirable restrictions are not needed, since a much simpler soft-switching implementation is possible as explained next.

Such current reversal of i_2 and the soft-switching for Q_1 is provided by utilizing the lagging current obtained by operating the LCC resonant circuit above resonance. The resonant frequency ω_o of LCC network is defined in terms of the input impedance $Z_i(\omega)$ in Eq. (6.8) which is repeated below and is illustrated in Figure 6.10(a), where:

$$Z_i(\omega) = \frac{1}{j\omega C_s} + j\omega L_2 + \frac{1}{j\omega C_p} // R_l \tag{6.21}$$

and the resonant frequency ω_o is the frequency when $Z_i(\omega)|_{\omega=\omega_o}$ is resistive. From Eq. (6.21), the resonant frequency ω_o is dependent on the load impedance of the LCC network as plotted in Figure 6.10(b). Before the lamp turns ON, the impedance of the lamp R_l is infinitely large and the LCC resonant circuit is unloaded. The unloaded resonant frequency ω_o is the parallel resonant frequency ω_{par}. If the switching frequency ω_s is set at or close to ω_{par}, the lamp will see a current source since the output impedance of the LCC network is infinitely large. After the lamp is turned ON, however, its impedance R_l drops. The resonant frequency ω_o will be reduced below ω_{par}. As an extreme, when the lamp load shorts or $R_l = 0$, the resonant frequency ω_o will be the lowest which is the series resonant frequency ω_{ser}.

Thus, once the lamp is on, the LCC network is nonzero loaded and the resonant frequency must be somewhere between ω_{ser} and ω_{par} as shown in Figure 6.10(b). Since the switching frequency ω_s is set near ω_{par}, which is the upper bound of the resonant frequency, the lamp ballast is operated above resonance when lamp is running, which means the input impedance $Z_i(\omega_s)$ of the resonant circuit is inductive and the resonant current i_2 *lags* behind the voltage v_{A-B_1} at the input port $A - B_1$ of the LCC network. It is this lagging current which acts as the reverse current to provide a soft-switching transition of Q_1.

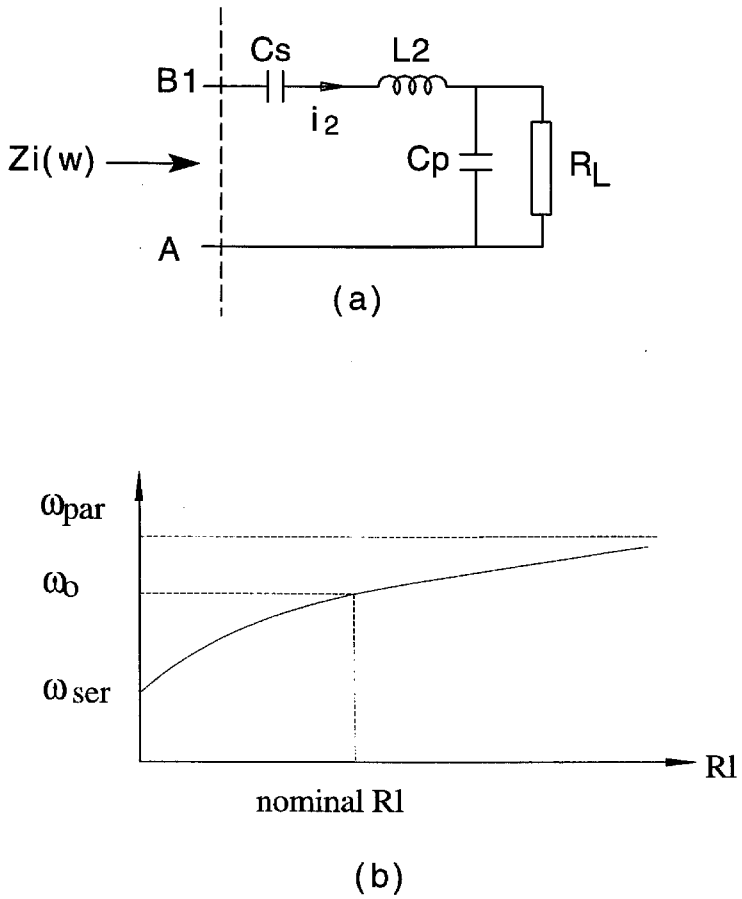

Figure 6.10: Illustration of LCC input impedance (a) and load-dependent resonant frequency ω_o (b).

Two resonant transition intervals tr_1 and tr_2, when both Q_1 and Q_2 are OFF, are introduced by delaying turn-on of one switch after the other is turned-off to facilitate soft-switching of the two MOSFETs, which are described with the corresponding schematic diagrams of Figures 6.11(a) and (b) where each current bi-directional switch Q is represented by a composite switch, consisting of a main channel S_Q, an antiparallel diode D_Q and the parasitic capacitance C_Q.

Since the durations of the two resonant transitions (tr_1 and tr_2) are short compared to the switching period, inductor currents i_1 and i_2 could be assumed constant during the two resonant transitions and represented by the dc current sources I_1, I_2, respectively.

The first resonant transition interval tr_1 starts when the switch Q_1 turns OFF, i.e.,

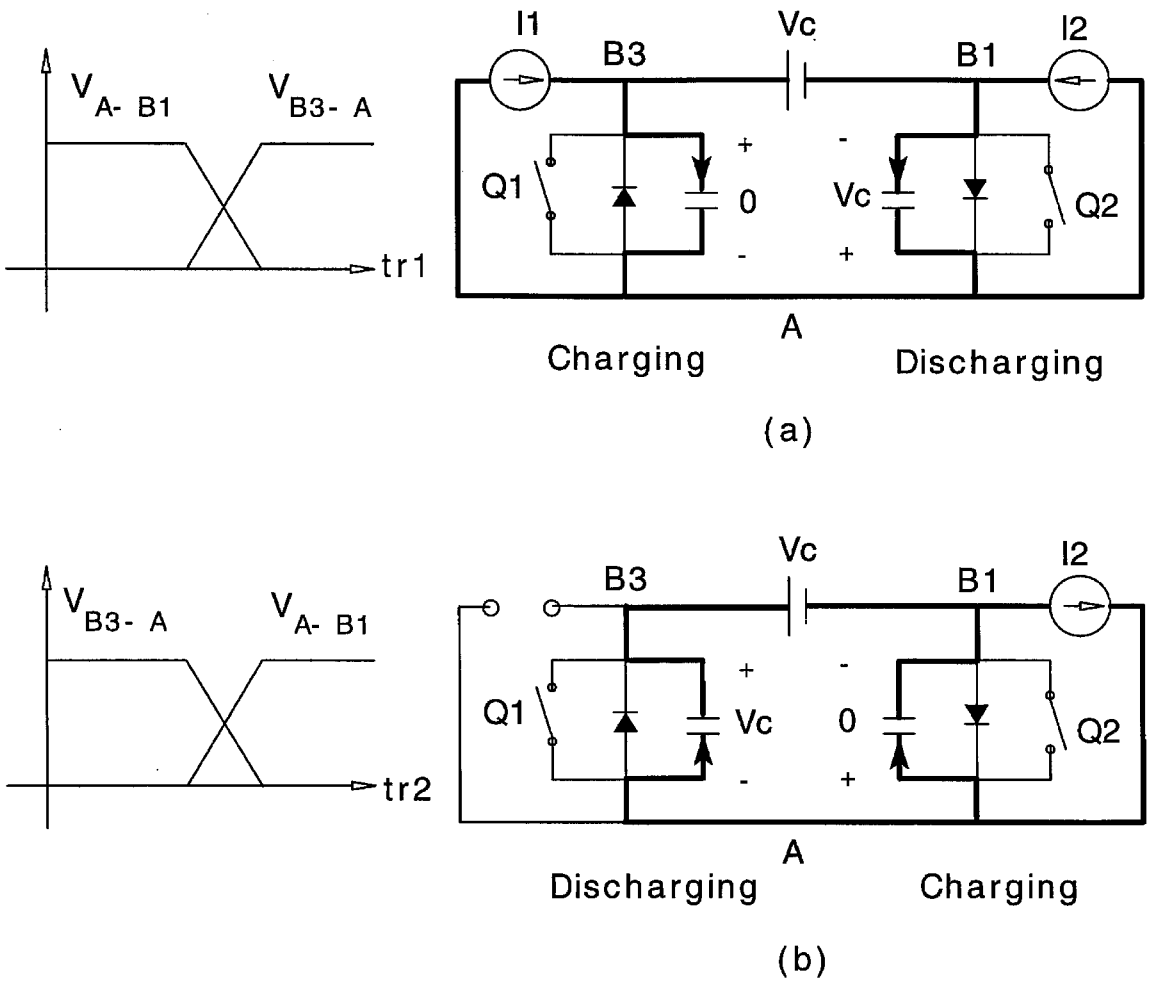

Figure 6.11: Soft-switching transitions of Q_1 and Q_2.

when t_1 interval ends. During tr_1, input inductor current i_1 is at its peak while resonant inductor current i_2 is also positive as shown in Figure 6.7 due to the phase lag with respect to the voltage v_{A-B1}. The two inductor currents i_1 and i_2 can be represented by the corresponding dc current sources I_1, I_2 respectively, as illustrated in Figure 6.11(a), where V_c is a dc voltage source representing voltage across the energy transfer capacitor C. The sum current $I_1 + I_2$ splits and charges and discharges the two capacitors C_{Q1} and C_{Q2} simultaneously. Thus capacitor C_{Q1} is charged and its voltage v_{B3-A} rises linearly from its initial value of zero. Capacitor C_{Q2} is simultaneously discharged and its voltage v_{A-B1} drops linearly from its full turn-off value of V_c to zero when the antiparallel diode D_{Q2} conducts, then voltages v_{B3-A} and v_{A-B1} are clamped at the V_c and zero, respectively. Now switch Q_2 can be turned on losslessly since v_{A-B1} is clamped at zero level and energy stored in C_{Q1} has been transferred into C_{Q2}. After Q_2 turns ON, the circuit starts its second interval t_2 as described in Figure 6.7.

The second resonant transition interval tr_2 starts when the active switch Q_2 turns OFF, i.e., when t_3 interval ends. During tr_2, input inductor current i_1 is zero owing to the DICM operation of L_1 while the output resonant inductor current i_2 is now negative as shown in Figure 6.7 owing to the phase lag with respect to the voltage v_{A-B1}, which can be represented by the corresponding dc current sources I_2, as illustrated in Figure 6.11(b). The current I_2 splits and charges and discharges the two capacitors C_{Q2} and C_{Q1} simultaneously. Similar to the process in tr_1, Q_1 can be turned ON losslessly. After Q_1 turns ON, the circuit goes to another switching cycle starting from its first interval t_1 as described previously in Figure 6.7.

During the first transition interval tr_1, large I_1 assists I_2 to implement soft-switching of switch Q_2, while during the second transition interval, tr_2, only I_2 is available to implement soft-switching of Q_1. Therefore soft-switching of Q_1 is more difficult to achieve, especially when the lamp is significantly dimmed and the lamp load is large enough so that the LCC network is operated marginally above resonance.

During the above-described resonant transitions of the MOSFETs, each switch is turned ON after its parasitic capacitor is fully discharged. Thus, the energy stored in the capacitances C_{Q1} and C_{Q2} is exchanged between them instead of being dissipated into

heat as in the hard-switching case. The above description shows turn-on switching loss have been eliminated, which also allows extra lossless snubber capacitance in the form of a discrete capacitor to be added to C_Q, i.e., to be placed directly across either switch Q_1 or Q_2 to reduce the turn-off loss. In addition, the slow body diode of MOSFETs can be fully utilized since there is no voltage immediately applied due to the conduction of the MOSFET after the body diode turns OFF [32]. Figure 6.12 shows the waveforms for the switch Q_1 with (b) and without (a) soft-switching to demonstrate the performance difference.

6.5 Circuit Design

Since the input current-shaping part and the output resonant ballast part are decoupled, the two parts can be designed separately after the intermediate voltage conversion ratio M is chosen. Switching frequency is usually chosen in the range of 20kHz to 100kHz so that high efficacy of the lamp can be obtained and circuit loss is still under control.

The first step in the design procedure is to select the intermediate voltage conversion ratio M. From Figure 6.6, large M provides high power factor. Once the M and switching frequency f_s are selected, the voltage V_c is calculated from $V_c = MV_m$. Duty ratio D can be chosen to be less but close to 0.5. Given a specific lamp, having nominal current i_l and nominal power P_l, the LCC component can be determined from

$$C_p = \frac{i_l}{\omega_s V_s(D)} \tag{6.22}$$

$$C_s = nC_p \tag{6.23}$$

$$L_2 = \frac{n+1}{n}\frac{V_s(D)}{\omega_s i_l} \tag{6.24}$$

where

$$V_s(D) = V_c\frac{\sqrt{2}}{\pi}sin(\pi D).$$

Parameter n provides a freedom to choose values of C_s and L_2. Large n makes large C_s and small L_2 as well as more harmonics in the lamp current; the minimum value of L_2 is $V_s(D)/\omega_s i_l$ when n is infinitely large. Small n makes the resonant circuit more selective so that clean sinewave current is obtained at the price of large L_2. The input inductor

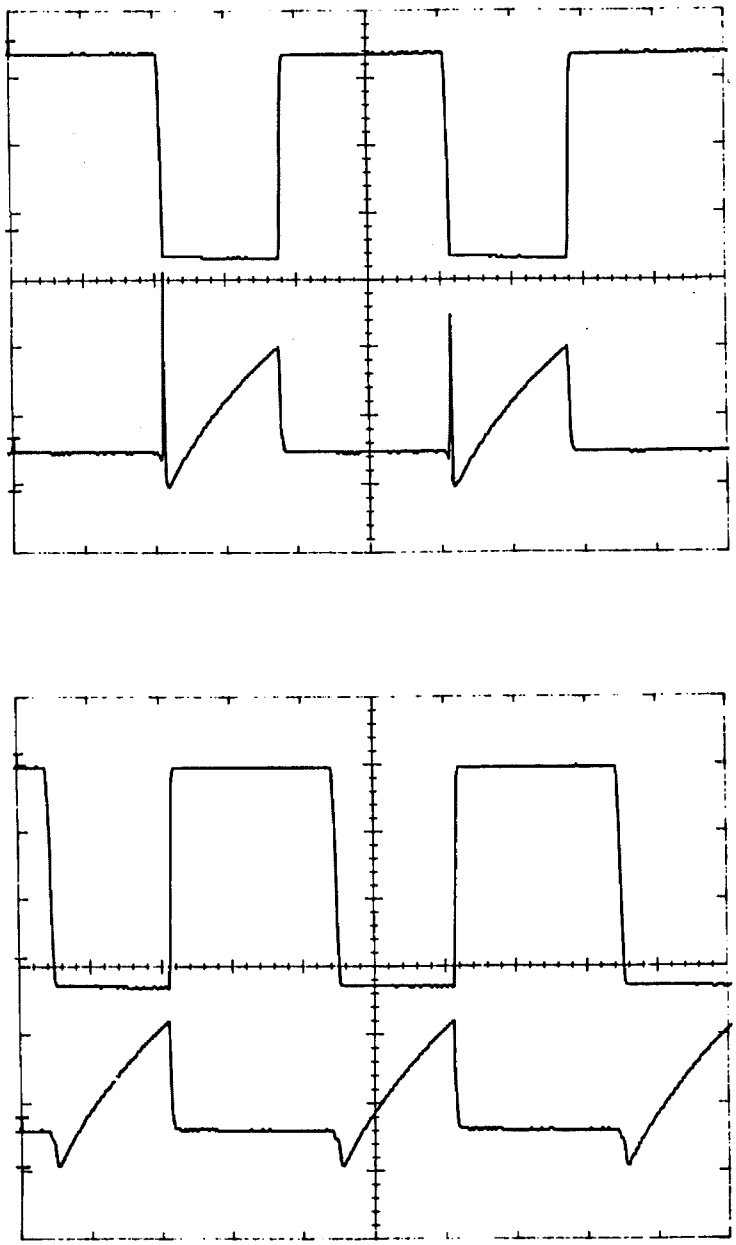

Figure 6.12: Switching waveforms of Q_1 without (a) and with (b) soft-switching. Voltage: 125V/div., current: 1A/div., Time: 5μs/div.

L_1 can be determined from

$$L_1 = \frac{M}{M-1}\frac{V_m^2 D^2}{4P_l f_s}. \tag{6.25}$$

The above results are obtained assuming no parasitics exist and 100% efficiency of power conversion.

6.6 Experimental Results

The input power factor is a function of voltage conversion ratio M as from Figure 6.6. Large M brings close to unity power factor but price is paid on peaky current i_1 and high voltage V_c so that high rating device is required and more loss is generated. M is chosen to be 2.7 in our circuit to ensure high power factor. The prototype built is shown in Figures 6.13, where the low-pass filter of L_f and C_f is placed between the bridge rectifier and front-end diode D_1 so that bridge rectifier only sees averaged line current and can be made of slow diode. Fluorescent lamp used is Sylvania Octron lamp (32W).

Drive circuits include conventional driver $DS0026$ and a simple polarized RC time delay network to generate the dead times tr_1 and tr_2 for soft-switching. Isolated drive for Q_2 is also provided in the drive circuit. Design is made based on the following data: M is 2.7, f_s is 50kHz, nominal lamp current i_l is 265mA and duty ratio is 0.4. Components used in the prototype: bridge rectifier: VH248, L_f: $180\mu H$, C_f: $1.5\mu F$, D_1: $50WF40F$, L_1: $880\mu H$, Q_1 and Q_2: $IRF840$, C: $10nF$, L_2: $2.40mH$, C_s: $31nF$, C_p: $5.0nF$, PWM controller: $UC3525$.

Major waveforms have been recorded and shown as follows. The input inductor current i_1 is shown in Figure 6.14 on the switching scale which clearly shows the DICM operation of the input inductor L_1. Current i_1 is averaged by the input low-pass filter L_f and C_f and unfolded by the bridge rectifier which results in the line current i_i nearly following the line voltage v_i as shown in Figure 6.15 on the line scale. On the other hand, low crest factor sinewave lamp current i_l is also achieved at the output by the LCC resonant circuit. Both lamp current i_l and lamp voltage v_l are shown on the different switching scale in Figure 6.16. It can be seen that lamp voltage and lamp current are in phase and lamp could be approximated as a resistance at the high frequency though

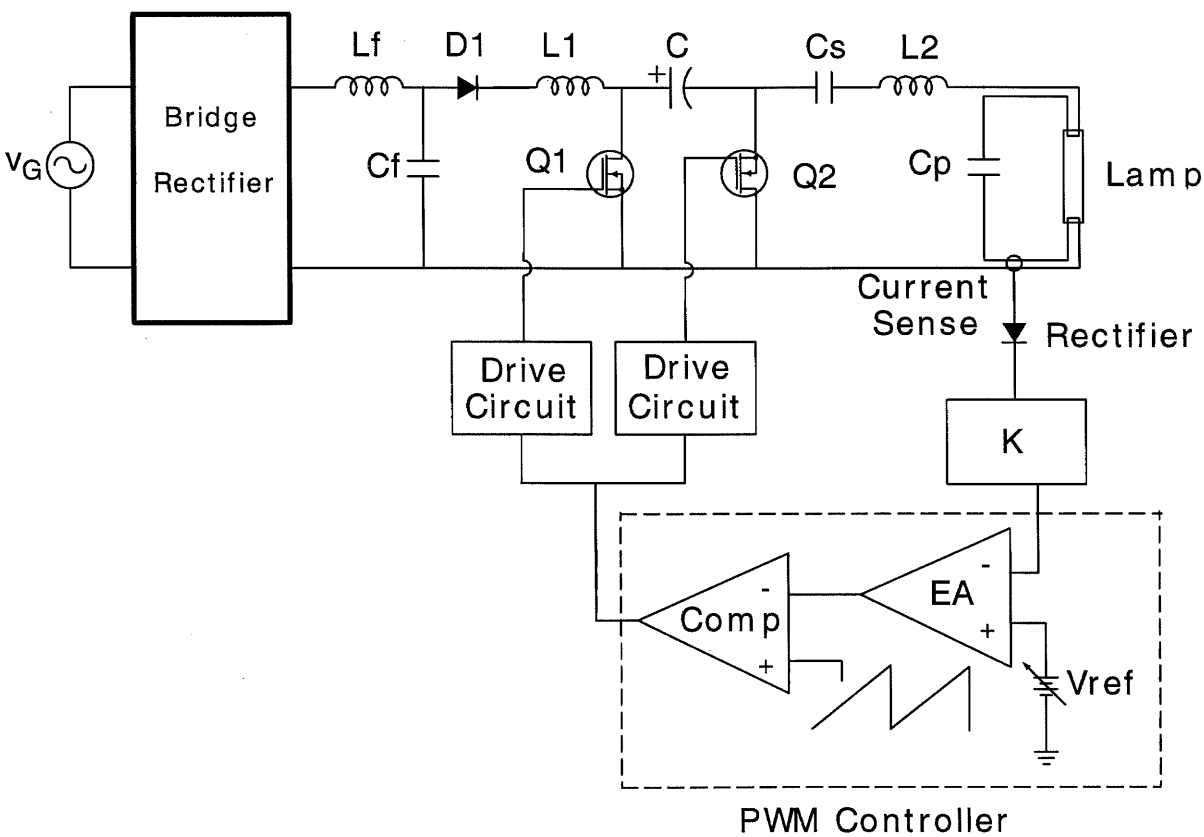

Figure 6.13: Experimental circuit.

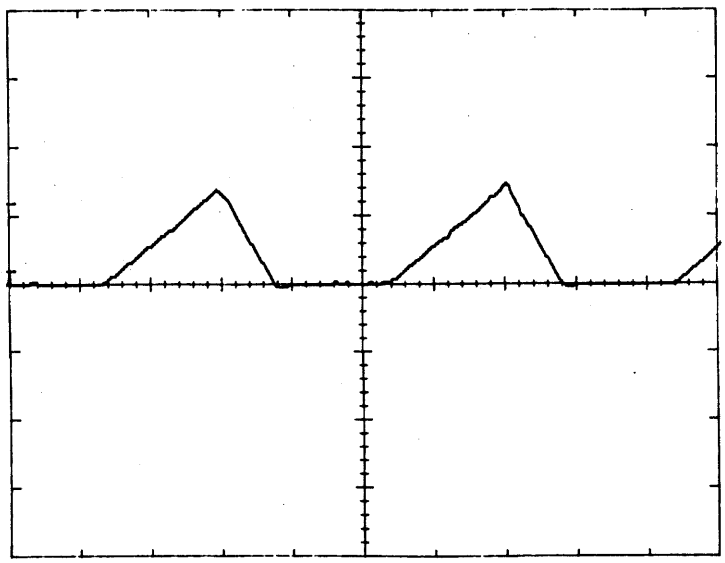

Figure 6.14: DICM operation of input inductor. Current: 1A/div., Time: 5us/div.

it is a function of the lamp current. Switch currents i_{Q1} and i_{Q2} are demonstrated in Figure 6.17, in which switch currents are the combination of the two inductor currents i_1 and i_2. It can be clearly seen that Q_2 has a large reverse current before its turn-ON due to the DICM operation of input inductor. The relatively small but critical reverse current comes from the resonant LCC matching network which makes Q_1 turn-ON at zero voltage and negligible current.

Major measured data are shown as follows. The major circuit loss comes from the two inductors L_1 and L_2 which experience substantial ac flux swing due to the respective resonant and DICM operation. The loss is measured at 1.2W for L_2 and 0.8W for L_1 based on the temperature rise when the input power is 40W. Drive circuit also consumes 1W power. The loss for the rest of the circuit is about 1W. The overall efficiency is estimated at 90%. Measured line frequency modulations on the lamp current are 13% for energy capacitor C of $10\mu F$ and 7% for C of $50\mu F$. Total harmonic distortion measured is less than 10% at the nominal lamp power. Measured power factor is above 0.99 due to the DICM operation of L_1 at high conversion ratio of $M = 2.7$.

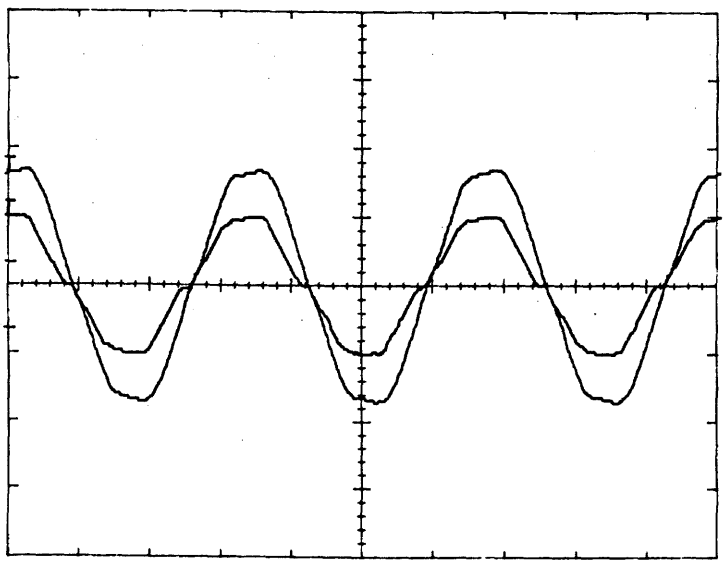

Figure 6.15: Input voltage (large waveform) and input current illustrate a high power factor of the front end. Voltage: 100V/div., current: 0.5A/div., time: 5ms/div.

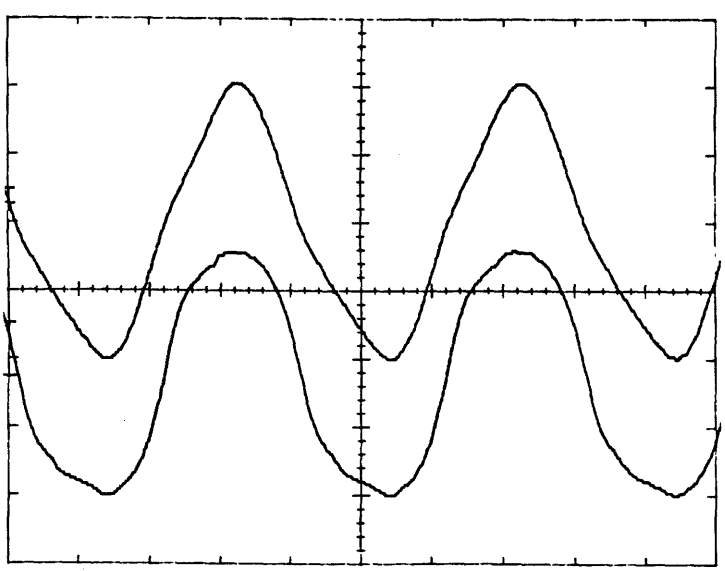

Figure 6.16: Fluorescent lamp voltage (upper) and current illustrate the desired low crest factor. Voltage: 100V/div., current: 0.2A/div., time: 5us/div.

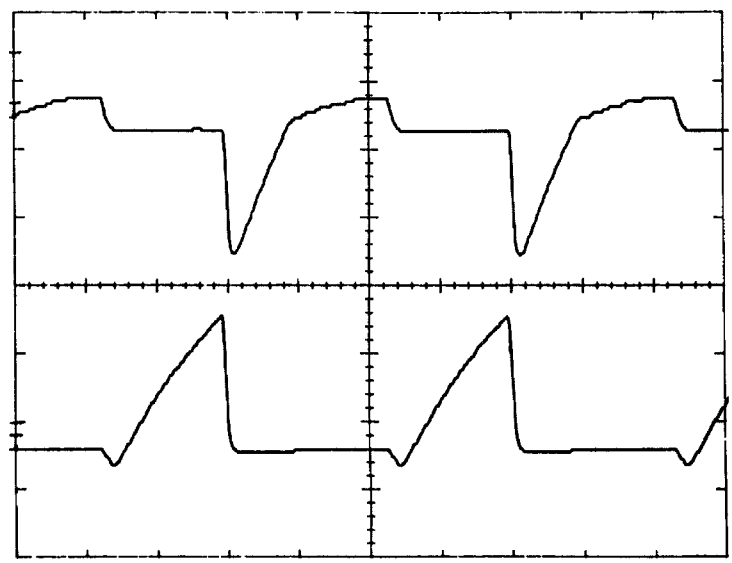

Figure 6.17: Switch currents of Q_1 (lower) and Q_2 indicate soft-switching feature. Current: 1A/div., time: 5us/div.

Chapter 7

Single Switch Unity Power Factor Lamp Ballasts

As another effort to further alleviate the compromise between the performance and the complexity, new single-switch ac-to-ac converters which are suitable for ballast applications are proposed based on the proper integrations of automatic current shapers and the single switch inverters, such as the Class E converter. The new circuits have the input part resembling its parent automatic shapers and the output part resembling the single switch inverter. The basic approach on which the new circuits are derived is introduced first. Prior to the derivations of new circuits, the operation of the Class E LCC ballast is illustrated and its soft-switching operation region is calculated and principles of automatic current shaping is briefly reviewed in Sections 2 and 3, respectively. The derivation of various single-switch, unity power factor lamp ballasts are then presented in Sections 4 and 5 followed by the description of the desirable mode of operation with illustration of major waveforms. Approximate analysis of the ballast circuits is given in Section 7. Section 8 demonstrates the experimental results.

7.1 Basic Approach

The single-stage, high power factor lamp ballast presented in the last chapter is derived from the Ćuk converter. The addition of a diode in series with the input inductor generates a new DICM mode operation, which decouples the input current-shaping from the high frequency output lamp ballasting function. Thus the ballast is also equivalent to an automatic boost current shaper loaded with an LCC resonant circuit.

More generally, it is recognized that more ballasts can be obtained by proper integrations of automatic current shapers and resonant inverters. The front-end automatic

current shapers provide the input current-shaping and internal energy storage and the resonant inverters offer a high frequency current source to drive the lamp. There are two advantages for automatic current shapers to be used in ballast applications. First, automatic current-shaping circuits perform current-shaping when the active switch operates at the constant duty ratio and switching frequency, which does not generate any extra line ripple when combined with resonant inverter. Second, the power level for a lamp ballast is usually below $100W$, which is within the range where automatic current shapers are applied without incurring large switch stresses. Proper integrations of the automatic shaper and resonant inverter can bring advantages from both sides into the combined circuit. For example, in Chapter 3, the single-stage high power factor ballast is a combination of boost automatic shaper and LCC inverter. By operating LCC network above resonance, soft-switching characteristics is inherited so that the combined circuit can shape the input current without switching losses.

Most automatic current shapers consist of a single active switch. Proper integrations of automatic current shapers and single-switch inverters such as Class E converter will generate new single active switch, ac-to-ac converters which are suitable for ballast applications as shown in Figure 7.1. As a result, the new circuits have the input part which resembles various automatic current-shaping circuits and the output part which resembles the Class E or other single switch inverters. Therefore, unity power factor lamp ballasts can be implemented by using a single active switch with the advantage of its compact structure. In addition, soft-switching feature is also retained from the Class E operation.

Prior to the derivation of new single switch, ac-to-ac converters, operation principle of the Class E converter and its soft-switching region will be introduced, followed by the presentation of automatic current shapers.

7.2 Class E Converter

The Class E converter [33] can be used as a ballast when a resonant matching network (LCC) is employed as shown in Figure 7.2. The dc voltage input V_{dc} connects a current bi-directional switch Q through a feed choke L_e, a resonant capacitor C_e is across the

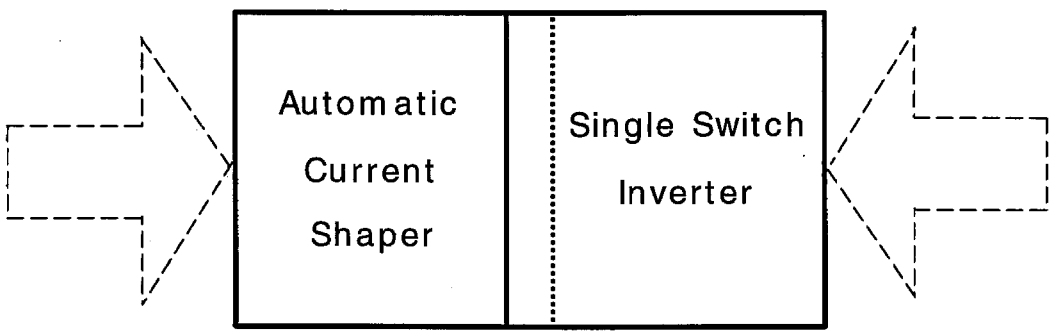

Figure 7.1: Basic approach: combination of automatic current shapers and single-switch inverter.

switch Q, an LCC resonant matching network with lamp load R_l is also placed across the switch Q.

The basic Class E converter has a single-switch configuration. The switch waveforms change in a resonant fashion so that in its ideal operating mode there is no switching losses. Figure 7.3 shows the major switching waveforms. When switch Q turns OFF, capacitor C_e delays the rise of switch voltage v_{ce} and thus reduces the overlap between the switch voltage and current. Therefore, turn-OFF loss is basically eliminated. v_{ce} rises initially and the resonant matching network is designed in such a way that v_{ce} eventually falls back to zero. The switch Q turns ON after v_{ce} drops to zero. So there is no turn-ON loss either. Because of this "lossless switching" operation, Class E converter is suitable for high frequency applications where switching losses are a major obstacle.

The Class E converter has a compact structure because of the tight correlations between its components. However, this inter-dependent relationships between its components impose a difficulty on the analysis of the fifth-order system. The object of the analysis is to derive the soft-switching region in the output plane for the ballast design

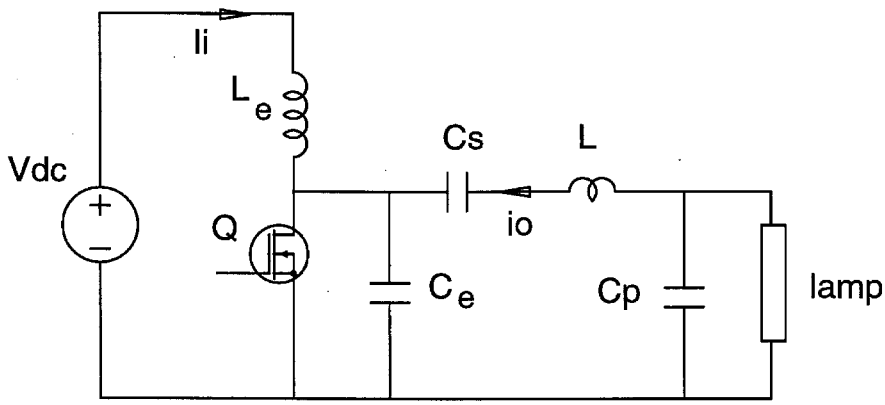

Figure 7.2: Class E converter used as a lamp ballast.

in Figure 7.2. To generate results of acceptable complexity, certain simplifications have to be made as follows [34]:

Inductor L_c is large enough to convert the dc voltage V_{dc} into a dc current I_i. LCC resonant network is highly selective and the current i_o flowing through it can be approximated by the fundamental component $i_c cos(\omega_s t) + i_s sin(\omega_s t)$ where ω_s is the angular switching frequency.

Other notations in Figure 7.3 are, α: interval (expressed in radians) when Q conducts positive current. Γ: interval (expressed in radians) when Q does not conduct either positive or negative current. D: duty ratio of the drive signal to Q.

The conditions of ideal (soft-switching) operation in terms of α and Γ are

$$\Gamma \leq 2\pi(1 - D) \tag{7.1}$$

and

$$\alpha \leq 2\pi D. \tag{7.2}$$

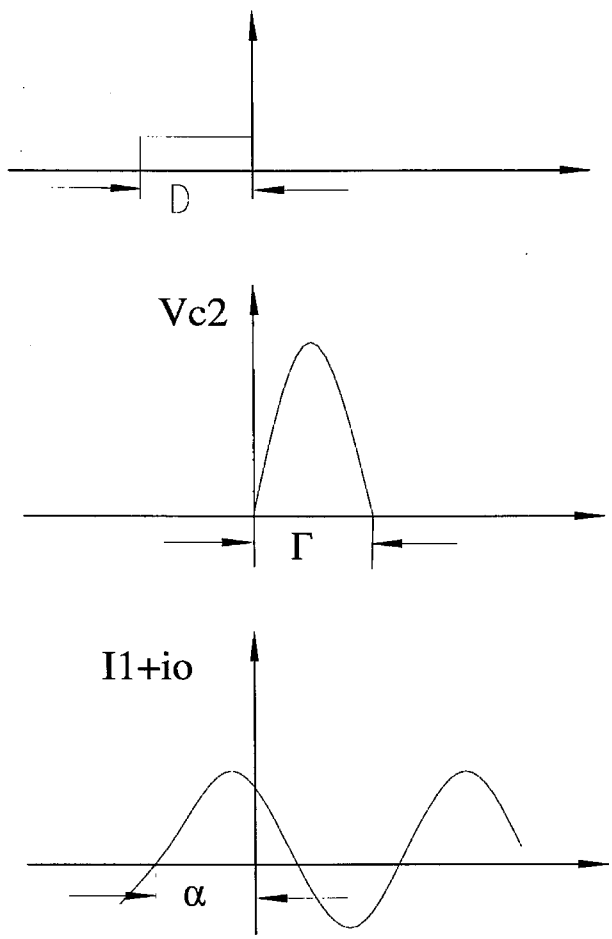

Figure 7.3: Major switching waveforms in the Class E converter.

In our case, it is assumed that the duty ratio is 50%. The above two constraints become

$$\Gamma \leq \pi \tag{7.3}$$

and

$$\alpha \leq \pi. \tag{7.4}$$

The combination of LCC network and lamp load R_l gives a complex impedance Z_i to the Class E switching cell:

$$Z_i = A + jB \tag{7.5}$$

where

$$A = \frac{R_l}{1 + (\omega_s C_p R_l)^2} \tag{7.6}$$

and

$$B = \omega_s L - \frac{1}{\omega_s C_s} - \frac{\omega_s C_p R_l^2}{1 + (\omega_s C_p R_l)^2}. \tag{7.7}$$

Calculations of the two boundaries for the soft-switching region in the normalized output plane are described next (Detailed derivations are shown in Appendix B).

The first boundary $\Gamma = \pi$ in the normalized output plane can be found through the following procedures: Step through load R_l, then solve for the switching frequency ω_s through equation

$$A'^2 + B'^2 = B' \left(\frac{\pi^2 - 4}{\pi^2} \right) - \frac{\pi^2 - 8}{4\pi^2} \tag{7.8}$$

where

$$A' \equiv \frac{A}{\omega_s C_e}, \tag{7.9}$$

$$B' \equiv \frac{B}{\omega_s C_e}. \tag{7.10}$$

Then the normalized current i_c/I_i can be calculated from

$$\frac{i_c}{I_i} = \frac{\pi(B' - 0.5) + 4/\pi}{2A'}. \tag{7.11}$$

The normalized load current i_R/V_{dc} in the unit of conductance is available from

$$\frac{i_R}{V_{dc}} = 1/\sqrt{0.5 A R_l \left[\left(\frac{i_c}{I_i} \right)^2 + \frac{\pi^2}{4} \right]}. \tag{7.12}$$

The second boundary $\alpha = \pi$ is determined via the following procedures: Step through Γ from 0 to π, solve for the switching frequency ω_s and load R_l from the following two equations:

$$A' = \frac{1}{2\pi} \frac{g_1(\Gamma)}{g_3(\Gamma)} \tag{7.13}$$

$$B' = \frac{1}{2\pi} \frac{g_2(\Gamma)}{g_3(\Gamma)} \tag{7.14}$$

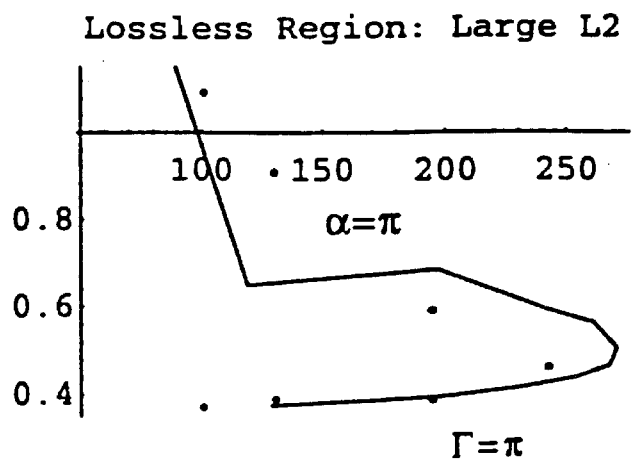

Figure 7.4: Boundaries of soft-switching region for the Class E converter.

where

$$g_1(\Gamma) = (\Gamma^2 cos\Gamma + \Gamma^2 + 4cos\Gamma - 4)(cos\Gamma - 1) \tag{7.15}$$

$$g_2(\Gamma) = \Gamma^3 - \Gamma^2 sin\Gamma cos\Gamma + 2\Gamma^2 sin\Gamma + 2\Gamma cos\Gamma - 2\Gamma + sin2\Gamma - 2sin\Gamma \tag{7.16}$$

$$g_3(\Gamma) = \Gamma^2 + 2\Gamma sin\Gamma + 2 - 2cos\Gamma. \tag{7.17}$$

The normalized load current i_R/V_{dc} is given by

$$\frac{i_R}{V_{dc}} = 1/\sqrt{0.5AR_l\left[\left(\frac{i_s}{I_i}\right)^2 + 1\right]}. \tag{7.18}$$

Based on the above procedures, boundaries of the soft-switching region (inside) can be calculated for a given LCC circuit as shown in Figure 7.4, where horizontal axis is load R_l and vertical axis is load current i_R (for $V_{dc} = 190V$). Figiur 7.4 also shows good fit between calculation (linked line) and experimental data points.

Fluorescent lamp can be approximated as a pure resistance R_l at the high frequency operation. The resistor R_l is a monotonically decreasing function of lamp current i_l due

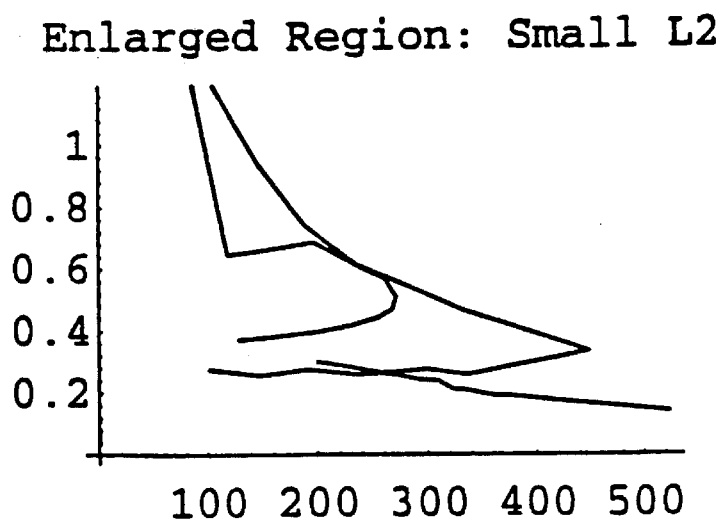

Figure 7.5: Boundaries of soft-switching region for Class E converter and lamp resistance are shown in the converter output plane.

to its negative impedance characteristics. When the lamp is given, LCC network can be designed to place its operating point inside the soft-switching region.

To assure voltage stress is minimum, operating point is generally placed close to the $\Gamma = \pi$ boundary. When the inductor L_e is reduced to the same order of magnitude as the resonant component, its ripple current allows an enlarged soft-switching region compared to the ideal case as shown in Figure 7.5 ($V_{dc} = 190V$). The lamp resistance is overlaid in the output plane to determine the operating point also shown in Figure 7.5.

7.3 Automatic Current Shapers

Some dc-to-dc converter topologies, when in their ac-to-dc applications and operated in DICM, yield unity or near-unity power factor without intelligent control. That is, the average input current is proportional to the input voltage even when the control (switching frequency and duty ratio) is held constant. In this sense, they are also called "automatic current shapers."

Automatic current shapers have been studied extensively [20] [35] [36] [37] [38]. They

can be divided into two categories according to how closely the input current follows the input voltage. The input current quality of one kind of automatic current shapers depends on the voltage conversion ratio $M = V_o/V_m$, like boost converter [20] [37]. High power factor is obtained at the price of high voltage conversion ratio, so they are also called "non-ideal" current shapers. Another kind of current shapers always have unity power factor, no matter what the voltage conversion ratio is, like buckboost (or flyback shaper) [20] [35].

The buckboost current-shaping converter and its inductor current i_L during a single switching period in DICM are shown in Figure 7.6. The input current i_i is the average of the rising slope of the inductor current i_L, that is

$$i_i = \frac{D^2 T_s}{2L} v_i \tag{7.19}$$

is therefore exactly proportional to v_i. Phsyically, the peak value of inductor current i_L during a single switching cycle is modulated by the instantaneous input voltage, so the area under the rising slope of i_L is proportional to the input voltage. In boost converter, input current is the average of entire i_L which consists of both parts of rising slope in $D_1 T_s$ interval and decreasing slope in $D_2 T_s$ interval. Since the $D_2 T_s$ interval is not fixed (also modulated by v_i), the input current $< i_i >$ does not exactly follow the input voltage.

Boost or flyback converter has a discontinuous input current. A low-pass filter has to be placed in front to remove the switching ripple and extract the average value. Another type of current shapers, which have two inductors in themselves, have continuous input current even operated in DICM. This is because the DICM operation is defined in terms of sum of two inductor currents and the inductor with smaller value will carry more switching ripple. Thus by choosing a large inductor at the input side input current will be continuous even without extra filtering. In addition, the two inductors can be coupled in such a way that all the switching ripple is steered away from the input side and no extra filtering is needed. Ćuk converter [38] belongs to this category. To illustrate the above situation, Ćuk current-shaping converter and its inductor currents i_{L1} and i_{L2} during a single switching period in DICM are shown in Figure 7.7. It can be shown that

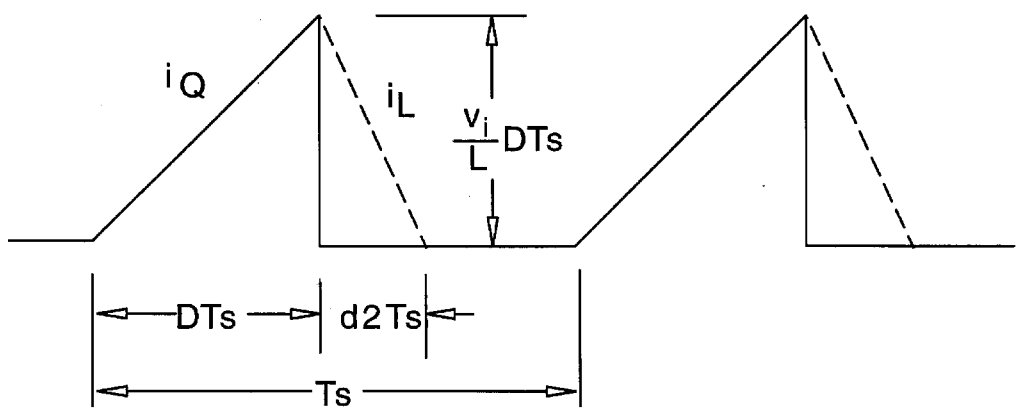

Figure 7.6: Inductor current waveform in buckboost current-shaping circuit.

input current [38] is:

$$i_i = \frac{D^2 T_s}{2L_e} v_i \tag{7.20}$$

where

$$L_e = L_1 // L_2.$$

So it is also an ideal current shaper just like buckboost circuit. Note the converters to which coupling inductance technique can be applied must at least have two inductors. They seem to be more complicated than the single inductor current-shaping circuits. But reflect on the fact that in single inductor converter extra filtering is always needed so the same number of reactive components are still maintained in both cases.

Major automatic current shapers are summerized in Figure 7.8.

The automatic current shapers introduced above operate based on the fact that the peak value of inductor current i_L during a single switching period is proportional to the instantaneous input voltage v_i. The inductor current waveform during a switching period is triangular, so it is straightforward to yeild the proportional or near proportional

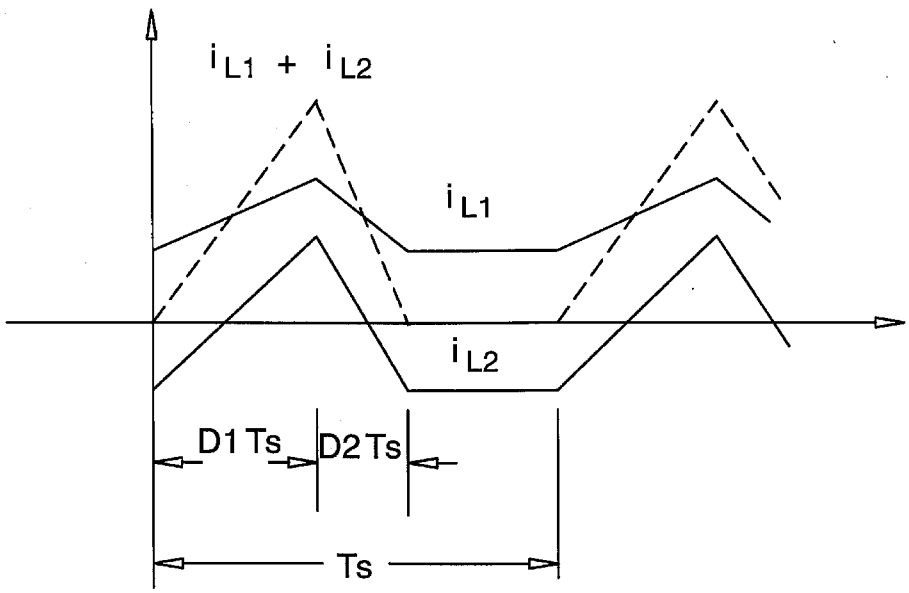

Figure 7.7: Inductor current waveforms in Ćuk current-shaping circuit.

relationship between the input voltage and input current. More generally, automatic current-shaping concept can be extended to a broader case when the peak value of inductor current i_L follows or nearly follows the input voltage even if the inductor current waveform is more complicated. Accordingly, coupling inductance technique can be applied to any inductors as long as they share a proportional voltage.

7.4 Derivation of New Topologies

New single-switch, ac-to-ac converter topologies are derived by proper combinations of the Class E converter and automatic current shapers, which are described in the last two sections, respectively.

A single switch high power factor ballast was first presented in [39] which is a combination of boost automatic current shaper and Class E converter as shown in Figure 7.9. Boost converter has a voltage conversion ratio larger than 1. When it is operated in the discontinuous inductor current mode (DICM), its output voltage (V_{c1}) has to be at least two times higher than the peak input (line) voltage as to maintain power factor close

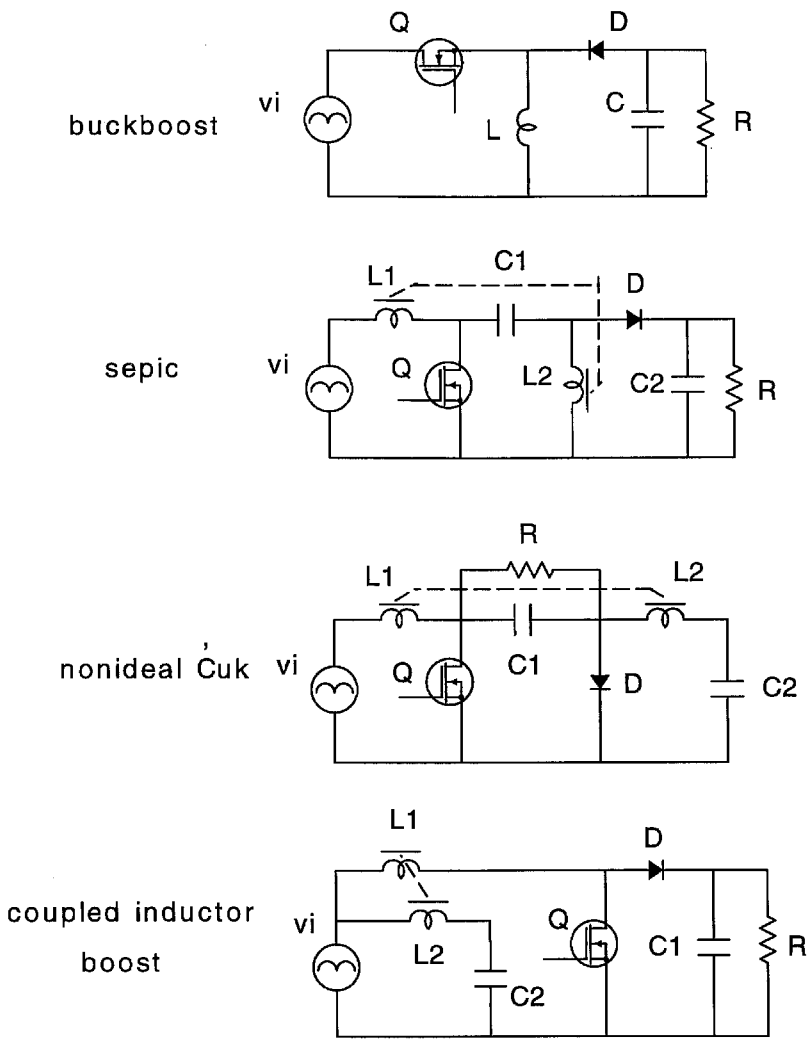

Figure 7.8: Some PWM automatic current shapers.

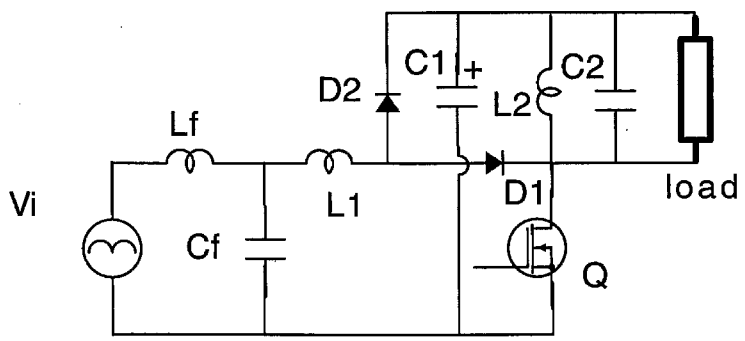

Figure 7.9: Previously proposed single switch ballast is a combination of boost shaper and Class E converter.

to unity, which may impose an unreasonably high voltage stress on the single switching device Q when the Class E converter operation is also taken into account.

Based on the similar reasoning, new circuits can be also derived by combining other automatic current shapers with the Class E converter. A new single switch unity power factor inverter is thus obtained as shown in Figure 7.10(a), which is a proper combination of buckboost automatic current shaper and the Class E converter. The proposed ballast physically consists of four parts: input network, power conversion stage, matching network and controller.

The input network of L_f, C_f and bridge rectifier provides rectified sinewave voltage and simultaneously averages and unfolds the up-ramp of the input inductor current i_1 to yield the bidirectional sinewave line current. The power conversion stage includes fast diodes D_1 and D_2, input inductor L_1, active switch Q, energy storage and transfer capacitor C_1, resonant capacitor C_2 and inductor L_2. The conversion stage converts the rectified line voltage from the input network to the high frequency pulsed half sinewave voltage, which is in turn converted by the matching network of L, C_s and C_p into the

necessary sinewave current source to drive the lamp. Functionally, L_1, Q, C_1, D_1, D_2 and input filter of L_f and C_f constitute an input part of the circuit which resembles a buckboost converter and C_1, Q, C_2, L_2 and the LCC matching network form an output part of the circuit which resembles a Class E converter.

It is well-known that DICM buckboost converter functions as an ideal resistor emulator when its active switch is operated at the constant switching frequency and duty ratio, i.e., unity power factor is automatically obtained despite its output voltage V_{c1} as long as the input inductor current i_1 is operated in DICM mode. Hence the voltage stress for the single switching device Q is considerably lower in the new circuit. Zero-voltage turn ON and OFF characteristics in Class E converter are retained by utilizing the resonance between C_2 and the resonant matching network so that the switching losses at high frequency operations are eliminated. Energy transfer capacitor C_1 provides the necessary internal energy storage so that lamp current contains negligible line frequency modulation.

Another new circuit in this class is derived by disconnecting the diode D_2 in the circuit of Figure 7.10(a), which is shown in Figure 7.10(b), where Z_{ac} is an ac load representing LCC network and lamp load R_l. The current shaping function in this circuit is performed by the "non-ideal DICM boost operation" in such a sense that when the switch Q is OFF, input inductor L_1 is connected completely to the approximate half sinewave voltage source v_{c2} as opposed to the stiff DC voltage source V_{c1} as in the "ideal" boost converter. Its parent automatic current shaper is shown in [40] which is a good automatic current shaper even if the input current can not be easily derived as a function of input voltage. A current-fed pushpull inverter can be derived by paralleling two Class E converters and driving them out of phase. Based on this, anothor topology is derived by paralleling the two circuits of Figure 7.10(b) as shown in Figure 7.10(c), where its output part of this circuit resembles a current-fed pushpull inverter and the input part resembles an interleaved "non-ideal DICM boost current shaper."

Combinations of coupled-inductor automatic current shapers with Class E converter result in further additions to this family as shown in Figures 7.10(d) (e) (f) (g) (h). In each case, the input part of converter has the same number of reactive components

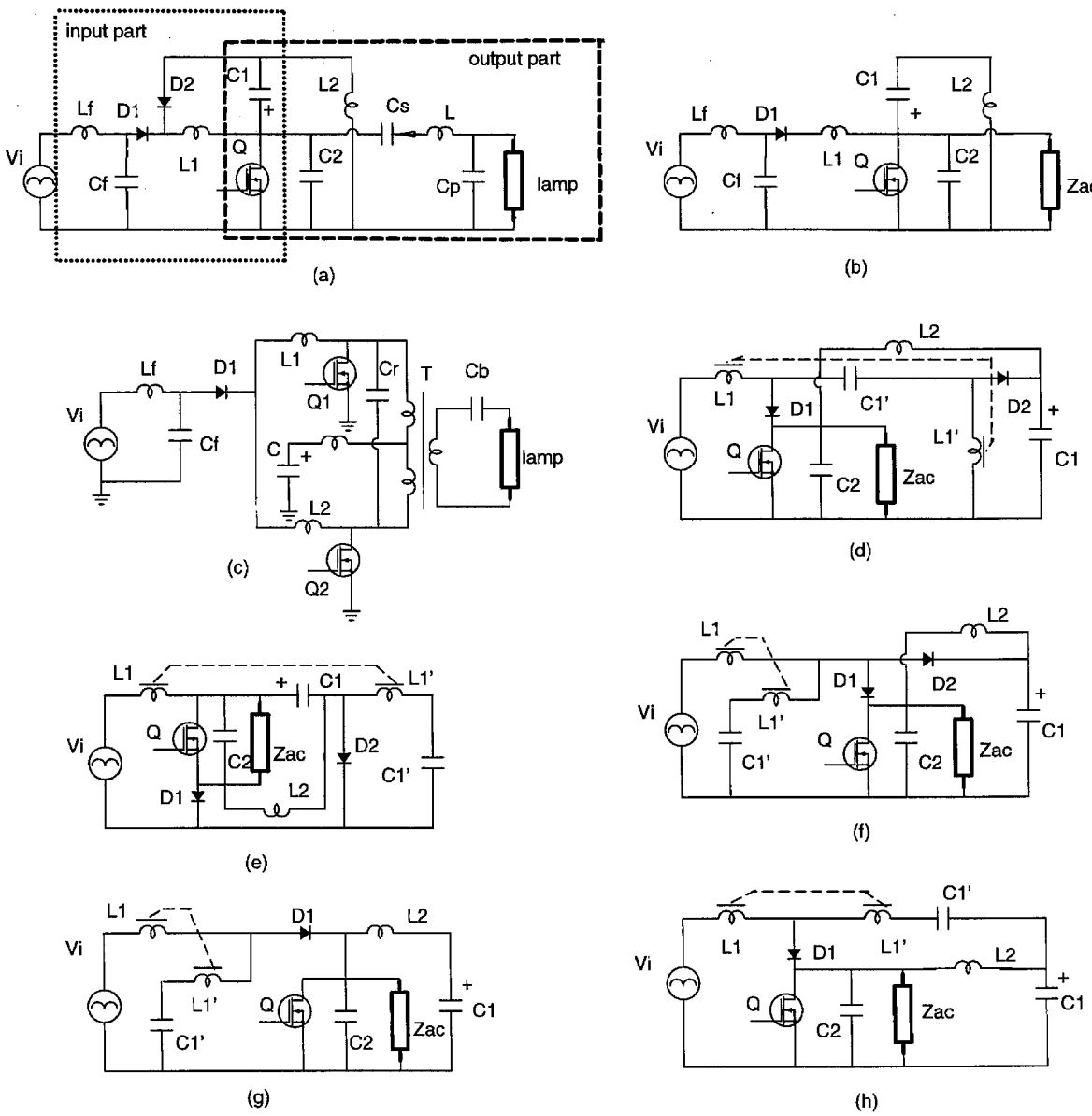

Figure 7.10: Proposed single-switch, unity power factor, lamp ballasts.

which resembles coupled inductor versions of SEPIC, Ćuk, boost, and nonideal boost converters, respectively. Circuit in Figure 7.10(g) can also be derived by disconnecting diode D_2 in the circuit of Figures 7.10(d) or (f). Circuit in Figure 7.10(h) can be derived by disconnecting diode D_2 in the circuit of Figure 7.10(e). The two inductors are coupled such that switching ripple on the input inductor is zero, and slight or no input filtering is needed. Isolated converters can be obtained by inserting transformer in the resonant matching networks.

Advantages of the Class E converter include single-switch configuration and soft-switching. But the switch has to stand about π times the DC input voltage, which for off-line applications, such as the ballast, may be a serious problem. Other single switch configurations which impose relatively lower voltage stress on the switching device is also applicable for ballast in the event that lower rating switch is more favorable than soft-switching, as shown in next session.

7.5 Other Single Switch Unity Power Factor ballasts

Another example of single switch inverter is forward inverter as shown in Figure 7.11. The inverter has a three winding transformer where the first winding is connected between the dc bus and the power switch, the second winding and the diode is to clamp switch OFF voltage to be less than π times V_{dc}, and the third winding is to provide the isolation. The switch duty ratio is less than 0.5. If turns ratio of first two windings is 1, then the switch voltage stress is $2V_{dc}$. If isolation is not a requirement, the resonant matching network and lamp can be connected directly to the second winding. Compared to the Class E converter, forward inverter has less voltage stress for the switch but loses the soft-switching feature.

Another family of single switch high power factor circuits is derived by proper integrations of automatic shapers and forward inverter as shown in Figure 7.12.

Combination of buckboost current shaper and forward inverter results in the circuit of Figure 7.12(a). Another circuit is derived by disconnecting diode D_2 in the circuit of Figure 7.12(a), which is shown in Figure 7.12(b), where again Z_{ac} is an ac load representing LCC network and lamp load R_l. The third circuit is generated by integrating

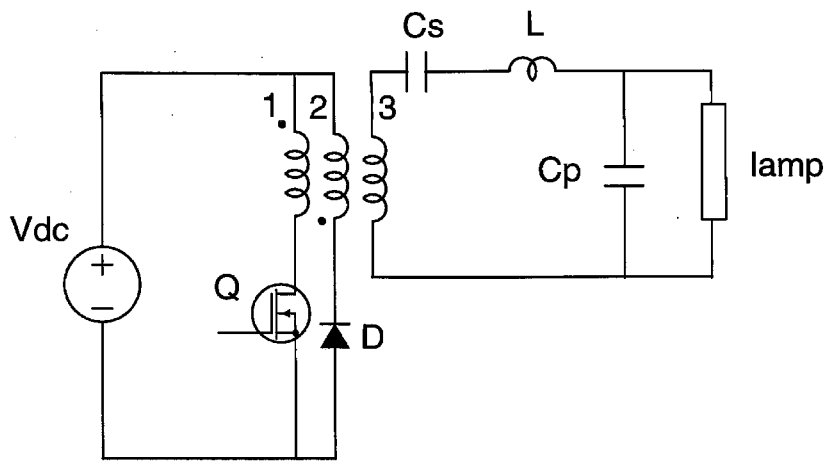

Figure 7.11: Forward inverter used as a lamp ballast.

boost current shaper and forward inverter as shown in Figure 7.12(c).

Combinations of coupled-inductor automatic current shapers with forward inverter result in further additions to this family as shown in Figures 7.12(d) (e) (f) (g). In each case, the input part of converter has the same number of reactive components which resembles coupled inductor versions of SEPIC, Ćuk, and boost converters, respectively. Circuit in Figure 7.12(g) can be derived by disconnecting diode D_2 in the circuit of Figures 7.10(e). The two inductors are coupled in such a way that switching ripple on the input inductor is steered away thus slight or no input filtering is needed.

7.6 Desirable mode of Operations

It has been shown that the new converter can be derived by properly combining automatic current shaper and single switch inverter. The operation of the combined converter is, nevertheless, not of simple cascade of two functionally different parts. For example, automatic shaper is mainly operated with squarewave voltage while the Class E converter is switched with resonant (half sinewave) voltage. When two circuits are

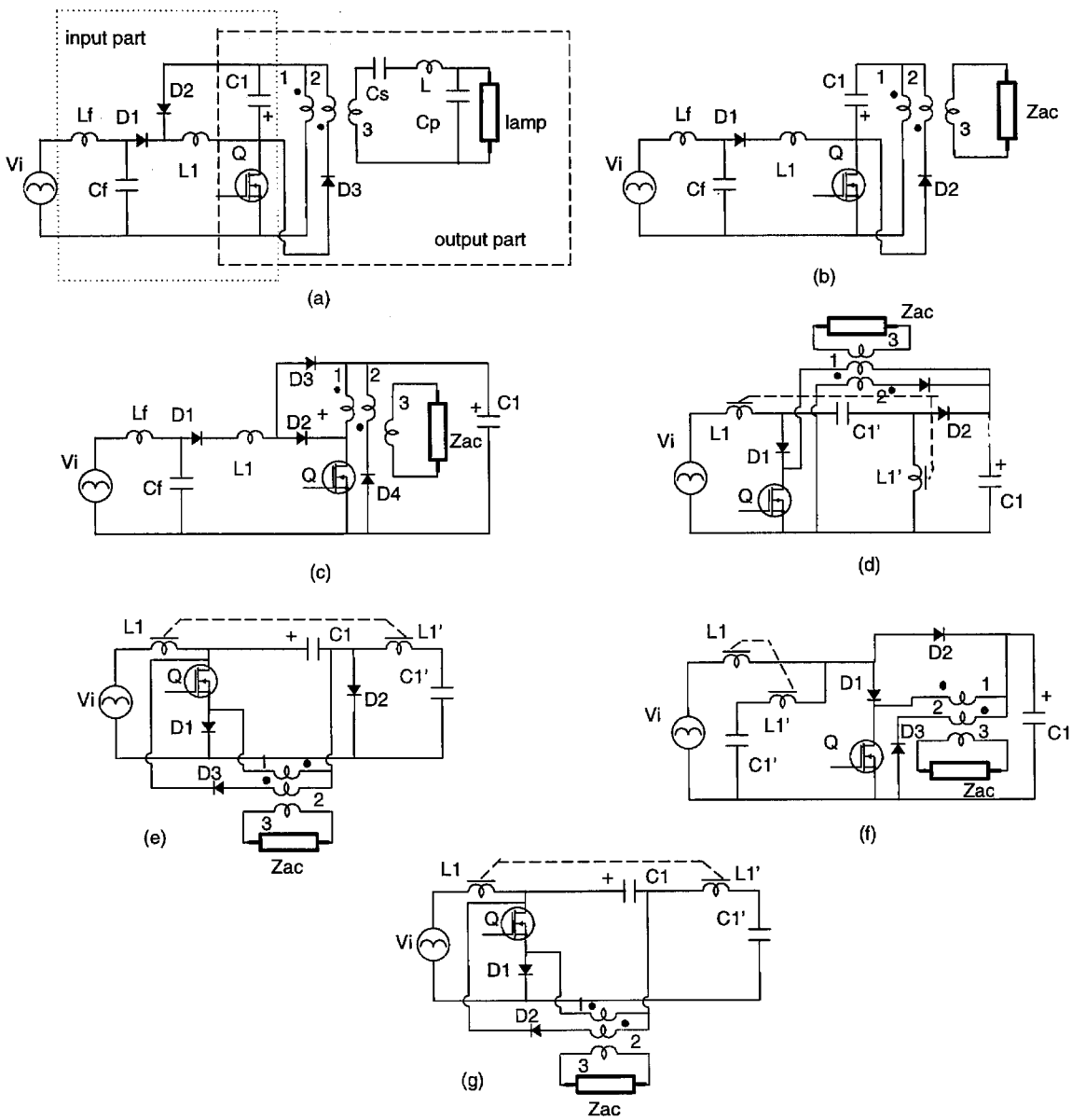

Figure 7.12: Another family of proposed single-switch, unity power factor, lamp ballasts.

combined, new operating modes appear owing to the interactions between them, which makes the circuit operation rather complicated.

In this section, as a typical example, operation of the proposed circuit in Figure 7.10(a) is described with its major waveforms both during a single switching period and in a line period. It will be shown that when buckboost automatic current shaper and the Class E converter are combined, certain interactions occur between them. As a result, the input part of the combined circuit merely resembles but no longer functions exactly like its parent converter; neither does its output part.

Several operating modes exist in the proposed circuit, where the desirable mode occurs when the input inductor L_1 is less than its critical value so that i_1 is discontinuous and input part of the circuit resembles the automatic current shaper. Only the preferred mode of operation is described here. Complete operation of the circuit in Figure 7.10(a) comprises six switching intervals during one switching period as shown in Figure 7.13. The cycle starts when the active switch Q turns OFF. The resonant capacitor C_2 is charged by resonant current i_o and input inductor current i_1. The voltage v_{c2} increases almost linearly to $V_{c1}+\sqrt{2}|v_i|$ and the diode D_2 closes and D_1 opens at the time t_1. Now the energy storage capacitor C_1 is placed across the input inductor L_1, its current i_1 decreases linearly to zero due to the DICM operation and diode D_2 opens at t_2. Meanwhile, switch voltage v_{c2} changes in the resonant way. When v_{c2} drops below the input voltage $|v_i|$ at time t_3, diode D_1 turns ON again and inductor current i_1 starts to flow. After the v_{c2} drops to zero at time t_4, the full line voltage is applied to the input inductor L_1 and its current i_1 increases linearly. The active switch Q can be turned ON at zero voltage at t_5. The next cycle starts when the switch Q turns OFF at T_s.

Several things make the combined circuit different from its parent circuits due to the interactions between the input and output parts. First, the input voltage $|v_i|$ is rectified sinewave $V_m sin\omega_l t$. When $|v_i|$ is low, the peak value of i_1 is also low so that i_1 can be discharged to zero even before v_{c2} rises to $V_{c1}+v_i$. Hence the switching intervals $0-t_1-t_2$ do not even exist when $|v_i|$ is low. In that case, the two intervals are reduced to one interval that ends when the i_1 is discharged to zero and D_1 turns OFF. The above variation of operation during a line period causes a certain amount of line ripple on top

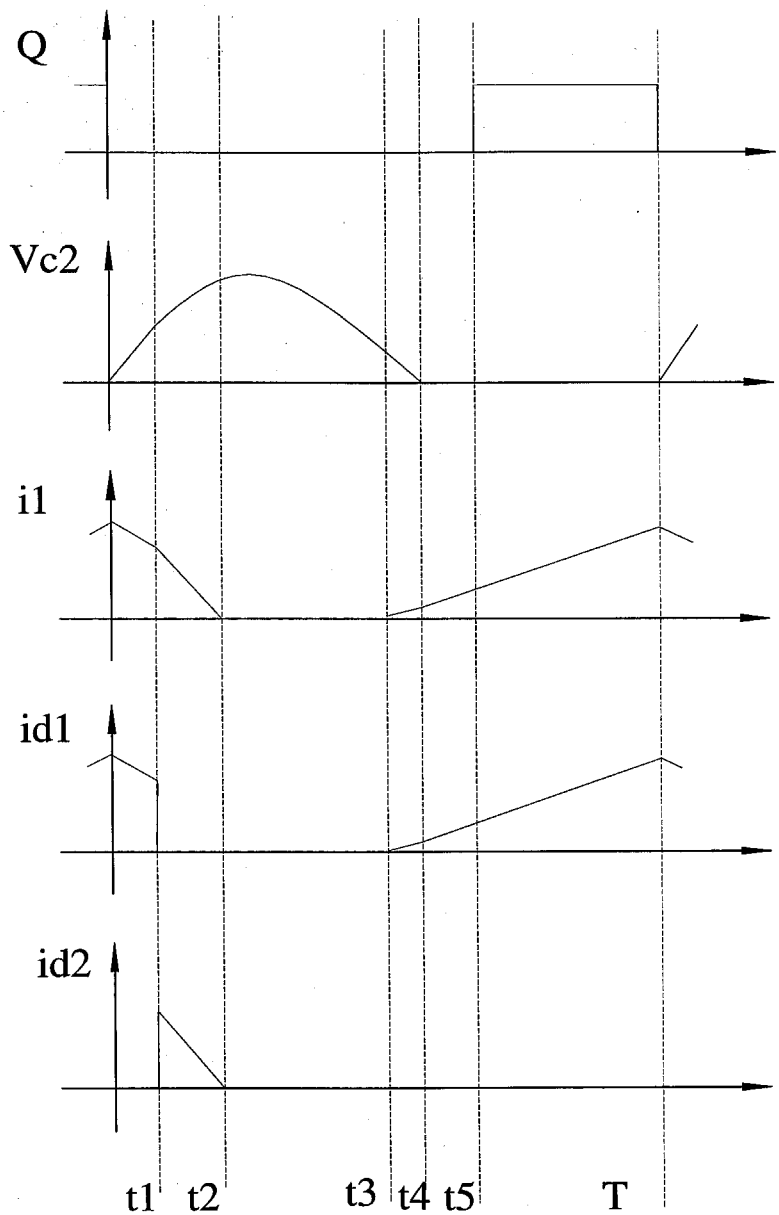

Figure 7.13: Major switching waveforms in the circuit of Figure 7.9(a).

of the voltage v_{c2} and on the converter output. Second, the charging of the resonant capacitance C_2 after Q turns OFF consumes part of the input inductor current i_1 when $|v_i|$ is high and all the current when $|v_i|$ is low which should otherwise charge capacitor C_1 in the event of buckboost converter. Third, the existence of the switching interval $t_3 - t_4$ makes input inductor current i_1 start to rise at a different time which makes the effective duty ratio variant and larger than it is desired. In addition, the early rise of i_1 (especially when $|v_i|$ is high) delays v_{c2}'s drop-back to zero so that the time t_4 is also variant resulting in a reduced soft-switching region. The above interactions make the input current shaping part of the circuit deviate from its parent current shaper. The output part of the circuit is also degraded owing to the superimposed line ripple and reduced soft-switching region. However, the desirable DICM operation of L_1 will keep the above interactions to the minimum since during $t_3 - t_4$ interval current i_1 is still close to zero.

Major waveforms on the line scale are shown in Figure 7.14 to further illustrate the circuit operation. The inductor current i_{L1} in DICM operation is modulated by the rectified input voltage $|v_i|$ as shown in Figure 7.14(a). As demonstrated in Figure 7.13, when $|v_i|$ is high, i_{L1} is equal to the i_{D1} during the interval $t_3 - t_4 - t_5 - T_s - t_1$ and is equal to the i_{D2} during the interval $t_1 - t_2$, which is shown in Figure 7.14(b) and (c) on the line scale. When line voltage $|v_i|$ is cycled to a lower value, interval $0 - t_1 - t_2$ does not exist and i_{D1} is equal to i_{L1} while i_{D2} remains zero. From perspective of line scale, input part of the circuit tends to be a buckboost automatic current shaper when line voltage $|v_i|$ is close to its peak and resembles a boost automatic current shaper when line voltage $|v_i|$ is close to zero. Qualitatively, the operation of the input part of the circuit is somewhere between a buckboost and a boost automatic current-shaping circuit. Since the peak value of i_{D1} is modulated by the input voltage $|v_i|$, the input current i_i, which is the average of current i_{D1}, therefore closely follows the input voltage $|v_i|$ as shown in Figure 7.14(a). The resonant voltage v_{c2} also carries a small amount of line ripple due to the above interactions as shown in Figure 7.14(d), which is passed on to the lamp current waveform as shown in Figure 7.14(e).

The complexity of the switching intervals in the described operating mode makes

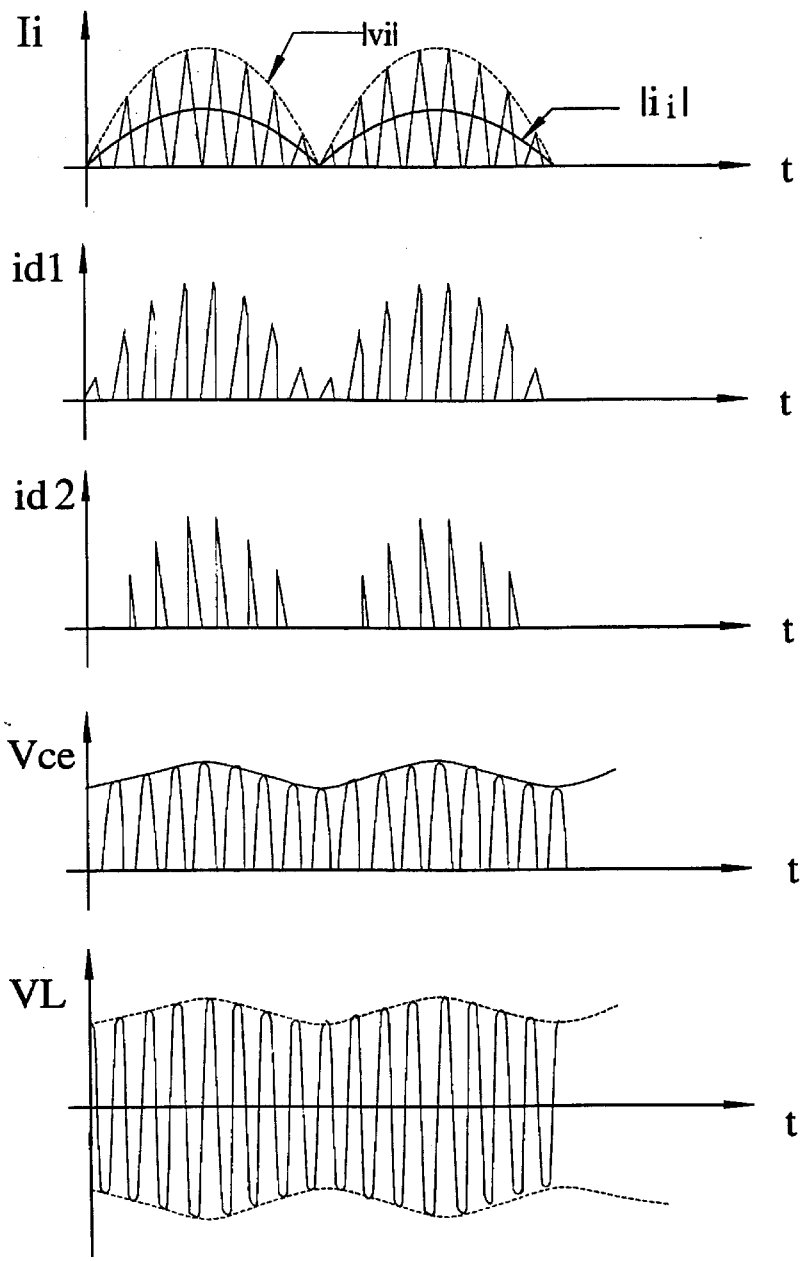

Figure 7.14: Major waveforms in the circuit of Figure 7.9(a) on line scale.

the exact analysis of the whole circuit rather difficult. Despite the above effects, certain assumptions can still be made based on the practical situations, which give acceptable results. More accurate analysis has to rely on computer simulations.

7.7 Analysis Considerations

As a first order approximation, the combined circuit is decoupled into the input and output part. The input part determines the converter power factor and stress for the switching device. The output part determines the soft-switching operation region and lamp operating point.

The right mode for input current shaping is to operate input inductor L_1 in DICM so that the input part resembles its parent automatic current shaper. The voltage across the switch v_{c2} is not a squarewave so that input inductor current i_1 no longer starts to rise uniformly at switch turn ON but sometimes before v_{c2} drops to zero, determined by

$$v_{c2} = |v_i|. \tag{7.21}$$

As $|v_i|$ is different for each switching period, the effective conduction duty ratio for i_1 is variant and larger than 0.5 even if the switching duty ratio D is 0.5. At the boundary between DICM and CCM, the conversion ratio $M = V_{c1}/V_m$ for the input part of circuit is approximately twice that of buckboost current shaper ($M = 1$ for $D = 0.5$) since the effective duty ratio is significantly increased. As a direct result, the voltage stress is approximate $2\pi V_m$ for $D = 0.5$.

Input inductor L_1 for this circuit can be determined by the first order equation:

$$L_1 \simeq \frac{0.6^2 V_m^2}{2P_l f_s} \tag{7.22}$$

where P_l is the nominal lamp power and f_s is the switching frequency.

The characteristic comparisons for the input part of the converters in Figure 7.10 are similar to their parent automatic shapers. The ballasts whose input parts resemble ideal automatic current shapers have the same voltage stress which is approximately $2\pi V_m$ for $D = 0.5$. On the other hand, the ballasts whose input parts resemble non-ideal automatic current shapers have a higher voltage stress which is approximately $4\pi V_m$ for

$D = 0.5$. For example, circuits in Figure 7.10 (a) and (d) have lowest voltage stress as opposed to the circuits in Figure 7.10(e) and (f) which have highest voltage stress. Also, ideal shaper based circuits have a better current shaping than that of non-ideal shaper based circuits at the price of larger current stress.

Soft-switching of the combined circuit is mainly determined by the output part of the Class E converter. The influence of the input current shaper on the Class E inverter can be ignored if the ripple component is negligible which is true in most cases.

The operation and analysis for another family of circuits incorporating automatic current shapers and forward inverter as shown in Figure 7.12 are more straightforward. Since the switching waveform is square wave, there is no interactions between the input and output parts of the circuit which greatly simplifies their analysis and design. Better current shaping is also obtained.

7.8 Experimental Results

The circuit shown in Figure 7.10(a) is built. Design is based on the following data: f_s is 100kHz, nominal lamp current is 265mA. V_{C1} is 190V, operating point can be determined in the output $R_l - i_R$, plane as shown in Figure 7.5, where the boundaries of the soft-switching regions for large and small L_2 are plotted and the lower straight line is the measured lamp resistance.

Components used in the prototype are listed below: Bridge rectifier: $VH248$, input filter of L_f: 600μH, C_f: 0.1μF, input inductor L_1: 728μH, switch Q: $IRFPE30$, fast recovery diodes D_1 and D_2: $10CTF40$, energy storage capacitor C_1: 33μF, resonant capacitor C_2: 1.6nF, inductor L_2: 2.57mH. LCC resonant matching network of L: 1.6mH, C_s: 5.76nF, C_p: 2.6nF. Operating frequency f_s: 105kHz.

Measured waveform and data are shown as follows. The input inductor current i_1 is shown in Figure 7.15 on the switching scale to demonstrate the DICM operation in the desired mode. Current i_1 is averaged by the input filter and unfolded by the bridge rectifier which results in the line current following the line voltage v_i as shown in Figure 7.16. Lamp current i_l and voltage v_l are shown in Figure 7.17. Switch voltage v_{c2} are given in Figure 7.18 to demonstrate the soft-switching operation. Negligible line

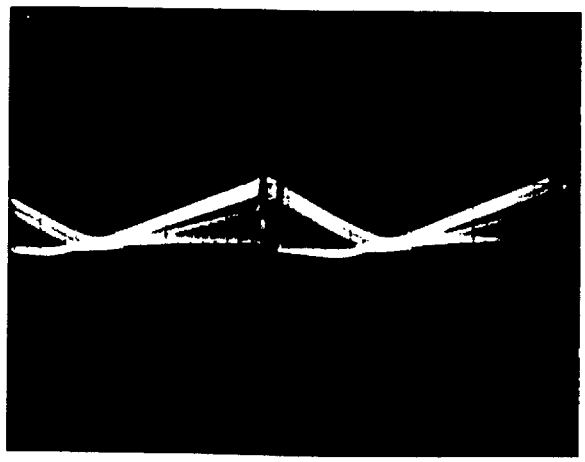

Figure 7.15: DICM operation of input inductor. Current: 1A/Div., Time: 2μS/Div.

ripples are observed at the output.

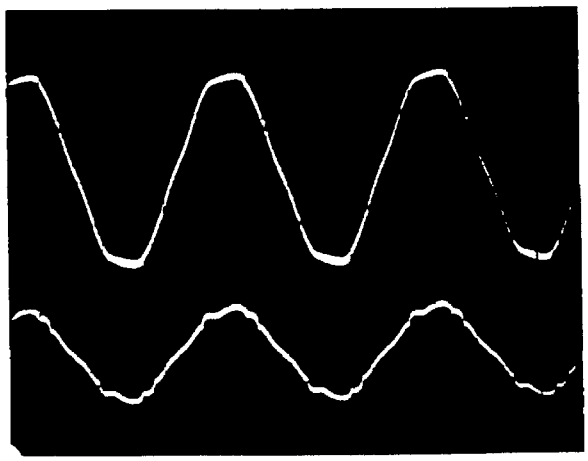

Figure 7.16: Input voltage (upper trace) and input current illustrate a close to unity power factor at the front-end. Voltage: 100V/Div., Current: 0.5A/Div., Time: 5mS/Div.

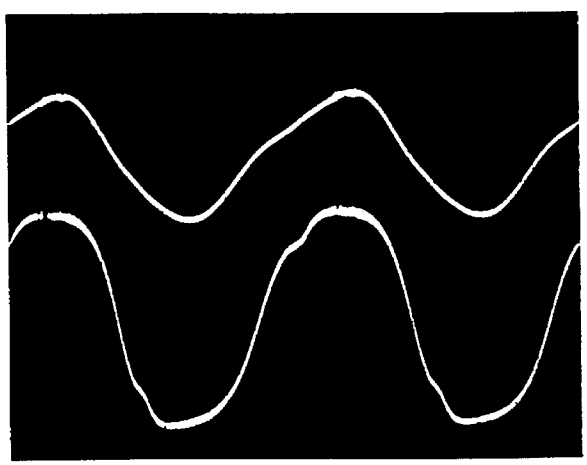

Figure 7.17: Lamp volatge (upper trace) and current show the desired waveform. Voltage: 100V/Div., Current: 0.2A/Div., Time: 2μS/Div.

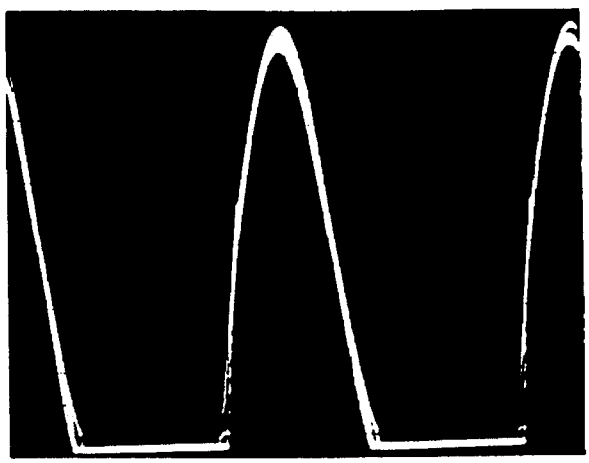

Figure 7.18: Switch voltage v_{c2} indicates the low switching loss operation. Voltage: 100V/Div., Time: 2μS/Div.

Chapter 8

Conclusions

The quest for low harmonic distortions and high power factor requires effectively two cascaded power conversion stages of a lamp ballast resulting in increased circuit complexity, lower efficiency and reduced reliability. It is expected that the discovery of new ballast topologies can overcome the above difficulties in such a way that input current-shaping and high frequency ballasting are combined into a single power conversion stage.

In the first phase of this research, a single-stage, high power factor lamp ballast is proposed, which is derived from the Ćuk converter. A new discontinuous inductor current mode of its input inductor makes this possible by separating the input current-shaping from high frequency output lamp ballasting function. The desirable mode of operation is presented with the illustrations of major waveforms. The high efficiency is further enhanced by soft-switching improvement, which is provided naturally through the lagging current of the output resonant matching network. Design equations are given. The performances of the proposed single-stage, high power factor lamp ballast are verified by the experimental results.

In the second phase of this work, single-switch, unity power factor ac-to-ac converter topologies based on proper integrations of automatic current shapers and the single switch inverters, such as the Class E converter, are presented, which are suitable for lamp ballast applications. The ballasts have the compact structure of single active switch, high input power factor and low crest factor lamp current as well as soft-switching. Descriptions of desirable mode of operations and the first order analysis are given. Experimental results confirm all the performances.

The proposed single-stage, power processing ballasts are expected to be applicable to the state-of-the-art smart power technology and to provide more cost-effective solutions for the ballast designers.

Appendix A

Derivations of Lamp Incremental Impedance $Z_l(s)$

Francis equation [2] is:

$$\frac{dy}{dt} = Aw - By \tag{A.1}$$

where y is lamp conductance, w is lamp power and A, B are positive constants. It states that the change of lamp conductance is proportional to its power and in reverse proportionality to its conductance. At the steady-state, it becomes

$$AW = BY \quad or \quad V^2 = B/A \tag{A.2}$$

when $W = VI$ and $Y = I/V$ are substituted. If the lamp carrier is dc, then the steady-state solution is just its dc operating point. If the lamp carrier is high frequency sinewave, then the steady-state operating point represents its rms values since switching period is much smaller than the ionization constant and conductance can be considered as constant.

From Eq. (A.1) the small-signal impedance $Z_l(s)$ can be derived. First y can be presented by:

$$y = \frac{i}{v} \tag{A.3}$$

and w is

$$w = iv. \tag{A.4}$$

Substitute Eqs (A.3), (A.4) into Eq. (A.1)

$$v\frac{di}{dt} - i\frac{dv}{dt} = Av^3i - Bvi \tag{A.5}$$

then i and v are decomposed into:

$$i = I + \hat{i}, \quad v = V + \hat{v}. \tag{A.6}$$

Substitute Eq. (A.6) into Eq. (A.5)

$$v\frac{d\hat{i}}{dt} - AV^3\hat{i} + BV\hat{i} = i\frac{d\hat{v}}{dt} + 3AV^2i\hat{v} - B\hat{v}i \tag{A.7}$$

apply Laplace transform

$$\hat{i}(sV - AV^3 + BV) = \hat{v}(sI + 3AV^2I - BI). \tag{A.8}$$

Finally substitute Eq. (A.2), $Z_l(s)$ can be obtained as

$$Z_l(s) = \frac{\hat{v}}{\hat{i}} = \frac{V}{I}\frac{s}{s + AV^2(A^2 - 1)}. \tag{A.9}$$

Similarly, for the modified model

$$\frac{dy}{dt} = \frac{Ai}{G(i)} - By. \tag{A.10}$$

The small-signal impedance derived from Eq. (A.10) is

$$Z_l(s) = \frac{V}{I}\frac{s + AVIG'(I)/G^2(I)}{s + VA/G(I)}. \tag{A.11}$$

Appendix B

Derivations of Soft-switching Boundaries of Class E Converter

Following assumptions are made to simplify the derivation: Inductor L_e is large enough to convert the dc voltage V_{dc} into a dc current I_i. LCC resonant work is highly selective and the current i_o flowing through it can be approximated by the fundamental component

$$i_o = i_c cos\theta + i_s sin\theta \tag{B.1}$$

where $\theta = \omega_s t$ and ω_s is the angular switching frequency. The current throught the switch is

$$i_s = i_c cos\theta + i_s sin\theta + I_i. \tag{B.2}$$

In our case, it is assumed that the duty ratio is 50%. The conditions of ideal (soft-switching) operation in terms of α and Γ are

$$\alpha \leq \pi \quad or \quad i_s(-\alpha) = I_i + i_c cos\alpha - i_s sin\alpha = 0 \tag{B.3}$$

and

$$\Gamma \leq \pi \quad or \quad \int_0^{\Gamma} i_s(\theta) d\theta = 0. \tag{B.4}$$

The combination of LCC network and lamp load R_l gives a complex impedance Z_i to the Class E switching cell:

$$Z_i = A + jB \tag{B.5}$$

where

$$A = \frac{R_l}{1 + (\omega_s C_p R_l)^2} \tag{B.6}$$

and

$$B = \omega_s L - \frac{1}{\omega_s C_s} - \frac{\omega_s C_p R_l^2}{1 + (\omega_s C_p R_l)^2}. \tag{B.7}$$

Assume the voltage across the switch Q is

$$v_{ce} = a_1 cos\theta + b_1 sin\theta + a_0, \quad 0 \leq \theta \leq \Gamma. \tag{B.8}$$

Also

$$v_{ce} = -i_o Z_i \tag{B.9}$$

therefore

$$i_c B - i_s A = b_1, \quad -i_c A - i_s B = a_1. \tag{B.10}$$

From Eqs. (B.4), (B.8) and (B.10), following relations are found

$$\frac{i_c}{I_i} = f_1(\Gamma, A', B') \tag{B.11}$$

$$\frac{i_c}{I_i} = f_2(\Gamma, A', B')$$

where

$$A' \equiv \frac{A}{\omega_s C_e},$$
$$B' \equiv \frac{B}{\omega_s C_e}.$$

Substitute $\Gamma = \pi$ into Eq. (B.11)

$$A'^2 + B'^2 = B' \left(\frac{\pi^2 - 4}{\pi^2} \right) - \frac{\pi^2 - 8}{4\pi^2} \tag{B.12}$$

and normalized current i_c/I_i can be calculated from

$$\frac{i_c}{I_i} = \frac{\pi(B' - 0.5) + 4/\pi}{2A'}. \tag{B.13}$$

From power balance

$$V_{dc} I_i = \frac{1}{2}({i_c}^2 + {i_s}^2)A = \frac{1}{2} {i_l}^2 R_l. \tag{B.14}$$

Therefore, the normalized load current i_R/V_{dc} in the unit of conductance is available from

$$\frac{i_R}{V_{dc}} = 1/\sqrt{0.5AR_l\left[\left(\frac{i_c}{I_i}\right)^2 + \frac{\pi^2}{4}\right]}. \tag{B.15}$$

For the second boundary $\alpha = \pi$, from Eq. (B.3)

$$\frac{i_c}{I_1} = 1. \tag{B.16}$$

Substitute Eq. (B.16) into Eq. (B.11), following relations are obtained

$$A' = \frac{1}{2\pi}\frac{g_1(\Gamma)}{g_3(\Gamma)} \tag{B.17}$$

$$B' = \frac{1}{2\pi}\frac{g_2(\Gamma)}{g_3(\Gamma)} \tag{B.18}$$

where

$$g_1(\Gamma) = (\Gamma^2 cos\Gamma + \Gamma^2 + 4cos\Gamma - 4)(cos\Gamma - 1) \tag{B.19}$$

$$g_2(\Gamma) = \Gamma^3 - \Gamma^2 sin\Gamma cos\Gamma + 2\Gamma^2 sin\Gamma + 2\Gamma cos\Gamma$$
$$-2\Gamma + sin2\Gamma - 2sin\Gamma \tag{B.20}$$

$$g_3(\Gamma) = \Gamma^2 + 2\Gamma sin\Gamma + 2 - 2cos\Gamma. \tag{B.21}$$

Step through Γ from 0 to π, solve for the switching frequency f_s and load R_l from the above equations. Finally

$$\frac{i_l}{V_{dc}} = 1/\sqrt{0.5AR_l\left[\left(\frac{i_s}{I_i}\right)^2 + 1\right]}. \tag{B.22}$$

References

[1] J. Waymouth, *Electric Discharge Lamps*, Cambridge, Mass.: MIT Press, 1971.

[2] V. J. Francis, *Fundamentals of Discharge Tube Circuits*, London: Methuen & Co. Ltd., 1948.

[3] J. H. Campbell, *The history and technical evolution of high frequency fluorescent lighting*, Lawrence Berkeley Laboratory Report, No. 7810, December, 1977.

[4] E. E. Hammer, "Fluorescent Lamp Operating Characteristics at High Frequency," Journal of Illuminating Engineering Society, October, 1984, pp. 211-224.

[5] J. E. Jewell, S. Selkowitz and R. Verderber, "Solid-state Ballasts Prove to Be Energy Savers," Lighting Design and Application, January, 1980, pp. 37-42.

[6] N. Aoike, K. Yuhara and Y. Nobuhara, "Electronic Ballast for Fluorescent Lamp Lighting System of $100 lm/W$ overall efficiency," Journal of Illuminating Engineering Society, October, 1984, pp. 225-231.

[7] E. L. Laskowski and J. F. Donoghue, "A model of a Mercury Arc Lamp's Terminal V-I behavior," IEEE Trans. on Industry Applications, Vol. IA-17, No. 4, July/August, 1981, pp. 419-426.

[8] S. C. Peck and D. E. Spencer, "A Differential Equation for the Fluorescent Lamp," IES Transaction, April, 1968, pp. 157-166.

[9] P. R. Herrick, "Mathematical Models for high-Intensity Discharge Lamps," IEEE Trans. on Industrial Applications, Vol. IA-16, No. 5, September/October, 1980, pp. 648-654.

[10] J. C. Engel and H. B. Hamilton, "Design and Analysis of a Closed Loop-Dynamic Metal Vapor Lamp Ballast," IEEE Industrial General Applications Society Annual Meeting, Conference Record 1969, pp. 371-379.

[11] M. Gulko and S. Ben-Yaakov, "Current-sourcing Push-pull Parallel-resonant Inverter (CS-PPRI): Theory and Application as a Fluorescent Lamp Driver," IEEE Applied Power Electronics Conference and Exposition, Conference Proceedings 1993, pp. 441-417 (IEEE Publication 93CH3271-4).

[12] L. O. Chua, C. A. Desoer and E. S. Kuh, *Linear and Nonlinear Circuits*, New York: Mcgraw-Hill Book Company, 1987.

[13] J. C. Doyle, B. A. Francis and A. R. Tannenbaum, *Feedback Control Theory*, New York: Macmillan Publishing Company, 1992.

[14] B. C. Kuo, *Automatic Control Systems,* Englewood Cliffs, New Jersey: Prentice Hall, Inc., 1991.

[15] R. D. Middlebrook and S. Cuk, "A General Unified Approach to Modeling Switching-Converter Power Stages," IEEE Power Electronics Specialists Conference, 1976 Record, pp. 18-34 (IEEE Publication 76-CH-0-1084-3AES).

[16] R. D. Middlebrook, "Input Filter Considerations in Design and Application of Switching Regulators," IEEE Industry Applications Society Annual Meeting, 1976 Record, pp. 366-382 (IEEE Publication 76-CH-1122-1-IA).

[17] S. R. Sanders, J. M. Noworolski, X. Z. Liu and G. C. Verghese, "Generalized Averaging Method for Power Conversion Circuits," IEEE Power Electronics Specialists Conference, 1990 Record, pp. 333-340 (IEEE Publication 90CH2873-8).

[18] C.T. Rim and G.H. Cho, "Phasor Transformation and its Application to the DC/AC Analyses of Frequency Phase-Controlled Series Resonant Converters (SRC)," IEEE Trans. on Power Electronics, Vol. 5, No. 2, April 1990, pp. 201-211.

[19] E. Young, F. C. Lee and M. M. Jovanovic, "Small-Signal Modeling of Power Electronic Circuits Using Extended Describing Function Technique," Proceedings of the

Virginia Power Electronics Center Seminar, Blacksburg, VA, September 15-17, 1991, pp. 167-178.

[20] S. Freeland, Part II, "Input-Current Shaping for Single-Phase Ac-Dc Power Converters," Ph.D thesis, California Institute of Technology, October, 1987.

[21] B. Christiansen, "Electronic Ballasts Improve Fluorescent Lamp Performance," Lighting Design and Application, pp. 13-18, January, 1990.

[22] P. Wood, "High Frequency Discharge Lamp Ballasts Using Power MOSFETs, IGBT'S and High Voltage Monolithic Drives," Proc. PCI '89, pp. 307-324.

[23] J. Spangler, B. Hussain and A. K. Behera, "Electronic Ballast Using a Power Factor Correction Technique for Loads Greater Than 300 Watts," IEEE Applied Power Electronics Conference and Exposition, Conference Proceedings 1991, pp. 393-399 (IEEE Publication 91CH2992-6).

[24] M. Jordan and J. O'Connor, "Resonant Fluorescent Lamp Converter Provides Efficient and Compact Solution," IEEE Applied Power Electronics Conference and Exposition, Conference Proceedings 1990, pp. 792-801 (IEEE Publication 93CH3271-4).

[25] G. Lutteke and H. C. Raets, "High Voltage High Frequency Class-E Converter Suitable for Miniaturization," IEEE Power Electronics Specialists Conference, 1984 Record, pp. 54-61 (IEEE Publication 84-CH-2073-5).

[26] G. Lutteke, H. C. Raets, "220V Mains 500kHz Class-E Converter Using a Bimos," IEEE Power Electronics Specialists Conference, 1985 Record, pp. 127-135 (IEEE Publication 85CH2117-0).

[27] L. Dixon, "High Power Factor Preregulator for Off-Line Power Supplies,"Unitrode Power Supply Design Seminar, SEM-800, 1991, pp. I2.1-16.

[28] S. Ćuk and R. D. Middlebrook, *Advances in Switched-Mode Power Conversion*, Vol. II TESLAco., 1981.

[29] M. Madigan, R. Erickson and E. Ismail, "Integrated High Quality Rectifier-Regulators," IEEE Power Electronics Specialists Conference, 1992 Record, pp.1043-1051 (IEEE Publication 92CH3163-3).

[30] C. Henze, H. Martin and D. Parsley, "Zero-Voltage Switching in High Frequency Power Converters Using Pulse Width Modulation," IEEE Applied Power Electronics Conference and Exposition, Conference Proceedings 1988, pp. 33-40 (IEEE Publication 88CH2504-9).

[31] S. Ćuk and E. Deng, "Single Stage, High Power Factor, Gas Discharge Lamp Ballast," U. S. Patent 5,416,387, May 16, 1995.

[32] R. L. Steigerwald, "A Comparison of Halfbridge Resonant Converter Topologies," IEEE Trans. on Power Electronics, Vol. 3, No. 2, April 1988, pp. 174-182.

[33] N. O. Sokal and A. D. Sokal, "Class E-A New Class of High-Efficiency Tuned Single-Ended Switching Power Amplifier," IEEE Journal of Solid-State Circuits, Vol. SC-10, pp. 168-176, June 1975.

[34] R. Redl, B. Molnar and N. Sokal, "Class E Resonant Regulated DC/DC Power Converters: Analysis of Operations, and Experimental Results at 1.5 MHz," IEEE Trans. on Power Electronics, Vol. PE-1, No. 2, April 1986, pp. 111-120.

[35] R. Erickson, M. Madigan and S. Singer, "Design of a Simple High-Power-Factor Rectifier Based on the Flyback Converter," IEEE Applied Power Electronics Conference and Exposition, Conference Proceedings 1993, pp. 424-431 (IEEE Publication 90CH2873-8).

[36] J. Sebastian, J. Uceda, J. A. Cobos, J. Arau and F. Aldana, "Improving Power Factor Correction in Distributed Power Supply Systems Using PWM and ZCS-QR Sepic Topologies," IEEE Power Electronics Specialists Conference, 1991 Record, pp. 780-791 (IEEE Publication 91CH3008-0).

[37] K-H Liu and Y-L Lin, "Current Waveform Distortion in Power Factor Correction Circuits Employing Discontinuous-Mode Boost Converters," IEEE Power Electronics Specialists Conference, 1989 Record, pp. 825-829 (IEEE Publication 89CH2721-9).

[38] M. Brković and S. Ćuk, "Input Current Shaper Using Ćuk Converter," International Telecommunication Energy Conference, Proceedings 1992, pp. 532-539 (IEEE Publication 92CH3195-5).

[39] A. Hiramatsu, K. Yamada, F. Okamoto and M. Mitani, "Low THD Electronic Ballast with a New AC-DC Converter Operation," Annual Conference of Illuminating Engineering Society of North America, Conference Proceedings 1992, pp. 341-360.

[40] E. Ismail and R. Erickson, "A New Class of Low Cost Three-Phase High Quality Rectifiers with Zero-Voltage Switching," IEEE Applied Power Electronics Conference and Exposition, Conference Proceedings 1993, pp. 182-189 (IEEE Publication 93CH3271-4).